Primary and secondary membrane damage by small β-barrel pore forming toxins and their implications for membrane repair

Dissertation

to obtain the degree

Doctor of Science

At the Department of Biology

The Johannes Gutenberg University Mainz

submitted by

Qianqian Qin

born in Shandong, China

Mainz, 2020

Dean: Prof. Dr. [redacted]

1. **Supervisor: Prof. Dr.** [redacted]

2. **Supervisor: Prof. Dr.** [redacted]

Day of the oral exam: 27th October, 2020

Dedicated to [redacted] and [redacted]

Contents

Summary

A thin lipid bilayer, the plasma membrane (PM), separates the interior milieu of cells of all living organisms from the outside world. Physiological trans-membrane channels and transporter proteins permit the regulated transport of ions, nutrients and water, which is essential for cellular homeostasis. In contrast, pore-forming toxins (PFTs), e.g. toxins produced by bacteria, permeabilize the plasma membranes of target cells to disturb cellular homeostasis. However, host cells can survive such an attack by PFTs and it is this remarkable ability of mammalian cells which is the principal subject of the present thesis.

The earliest experiments in the field of membrane repair documented that mechanical perforation of oocyte membranes is reversible. Rapid influx of calcium turned out to be essential for repair in this model. In the mid-nineties, following up on the findings of Thelestam and Mollby, our group started to investigate the mechanisms of repair for defined, circumscribed lesions caused by PFTs. A key finding was that repair of the plasma membrane was comparably fast for the relatively large pores formed by streptolysin O (SLO, ca. 30 nm diameter), as compared to *S. aureus* α-toxin, which forms far smaller pores (ca. 1.2 nm). Further, it turned out that repair after SLO- but not α-toxin attack requires extracellular calcium, thus resembling repair in the oocyte model while α-toxin triggered slower p38 MAPK dependent repair, which did not depend on extracellular calcium. These findings indicated that membrane repair is diverse, and raised the question whether overall pore size/conductance, or structural differences between SLO (a cholesterol dependent cytolysin) and α-toxin (a member of the small β-barrel family of PFT), or yet other differences, account for differential susceptibility of various PFT for rapid, calcium-influx dependent repair (CIDRE).

In the first part of this work, a new small β-PFT, i.e., Phobalysin P of *Photobacterium damselae* subsp. *damselae.* (PhlyP) is discussed, which we exploited as a unique experimental tool to tackle the above question. This was promising, because PhlyP, despite being a small β-PFT like α-toxin, forms pores, which are permeable for vital dyes. This is also in contrast to the closely related *Vibrio cholerae* cytolysin (VCC), which has about 50% homology at the amino acid level with PhlyP and a pore channel

diameter of approximately 1.2 nm. Homology based modelling using VCC toxin as a template indicated that PhlyP has a slightly wider channel diameter and fewer charged residues at pore channel. Comparative studies on PhlyP and VCC revealed that these differences have significant consequences for PFT primary toxicity and host membrane repair. In essence, PhlyP causes more rapid fluxes of ions, including of calcium ions (Ca^{2+}), and these changes are largely reversible. The mechanisms of repair are similar to those previously described for SLO, i.e., involving rapid influx of calcium, exocytosis, and production of ceramide by acid sphingomyelinase and caveolin-dependent processes, presumably endocytosis of toxin. In contrast, VCC pores are less conductant, leading to slower fluxes of (cat-) ions (K^+ and Ca^{2+}). Importantly, these changes are usually not reversible, but ultimately lead to the death of a cell. By swapping amino acid moieties forming the presumed channel narrow points of VCC and PhlyP, the importance of channel width for both primary toxicity and susceptibility for rapid repair became evident. Therefore, it is concluded that not the affiliation of a PFT with a certain structural family, but pore size and conductance for calcium ions determine the capacity to trigger rapid repair.

The second part of this work deals with the question how secondary effects may account for changes caused by a PFT, in particular small β-PFTs. Two observations led to this question: first, VCC, although permitting comparably slower influx of ions, did ultimately increase the levels of cellular Ca^{2+} concentration, an effect that was sensitive to suramin, an inhibitor of P2X7 channels. Second, α-toxin has been proposed to form small pores or large pores depending on the concentration of toxin. However, the nature of the different pore types is unclear. By studying α-toxin dependent changes of Fluo-8 signals in epithelial cells, it became clear that only toxin concentrations, which are well beyond the threshold that triggers potassium (K^+) influx lead to rapid influx of calcium, suggesting that indeed two types of lesions do exist.

Further analysis indicated that neither zvad-fmk nor necrosulfonamide prevented influx of PI under these conditions. Therefore, large pores seem not to be secondary to caspase-1 dependent activation of gasdermin D (GSDMD), and the formation of large pores from the cytosolic side, or formation of similar pores by Mixed lineage kinase domain like pseudokinase (MLKL). Although GSDMD-activation was detectable after α-toxin treatment in cells transiently transfected with N-terminally tagged GSDMD,

these events occurred too late to account for the observed fluxes of PI or calcium ions. In contrast, glycine, partially prevented influx of PI in α-toxin (high dose)-treated cells. Therefore, the mechanism of “large-pore formation” by α-toxin appears to be swelling-induced rupture. This is also in agreement with the observation of LDH-efflux at high toxin doses.

To sum up, pore size is an important parameter, which co-determines toxicity and repair of a given small β-barrel PFT. Further, secondary damage including by endogenous channel forming proteins may account for a plethora of cellular responses to PFT and for apparently divergent results obtained by different researchers.

Abbreviations

ADAM10	A disintegrin and metalloprotease 10
ASIC	Acid sensing ion channel
ATP	Adenosine triphosphate
ADP	Adenosine diphosphate
AMPK	Adenosine monophosphate-activated protein kinase
α-toxin or **Hla**	*Staphylococcus aureus* α-hemolysin
BSA	Bovine serum albumin
Ca^{2+}	Calcium ion
CIDRE	Calcium influx-dependent repair-mechanisms
CD59	CD59 glycoprotein
CDC	Cholesterol-dependent cytolysin
Da	Dalton
DMSO	Dimethyl sulfoxide for molecular biology
E. coli	*Escherichia coli*
eIF2α	Eukaryotic initiation factor 2α
ERK	Extracellular signal–regulated kinases
ESCRT	The endosomal sorting complexes required for transport
g	gram
GCN2	General control, non-derepressible 2
GSDMD	Gasdermin D
GPI receptor	Glycosyl phosphatidyl– anchored receptors
GRAF1	GTPase regulator associated with focal adhesion kinase-1

HBSS	Hanks' balanced salt solution
HaCaT	Human non-virally transformed keratinocytes
IL 1β	Interleukin 1 beta
JNK	c-Jun N-terminal kinase
k	Kilo-
K^+	Potassium ion
LAMP-1	Lysosome associated-membrane protein 1
LDH	Lactate dehydrogenase
LLO	Listeriolysin O
l	Liter
M	Molar mass
m	Milli-
min	Minute
MAC	Membrane attack complex
MACPF	MAC perforin domain
MAPK	Mitogen-activated protein kinase
MLKL	Mixed lineage kinase domain like pseudokinase
MEFwt	Mouse embryonic fibroblast wild type
MEFcav$^{-/-}$	Mouse embryonic fibroblast caveolin deficient
Na^+	Sodium ion
n	Nano-
NO	Nitric oxide
NF- κB	Nuclear factor kappa-light-chain-enhancer of activated B cells
NK cells	nature killer cells

PAS	Phagophore assembly site/pre autophagosomal structure
PBS	Phosphate-buffered saline
PCR	Polymerase chain reaction
PFA	Paraformaldehyde
PFO	Perfringolysin
PFP	Membrane pore-forming protein
PFT	Bacterial membrane pore-forming- toxin
PhlyP	Phobalysin P of *Photobacterium damselae* subsp. *damselae*
PM	Plasma membrane
PI	Propidium iodide , a fluorescent intercalating agent
PKR	Protein kinase R
P38 MAPK	P38 mitogen-activated protein kinase
ROS	Reactive oxygen species
RIPK	Receptor-interacting protein kinase
RMP	Resting membrane potential
RTX	Repeats in toxin protein sequence
SLO	Streptolysin O
TLR	Toll-like receptor
UPR	Unfolded protein response
Vac A	*Helicobacter pylori* vacuolating toxin A
VCC	*Vibrio cholerae* cytolysin
zvad-fmk	Z-VAD(OMe)-FMK, the broad-spectrum caspase inhibitor
µ	Micro-

1 Introduction

1.1 Biological membranes

Biological membranes exist in virtually all organisms, although transient existence of life without membrane has been documented (Kim et al., 2001). The plasma membrane (PM) functions as a barrier surrounding cells to separate intra- and extra-cellular components, therefore forming an independent and compartmentalized intracellular environment. Moreover, the PM is an essential tissue in living organisms as it takes part in most cellular processes. Nearly all the PM shares the basic lipid bilayer structure that is composed of two-sheets of lipids with various inserted proteins and carbohydrate.

PMs of different origin share a basic lipid bilayer structure. The PM is amphipathic with two leaflets of phospholipid molecules that constitute the bilayer. Specifically, each lipid molecule has two hydrophobic fatty acid chains and one hydrophilic phospholipid head. Due to water's polarity, the charged hydrophilic heads are attracted to intra- and extracellular water and form a flat lipid surface, while the hydrophobic tails interact with the other lipid tail region on the complementary leaflet. Lipids build up the basic bilayer membrane structure softly and strongly that provide the foundation of the PM flexibility. Three major types of lipids occur in the PM, including glycerophospholipids, sphingolipids and cholesterols. Among them, phospholipids (glycerophospholipid and sphingolipid) constitute the main fabric of membrane structure and are the majority percentage of the PM composition. Cholesterol is usually present in mammalian cells and mycoplasmas bacteria where it can regulate the fluidity, thickness and compressibility of the PM in diverse ways (Brown, 1996; Yang et al., 2016). The carbohydrate components only localize on the outside surface of the lipid bilayer where they play a role in recognition function of cellular signal molecules. They usually attach to lipids through covalent bonds forming glycolipids, or link to PM proteins covalently forming glycoproteins (Lein et al., 2015; Watson, 2015).

Proteins are the second major component of the PM and carry on many specific cellular activities. Proteins can constitute between 20–70% of the PM by mass in different organisms. The PM proteins carry out many functions which are helpful for the survival and metabolism of cells. Membrane proteins usually exist in two forms in lipid bilayer, i.e., integral and peripheral proteins. Integral membrane proteins tightly attach to the lipid bilayer by the interaction of their hydrophobic regions. They insert or cross the lipid bilayer structure one or multiple times to form a stable structure which can only be removed by treatment of detergents or organic solvent liquid. The peripheral proteins usually attach to the lipid head group of the PM or to the integral protein by non-covalent bonds. The inner and outer surfaces of the PM have different compositions to perform different biological functions; for example, signal recognition usually happens on the outer surface, while the immunity responses mostly take place on the inner surface (Watson 2015; Stillwell 2013).

The PM provides an enclosed space for cells to form compartments which maintain the cellular inner environment. In the cytosol, the PM functions in forming different organelles by making cellular compartments with specific pH value, voltage and enzymes (Watson, 2015). Also, with the help of the PM, organelles can be connected and work together to respond to sequential physiological and biochemical processes. Meanwhile, the PM is a main platform where many metabolic reactions occur. It is characterized by two significant features: selective permeability and fluidity. Many cellular processes are dependent on the selective permeability of the PM, such as the exchange of substances between outer- and inner-cellular environment, the prevention of the entry of toxic or unneeded substances, and the transportation of metabolites or other molecules. The PM fluidity is mainly based on the rotation around the bonds of tails on lipid molecules. The structure of the PM has been described as a mosaic of lipids, proteins, cholesterol and carbohydrates composing the lipid bilayer, which is called the mosaic model (Singer and Nicolson, 1972). Both the fluidity and the mosaic model ensure a membrane structure between liquid and solid, thus providing the living cell a prerequisite to be an individual unit of life (Watson, 2015).

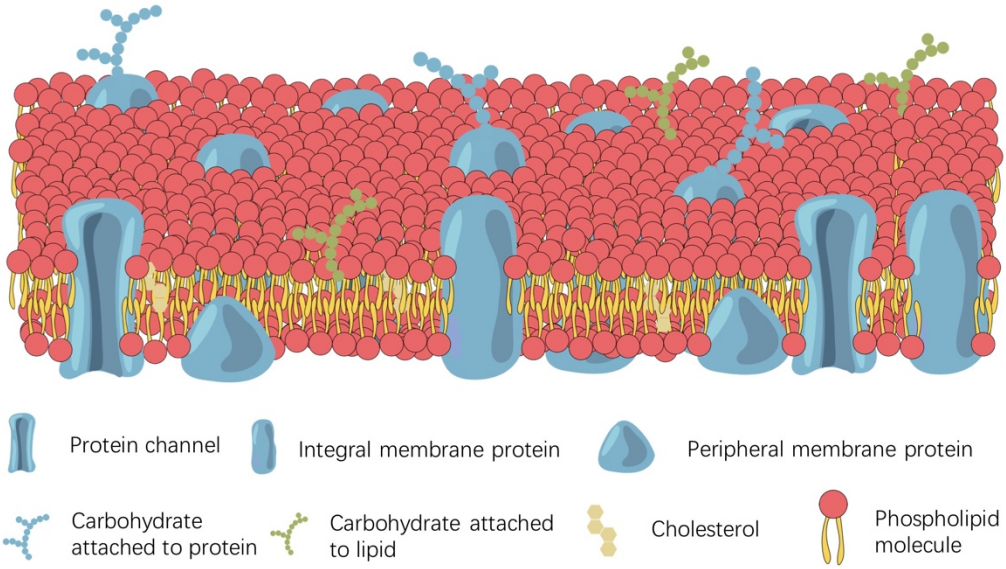

Figure 1: The scheme of the biological plasma membrane (PM). The PM is amphipathic with two leaflets of phospholipid molecules to constitute the bilayer. Lipids, proteins and carbohydrates are the three major components of the PM. Carbohydrates attach to the lipids through covalent bonds forming glycolipids, or link to the proteins covalently forming glycoproteins. The PM proteins usually exist in two forms, integral and peripheral proteins. Cholesterols usually occur in mammalian cell membrane. Ion channels are constituted by integral proteins and universally distributed in the PM (https://openstax.org/details/books/biology-2e).

In all cells, there is a voltage difference between the inner and outer sides of the PM with the interior electrically being negative and the outer being positive. This is called the Resting Membrane Potential (Braun et al., 2007) (Fig. 2). The RMP is the fundamental of the bioelectricity. Two factors are responsible for the generation of the RMP between inner and outer sides of the PM: 1) the uneven distribution of sodium and potassium positive ions on two sides of the PM. The intracellular environment has higher concentration of K^+ and lower concentration of Na^+ than the extracellular environment; 2) In certain contexts, the selective permeability of the PM to various ions is different. In particular, the intracellular K^+ concentration is higher than the extracellular environment, while the concentrations of Na^+ and Cl^- are lower that the exterior. Furthermore, organic anions are only maintained inside cells. The PM has higher permeability to K^+ and lower permeability to Na^+. Nearly no ions can pass through the PM in quiescent situation except K^+. The main ion flow in this period is the efflux of K^+, which is driven by the potassium concentration difference between inner and outer sides of the PM. As a result, the positive charge of the PM interior decreases

and the extracellular positive charge increases, therefore forming a potential difference between the outside and inside of the PM. The outflow of K^+ cannot proceed without limitation. With the increase of K^+ concentration on the extracellular side, the movement of K^+ is stopped by the electric field force to reach an equilibrium.

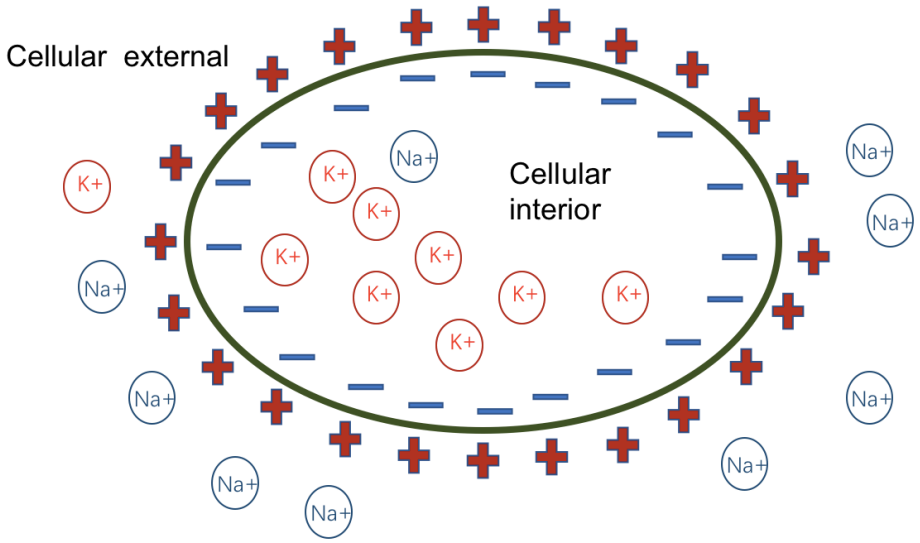

Figure 2: The resting membrane potential with interior electricity negative and outer positive. There is voltage difference between inner and outer sides of the PM in quiescent cells. The uneven distribution of the positive ions on both sides of the PM and the selective permeability of the PM are mainly responsible for the generation of the RMP.

The transport of ions and other solutes between intra- and extracellular environments is performed by pore-forming proteins located on the PM, referred to as ion channels (Subramanyam and Colecraft, 2015). The ion channels consist of integral proteins and universally distributed in the PM. A single ion channel is normally arranged in a circle by several separated homologous proteins to form a multi-subunits congregation with a small, water-filled pore in the core, which is typically 1–2 atoms of width (Hille and Catterall, 1994). The specificity of ions passed through is decided by the narrowest point of the ion channel and the charge of the ions. For example, K^+ - Na^+ channel is only permeable for K^+ and Na^+. The most distinctive features of ion channels are their high transporting speeds and metabolic energy-independent. The transporting rate of ion channels can be 10^6 ions per second and even higher. As the transport across ion channels is driven by ion concentration difference and thermodynamic tendency to decrease electrochemical gradients, there is no ATP consumption (Hille, 1978).

Ion channels have physiological relevance. For instance, they are involved in the contraction of cardiac and skeletal muscles, in the cell growth and proliferation, in the release of insulin, etc. (RamaKrishnan and Sankaranarayanan, 2016). Ion channels are controlled by gates (called ion channel gates), which are regulated by chemical agents, electrical signals, temperature, pH value, mechanical stress and other triggers. Based on the gated-feature, organisms can use toxins to attack prey by affecting their ion channels in order to palsy their nervous system. Therefore, ion channels also become the effective target point for new therapeutic applications (Heusser et al., 2016).

Ion channels are classified according to their gate features, specificity of ions passing through and ligands that they combine with. Voltage-gated ion channels, including sodium channels, potassium channels, calcium channels and transient receptor cation channels, depend on the membrane potential to open or close. Ligand-gated ion channels (ionotropic proteins), are activated by binding some specific ligand molecules to membrane receptor proteins. These channels involve Nicotinic acetylcholine receptors, glutamate receptors, P2X receptors activated by ATP, GABA receptor triggered by gamma-aminobutyric acid. Some other types of ion channels cannot be classified easily by voltage or ligand, such as Acid sensing ion channel (ASIC), which is activated by extracellular H^+ (RamaKrishnan and Sankaranarayanan, 2016).

Porins are also membrane channels that responsible for substance transport, which are also named as channel protein. They are water-filled pores formed by β-barrels spanning the cellular lipid bilayer, to promote the absorption of hydrophilic substances (Nakae, 1976). Porins are quite different than the other typical membrane channels in their structure as they are composed of transmembrane antiparallel β-strands and connected by many extraplasmic loops, lacking of an archetypal hydrophobic region, which is a common structure domain in other membrane channel proteins (Fernandez and Hancock, 2012). Specifically, hydrophobic amino acids in porin subunits are facing towards the outside while hydrophilic amino acids are facing inside the protein structure. All amino acids assemble in a unique β-barrel with an extra-long loop folding back in to the cavity (Fernandez and Hancock, 2012). The structure solved out of membrane porins is a typical trimeric protein with 16 β-strands. Many other porin structures were determined to have small variations in the topology of the loops. Porins

are simply classified as belonging to either the 16-stranded or 18-stranded families. The 16-stranded porins are usually viewed as general porins which are permeable to many hydrophilic molecules without substance preferences, while the 18-standed porins have substance-specificity (Forst et al., 1998; Schirmer et al., 1995). Porins are highly expressed with 10^4 –10^6 copies per cell. The expression level can be adjusted in response to different stimuli, thus modulating the degree of the PM permeability (Fernandez and Hancock, 2012; Koebnik et al., 2000). As membrane channel proteins, the predominant activity of porins is to build large pores, which enable rapid diffusion of hydrophilic molecules. In addition, porins are also involved in many physiological processes, including antibiotic resistance, pathogenesis effectors, immunity system elements, and others (Achouak et al., 2001).

Pumps (also named ion pumps or ion transporters), are transmembrane integral proteins which transport ions or small molecules through the PM against their electrochemical or concentration gradients. Contrary to ion channels for which only selective ions pass through rapidly, transport by pumps is a process of thermodynamics increase, which obey the electrochemical or concentration gradients by expending energy released from ATP hydrolysis (Gadsby, 2009). ATP-powered pumps are classified into four types: The P, F, V class and ATP-binding cassette (ABC) superfamily. The P, F and V classes are responsible for ions transport while the ABC superfamily are responsible for both ions and small molecules movement. Taking the P-group as a typical case, these pumps are tetrameric proteins, typically composed of 2 α-subunits and 2 β-subunits normally (Lodish et al., 2000). The ATP-binding site is located on the α-subunits. To transport specific ions, one pump transporter has at least one α-subunit, which can be phosphorylated in the transport process. Unlike the P-group pumps, the F and V group pumps are mainly responsible for maintaining cellular H^+ concentration, and have more complex structures that labour at least 3 different types of transmembrane proteins and 5 polypeptides. The ABC superfamily pumps have at least 100 members. Each pump can specifically transport a single substance or one kind of related substances, such as ions, sugars, peptides and occasionally proteins. All pumps in this family have the universal configuration that is composed of 2 transmembrane domains and 2 ATP-binding sites (Lodish et al., 2000).

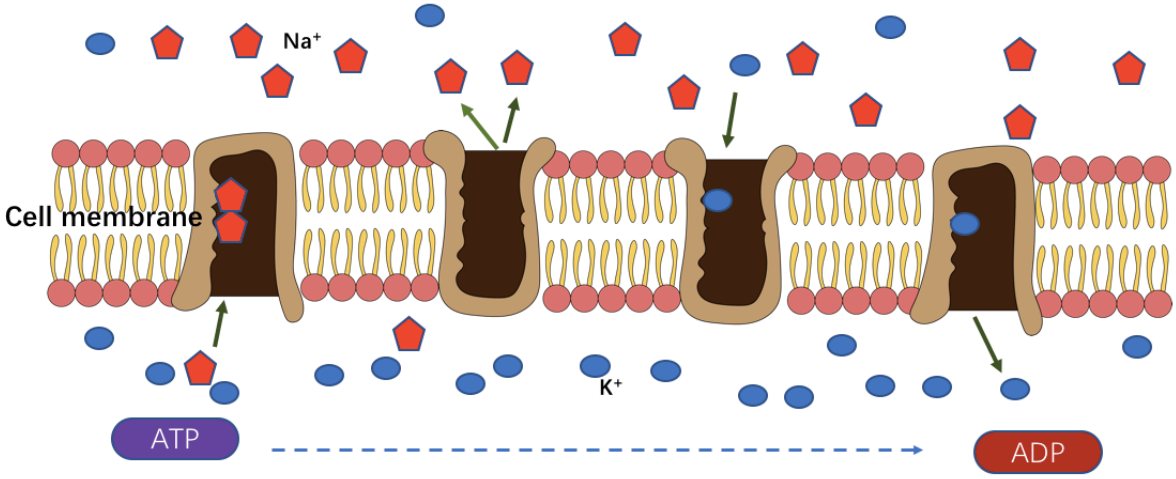

Figure 3: The scheme of sodium–potassium pump. Na^+ / K^+ - ATPase exports two K^+ and import three Na^+ by consuming one ATP molecule. One single positive charge is exported in each pump circle (https://openstax.org/books/biology-2e/pages/5-3-active-transport).

1.2 Membrane pore-forming proteins

Membrane pore-forming proteins (PFPs), are proteins that can make pores on the PM of target cells. By making pores, the PFPs destroy the boundary of cells, alter the permeability of the PM, eliminate the difference between intra- and extra-cellular environments to perform their specific functions. The PFPs are widely spread in many organisms from bacteria to human, and function as weapons to permeate the PM of target cells (Bischofberger et al., 2009; Parker and Feil, 2005).

1.2.1 Perforin (Perforin-1)

Perforins are PFPs which come from mainly nature killer (NK) cells and $CD8^+$ T cells. They play a significant role in the innate immune system by making pores on target cells to result cell death. The single molecule of perforin is around 70 kDa and composed of several hundred of amino acids that form 4 domains (Osinska et al., 2014). Among them, one domain possesses a special hydrophobic region of two β-sheets and one α-helix, which later merge into the lipid bilayer to exert their permeabilizing function.

There is a Ca^{2+} binding site at the N-terminal region of each perforin molecule, which plays an important role in the membrane permeabilization process (Law et al., 2010; Lasek and Malejczyk, 2007). Perforin can be activated by the binding of Ca^{2+} to make pores on a target membrane (Law et al., 2010; Osinska et al., 2014). Some proteins in cells can adjust the activation of perforins. For example, calreticulin in cytolytic granules play a role on protecting perforins from activation by pre-emptively binding with Ca^{2+}, and inhibiting the oligomerization of perforin molecules (Andrin et al., 1998); Phospholipids, the major target of perforin, can increase the binding efficiency of perforin to the PM by combining with Ca^{2+} (Lasek and Malejczyk, 2007).

Perforins are released from granules of NK cells and T cells to recognize target cell specifically ($CD8^+$ T cells) or non-specifically (NK cells) before binding to the PM (Osinska et al., 2014). Following the polymerization, perforins form a cylindrical pore with diameter of 5 – 20 nm across the lipid bilayer (Liu et al., 1996). The pore-formation on the PM destroys membrane boundary and allows the movement of ions, molecules, water and even proteins by passive transport, which leads to the activation of apoptosis and eventually cell death (Liu et al., 1996). This is the basic mechanism used by NK cells and T cells to perform cytotoxic effects in the immune system. However, the unusual binding of perforins with the PM can result in resistance against the cytotoxic activation of NK cells and T cells, engendering many evading mechanisms of target cells against perforins (Lehmann et al., 2000).

1.2.2 Complement

Complement denotes a set of proteins which, besides fulfilling other functions, can lead to formation of a pore complex, the membrane attack complex (MAC) of the immune system (Young et al., 1986). As one of the most important effector proteins of the immune system, MAC targets pathogenic bacteria to make pores in their membrane by orderly activation of many complements: C3b, C5b, C6, C7, C8 and C9. Activated complement components form a complex and insert into target membrane to build a central, water-filled pore by polymerised protein C9 (Schreiber et al., 1979). The MAC formation starts from C3b, which is also the target for C9 polymerization. After the orderly activation of C5, C6, C7 and C8, the C9 polymerization is triggered. By refolding,

C9 form a loop with one side being a hydrophobic region and the other side is hydrophilic domain. The loop inserts into the target membrane by hydrophobic force and leaves the hydrophilic domain to compose a water-filled pore together with other C9 hydrophilic domains. The process of C9 monomer insertion is a completely physical action without any enzyme involved and no specific binding receptor for C9 complex (McCormack et al., 2013a).

1.2.3 Gasdermin D and Mixed Lineage Kinase Domain Like Pseudokinase

Recent studies reported two novel types of intracellular channel forming proteins, which were involved in programmed cell death: gasdermin D (GSDMD) and mixed lineage kinase domain like pseudokinase (MLKL) (Kovacs and Miao, 2017; Petrie et al., 2019; Wang et al., 2014). GSDMD belongs to human gasdermin family among GSDMA, GSDMB, GSDMC, GSDME, and NFNB59 (Shi et al., 2015). Gasdermin family members are mostly expressed in epithelial cells and play important role in cell proliferation and differentiation. Most members of the gasdermin family show pore-forming ability and share one similar molecular structure, which consists of one pore forming domain at the N-terminal and one repressor domain at the C-terminal, yet the linkers between N and C domains are different (Kovacs and Miao, 2017; Shi et al., 2015). GSDMD is currently recognized as the effector of pyroptosis, a type of lytic programmed cellular death (Kayagaki et al., 2015; Shi et al., 2015).

Pathogens sometimes attack cells or tissues without alarming the immune system, which can become a serious threat to the host. The most effective solution is to kill the infected cells by programmed cell death. Pyroptosis is one such cell death mechanism. The GSDMD molecule in humans was reported to be composed of an amino-terminal domain (N-domain) and a carboxy-terminal domain (C-domain) connected by a linker (Ding et al., 2016; Liu et al., 2016). The N-terminus forms an oligomeric pore on the cytosolic side of the cellular membrane after activation. In the pore formation process, the linker is cleaved by caspase-1/11, thus releasing the N-domain from the C-domain to merge into the PM and oligomerize into a GSDMD pore with a diameter of 10–15 nm (Aglietti et al., 2016; Ding et al., 2016; Liu et al., 2016). The MLKL protein functions

as the effector of another programmed cell death mechanism induced by the tumor necrosis factor (TNF), necroptosis, thus leading to membrane disruption by forming inner pores. Normally, TNF-α activates receptor-interacting kinase-1 (RIPK1) and RIPK3 to trigger necroptosis. Activated RIPK3 can recruit and phosphorylate MLKL. The phosphorylated N-terminals of MLKL protein translocate to the plasma membrane and oligomerize to form a cation selective inner channel (Fig. 4 and 5) (Zhang et al., 2018).

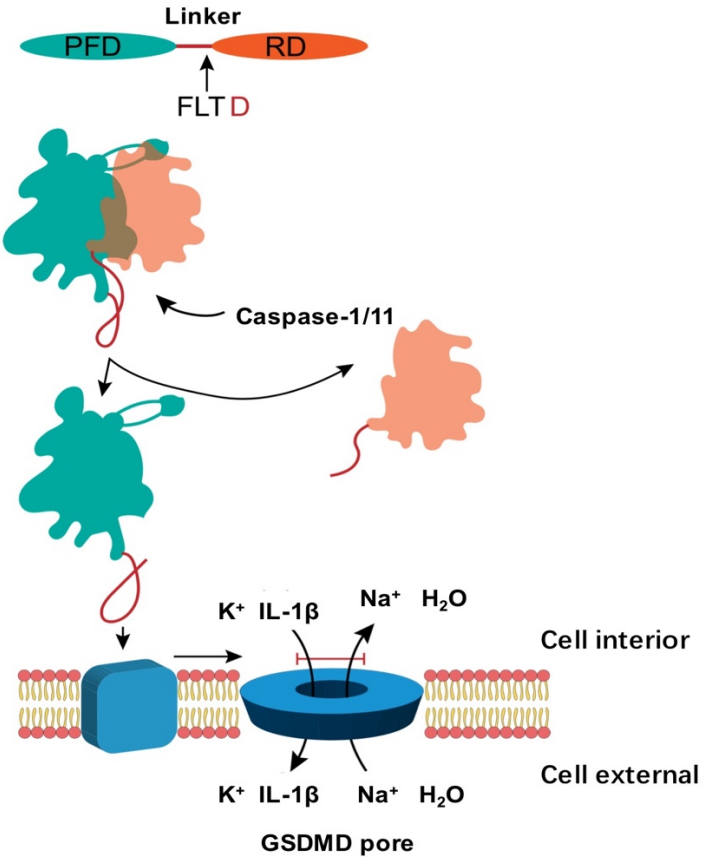

Figure 4: The schematic diagram of GSDMD pore forming. The linker is cleaved by caspase-1/11, thus releasing the N-domain from the C-domain to merger into the PM and oligomerize into a GSDMD pore with a diameter of 10-15 nm, which is big enough to pass small molecules. Picture was adapted from Trends in Cell Biology with copyright license number: 4721281171451 (Kovacs and Miao, 2017).

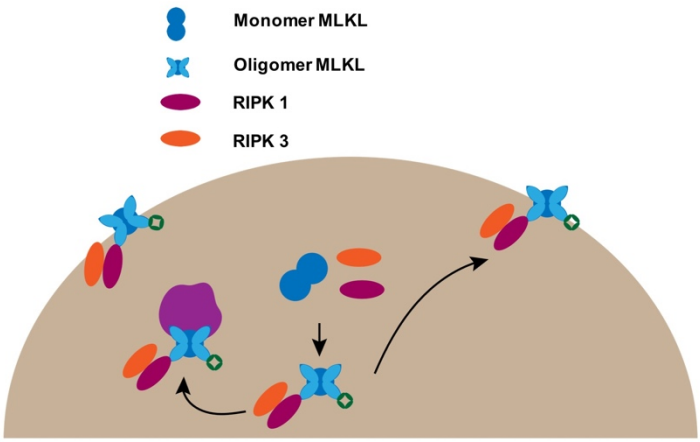

Figure 5: The schematic diagram of MLKL pore forming. Monomer MLKL is triggered by RIPK 1 and 3. Activated and phosphorylate MLKL proteins translocate to the plasma membrane and oligomerize to form a cation selective inner channel (Wang et al., 2014).

1.3 Pore forming toxins

Living organisms, such as insects, poisonous reptiles, plants, fungi and bacteria, can produce pore-forming toxins that destroy target cell membranes. These organisms employ toxins to make lesions or pores on the PM thus enhancing their attack ability. Bacterial pore-forming toxins (PFTs), the largest family of PFPs, account for a large percentage of bacterial toxins (Iacovache et al., 2008). PFTs are widely distributed and support pathogenicity. Unlike natural channels through the PM, the pores formed by PFTs are not selective for particular substances and do not usually respond to any ligands or voltage. Because of its unregulated and often non-selectivity characteristics, PFTs-pore channels cause severe disruptions to the intracellular environment.

In the bacterial infection process, PFTs are initially secreted as water soluble molecules and recognised by binding specific receptors. By binding particular receptors, water soluble monomers of PFTs assemble to increase their concentration on the target membrane and facilitate oligomerization. This is an indispensable step for the membrane insertion of all PFTs (Dal Peraro and Van Der Goot, 2016a). The insertion of PFT oligomers into their targets dependents on the hydrophobic surfaces formed in the oligomerization process.

PFTs can be classified according to several criteria. For example, according to their pore size, the way they bind to target cell membrane, and their particular properties. According to the study of secondary structure of pore channels, PFTs are generally classified into two main families: α-helical toxins and β-barrel toxins, based on their membrane spanning-domains are made up by α-helices or β-barrels (Gilbert, 2002). Other (sub)-families are distinguished by particular properties, such as cholesterol-dependent cytolysins (CDCs), because cholesterol plays an indispensable role for the function of CDCs.

α-helical PFTs have hydrophobic stretches in their primary sequence, which become helical in the subsequent dimensional changes to compose membrane-spanning elements. In contrast, β-barrel PFTs do not contain these kinds of hydrophobic stretches, but have only amphipathic β-filaments, which can combine to form multi-protein structures with a hydrophobic exterior that enable permeability. The β-barrel PFTs are further classified as big β-PFTs or small β-PFTs based on their pore channel diameter. Usually β-PFTs that form pore channel diameters < 3 nm are classified as small β-PFTs which allows only ions, water and other small molecules to pass through; while large β-PFTs form much larger channels. Whereas α-toxin (a small β-PFT) forms pore channel with an inner diameter of 2–3 nm, CDCs can form pores of 20–30 nm (Gonzalez et al., 2008). A number of PFT high resolution structures have been solved.

1.3.1 α-helical bacterial PFTs

1.3.1.1 The colicin family

Colicins are multi-peptides produced by *Escherichia coli* (*E. coli*), and able to make poses on the PM. By making pores on membranes, colicins function as weapons of *E. coli* to destroy cells thus seizing competitive advantageous living environments (Dal Peraro and Van Der Goot, 2016a). Interestingly, colicins are used to kill bacteria from the same specie. In order to protect themselves from colicins, the host bacteria secret immunity proteins to against the pore-forming function of colicins at the same time (Iacovache et al., 2008). Colicins play important role in stabilizing the microbial

biodiversities (Cascales et al., 2007), owing to their narrow target spectrum of the same bacteria species.

Colicins are secreted as water soluble molecules and synthesized in cytoplasm before released to cell external, where they occasionally or intentionally meet the target cells. Receptors are the important starting point of colicin membrane-translocation. Once bind to specific receptors, colicins undergo dimensional change (from 3D to 2D) to make preparation for translocation to the target PM (Parker and Feil, 2005). Three important steps are required by colicins to make pores on the target PM: bind to the receptors, change dimensional conformation and insert into the lipid bilayer. The structure of colicin molecule has been resolved and revealed a multi-domain protein (Cascales et al., 2007). According to these three pore-forming steps, the structure of colicins can be divided as binding-domain, translocation-domain and pore-forming domain.

Different colicins have different structures of binding and translocation domains. However, all pore-forming colicins share a similar channel-forming domain, named “Umbrella”. This is a spherical domain with a hydrophobic α-helical hairpin hiding inside of several amphipathic α-helices. When bind to specific receptors, the pore-forming domains go through the dimensional morph and change from a water-soluble conformation to a steady structure that insert into the lipid bilayer. The formation of colicin pore leads to ATP loss, ions fluxes and finally to cell death. Before, it was believed before that the amphipathic helices detach from the hydrophobic hairpin and insert during pore-forming. However, recent research indicate that pore formation by colicin is not only dependent on this specific hydrophobic hairpin structure, but also relies on other mechanisms, such as multimerization and low pH volume level at the membranes interface (Cascales et al., 2007). As a convincing model of colicin pore structure is lacking, the arrangement of the helices and the mechanism of the pore forming is still under known. More recent research showed that colicins not only work as pore forming proteins, but also act as DNAse or RNAse and travel to periplasmic compartment that disturb cell translation, transcription and block protein synthesis (Cascales et al., 2007; Lakey and Slatin, 2001).

1.3.1.2 Actinoporins

Sea anemone secrete many toxins to disable and digest their preys. Actinoporins are one of the most effective PFTs secreted by sea anemone, and act as a potent weapon against their predators. The most significant property of actinoporins is lipid-dependent binding, especially towards the target membrane that are affluent in sphingomyelin and phase-separated lipids. Equinatoxin II, produced by *Actinia equine*, and sticholysin II, secreted by *Sticholdactyla helianthus*, are two of the most well studied actinoporins. Sticholysin II monomer molecules contain a β-sandwich which is composed of many β-stands and flanked on both sides by two α-helices. An amphipathic helix is located in the N-terminal region, while the second α-helix at the other side of the β-sandwich has some aromatic residues. When merging into the target membrane, the N-terminal region moves away from the β-sandwich core and plugs into the lipid bilayer. All actinoporins share the same β-sandwich and α-helices wing structure (Barlic et al., 2004; Dal Peraro and van der Goot, 2016a).

According to structure and function studies of actinoporins, the pore forming process can be simply divided in three stages. Firstly, the actinoporins attach to the target membrane by identifying the specific lipid; secondly, the N-terminals of actinoporins move away from the β-sandwich and translocate to the connector between the water and the lipid; thirdly, the N-terminal segments undergo oligomerization and form a transmembrane structure. No pre-pore structure appeared in the formation of the whole architecture. Although actinoporins must oligomerize into multimers to establish a transmembrane pore, details about the pore forming process remain unclear and will require further research (Kristan et al., 2009; Rojko et al., 2016).

1.3.2 β-barrel PFTs

1.3.2.1 Cholesterol-Dependent Cytolysins (CDCs)

CDCs comprise more than 20 members. They are mainly produced by Gram-positive bacteria, such as *Clostridium, Bacillus, Streptococcus, Listeria* and *Arcanobacterium*. Some Gram-negative bacteria can also produce CDCs. As the name indicated,

cholesterol is an essential factor for carrying out the function of CDCs. CDCs were thought to take cholesterol as binding receptors, which is true in the context of Perfringolysin (PFO) (Savinov and Heuck, 2017). However, later studies uncovered the exceptions such as intermedilysin, which can choose different receptors including CD59 (Christie et al., 2018; Wickham et al., 2011). Cholesterols have also other functions besides acting as the binding receptor. However, the mechanisms of cholesterol in step-transition, oligomerization or insertion is varied among different CDCs. In addition to the notable feature of cholesterol-dependence, CDCs have another distinguishable characteristic, the big pore. Pore channels of CDCs are between 25–30 nm wide in diameter and composed of 20–50 subunits, with approximately 200 β-strands. More than 20 members of CDCs have been identified so far. These CDCs have a high degree of resemblance in sequence of about 40 - 80%, and have similar toxin activity and structure (Shatursky et al., 1999; Tweten, 2005).

Other than the water-soluble single molecules, the CDC pore configuration is still less known. Perfringolysin (PFO), an archetypical and well-characterized toxin in the CDC family, is an elongated, rod-shaped, multi domain hydrophilic protein that is full of β-sheets without any exterior facing hydrophobic residues. Usually the single molecule of PFO can be easily divided into 4 parts. Domain 1, 2 and 4 are arranged sequentially in the long part, while domain 3 is one globular segment located in the core of the molecule closed to domain 2 (Rossjohn et al., 1997; Shatursky et al., 1999; Solovyova et al., 2004). The whole molecule is rich in β-sheets, while domain 3 has several short α-helices undecapeptides, ECTGLAWEWWR, and 3 short hydrophobic loops which are involved in the binding step (Johnson and Heuck, 2014).

The pore-forming mechanism of PFO start by the binding of monomers to cholesterol receptors. After insertion of the several loops in domain 3, the oligomerization starts. Following the oligomerization of 40–50 monomers to a pre-pore conformation, domain 1, 2 and 4 concert the corresponding parts to form a barrel-shaped configuration, thus moving the hydrophobic β-hairpin (TMH1 and TMH2) close to the target membrane (Kacprzyk-Stokowiec et al., 2014). Each monomer contributes two hydrophobic β-hairpins to the final transmembrane β-barrel, which is a distinctive feature of CDCs other than the other PFT families. In water-soluble molecule, two β-hairpins

interestingly form a β-sandwich model flanked by several short α-helices. This β-sandwich model needs to be transformed from α-helices to β-sheets that is competent in membrane insertion. The β-hairpins cannot insert individually but need cooperation with neighbouring monomers to trigger the insertion together, displaying an all-or-nothing image (Solovyova et al., 2004).

After insertion of the large β-barrel, a mature pore is established at the PM. The pore channel is big enough for the macromolecule to pass. The oligomerization takes place by sequential addition of monomers or oligomers, but sometimes the CDCs form a partial pore rather than a complete one. Although the partial pore is not mature, it is still active to perform toxic activities. Structure data revealed that CDCs possess common membrane attack complex component / perforin (MACPF) domains like mammalian immune cells have. Mammalian immune cells use this complex domain to kill pathogens and infected cells. This pore forming mechanism is not unique for CDCs, but also utilized by the other organisms (Kondos et al., 2010).

1.3.2.2 The "Haemolysin Family"

a. Staphylococcus *aureus* α-hemolysin

Staphylococcus aureus α-hemolysin (α-toxin or HIa) is one of the best-understood toxin of the small β-PFT class (Bhakdi et al., 1991; Bhakdi and Tranum-Jensen, 1991). α-toxin molecules are secreted as approximately 32 kDa monomers, which bind to the target membrane and oligomerize into a heptameric pre-pore structure. The structural analysis revealed a mushroom-like architecture composed of 7 subunits (protomers) and comprises 14 -anti-parallel strands (Song et al., 1996).

To this end, the stem (the green loop in Figure 6) of each toxin molecule rearranges and inserts into the lipid bilayer (Fiaschi et al., 2016). The channel looks like a ring-castle structure with an outsider diameter of about 10 nm and an inner diameter of 2–3 nm (Arbuthnott et al., 1967; Fussle et al., 1981).

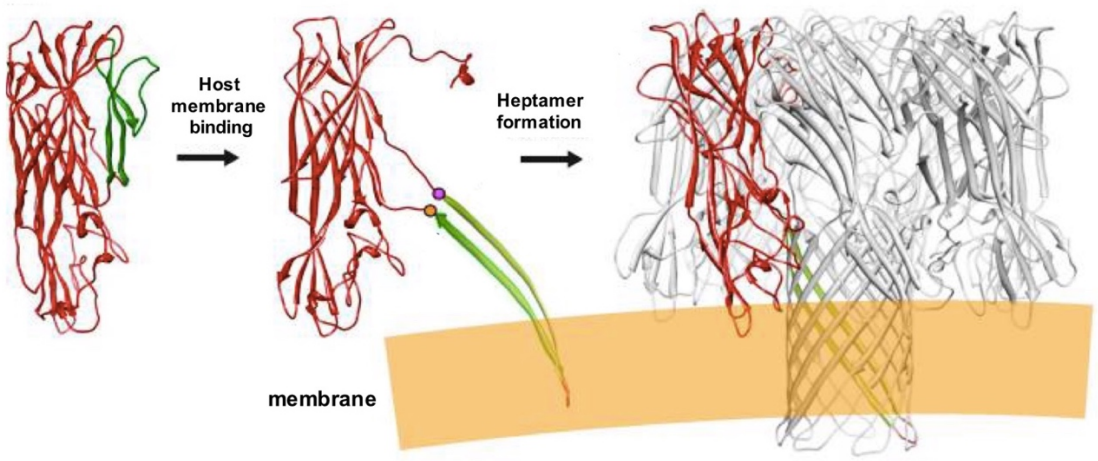

Figure 6: The schematic diagram of α-toxin pore forming process. α-toxin molecules bind to the target membrane before oligomerization into a heptameric pre-pore structure. After that, the stem of each molecule rearranges and inserts into lipid bilayer thus forming a mature toxin pore (Fiaschi et al., 2016).

The exact mechanism by which α-toxin interacts with the target membrane is an unresolved topic in this field. Many studies have revealed that α-toxin is potent at binding membrane lipids, interacting with the target membrane in a specific manner and interfacing with receptors (Berube and Bubeck Wardenburg, 2013). Notably, α-toxin has higher binding efficiency and affinity to rabbit red blood cells than to other cells (Hildebrand et al., 1991). Although, the PM of most animals seems to have an intrinsic ability to bind α-toxin, the high efficiency and affinity is sensitive to proteases, which may indicate some contributions of membrane proteins. Several membrane proteins have been discussed as binding partners of α-toxin, such as β1-integrin and caveolin-1 (Liang and Ji, 2006; Srivastava et al., 2009). However, caveolin-1 seems to play a dispensable role in α-toxin pore formation activity, due to the observation that some cells types free of caveolin-1 are highly sensitive to α-toxin (Husmann et al., 2009).

A disintegrin and metalloprotease 10 (ADAM10) has been revealed to act as a receptor of α-toxin (Wilke and Bubeck Wardenburg, 2010); it has been reported that ADAM10 improves binding efficiency of α-toxin (Wilke and Bubeck Wardenburg, 2010). Moreover, besides its role as a binding receptor, ADAM10 may also exert downstream biological effects (Becker et al., 2014; Hernandez et al., 2019; Inoshima et al., 2011; Inoshima et al., 2012; Powers et al., 2015; Powers et al., 2012). Actually, it has been

proposed that the activation of ADAM10 by α-toxin supports the idea that ADAM10 is the receptor for this toxin. However, supra-cytotoxic doses of α-toxin are required to trigger the activation of ADAM10-dependent cleavage of E-cadherin suggesting that activation of ADAM10 is a consequence of membrane damage, not a direct consequence of toxin-binding (von Hoven et al., 2016). In fact, high doses of α-toxin are also required to trigger significant Ca^{2+} influx (Walev et al., 1993; Walev et al., 1994). Although it has been proposed that Ca^{2+} influx occurs through the α-toxin pore, see (Reboud et al., 2017) and references therein, this issue is still debated (von Hoven et al., 2016), and the apparent existence of two different pore sizes, depending on toxin-concentrations has remained puzzling.

b. *Vibrio cholerae* cytolysin (VCC)

The *Vibrio cholera* belong to Gram-negative bacteria and usually lead to the serious diarrhoeal disease, cholera (Usmani et al., 2012). They produce many kinds of toxins to contribute their pathogenesis process. Some strains of VC secret *Vibrio cholerae* cytolysin (VCC). The VCC toxin is a member of the accessory toxins that makes tiny pores on target membranes to assistant the attack of VC bacteria. VCC is secreted in pro-architecture molecules called pro-VCC, which are approximately 72 kDa and have a pro-domain at the N-terminal (Nagamune et al., 1996). With the abundance of pro-domains by proteolytic reaction, mature VCC toxins are generated. A mature VCC molecule usually has three main different domains, the central cytolysin domain, the β-trefoil domain, and the β-prism I domain (Olson and Gouaux, 2005). The central cytolysin domain is the main insertion part which shares structural homology with other small β-PFTs. The other β-domains mainly contribute to the binding step (Kathuria and Chattopadhyay, 2018).

The transmembrane pore induced by VCC is a heptameric β-barrel architecture with diameter of 1–2 nm wide (De and Olson, 2011; Yuldasheva et al., 2001). These seven anti-parallel β-strand pairs come from seven water-soluble monomers of VCC. During the approach to the target membrane, the water-soluble molecule of VCC firstly binds to the target membrane and becomes a membrane-binding monomer. After that, seven membrane-binding monomers transform and convert into an intermediate assembly,

the pre-pore. In water-soluble VCC molecules, the β-strand pairs are kept packed and hidden in each monomer, called “pre-stem”. Following the formation of pre-pore oligomers on the target membrane, these pre-stem domains open up and reorganize before inserting into the lipid bilayer to form a functional channel-VCC pore (Kathuria and Chattopadhyay, 2018; Paul and Chattopadhyay, 2014; Rai and Chattopadhyay, 2015a, b).

The exact mechanism of how VCC interact with the target membrane remains unclear. Studies have shown that VCC can make pores both in biomembranes and the lipid bilayers of liposomes (Zitzer et al., 1997). It seems like no specific proteinaceous receptors are strictly required for VCC binding and pore formation. However, experimental results have shown that VCC binding and pore formation happened much more efficiently on biomembrane than on the lipid bilayers of liposomes (Zitzer et al., 1999). This indicates that there may be assisting interactions on biomembranes to promote effective pore formation. Recently, more evidences have revealed that multiple pathways are involved in the binding and pore formation process of VCC on biomembranes, however even these are not enough to explain the observed differences (Kathuria and Chattopadhyay, 2018).

Water-soluble VCC molecules have a special association property with amphipathic lipid bilayers, while they have non-specific associations with hydrophilic or hydrophobic bilayers. It is conceivable that the amphipathic property will drive VCC monomers to the lipid bilayers (Zitzer et al., 1997). VCC can both make pores on biomembranes and the lipid bilayers of liposomes, suggesting that only lipids are enough to trigger the VCC binding and pore formation process. However, the efficiency changes largely with different lipid bilayers of liposomes (Zitzer et al., 2000). It has been shown that phospholipids play a main role in the binding and pore formation event of VCC (Olson et al., 1999; Rai and Chattopadhyay, 2015a, b). Cholesterols and sphingolipids usually constitute the lipid rafts where GPI-receptor normally anchored. GPI-proteins are mostly the receptors of many β-PFTs such as aerolysin family. However, the interaction of VCC with cholesterols and sphingolipids needs further investigations (Brown and London, 2000; Fivaz et al., 2002). No receptor was proved to be specific to VCC while recent studies have shown that TLR2/TLR6 complexes

could be the potential VCC receptor in monocytes and macrophages (Khilwani et al., 2015).

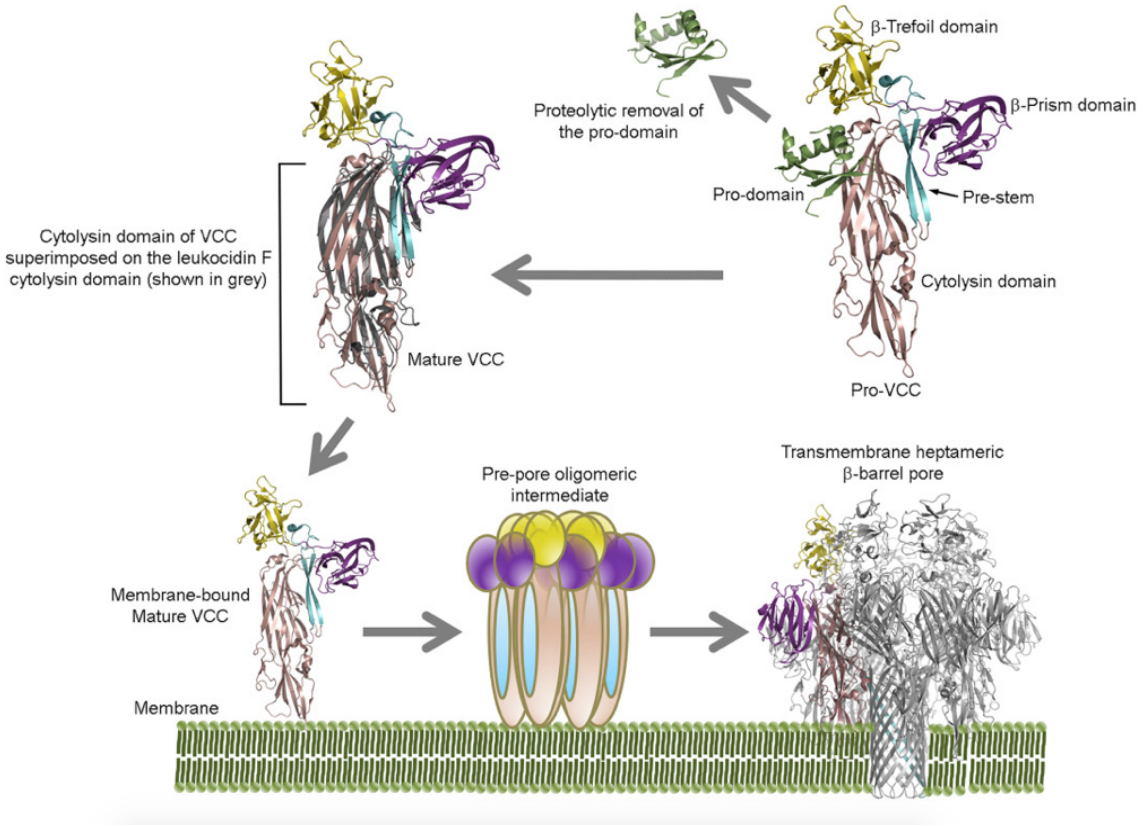

Figure 7: The schematic diagram of VCC molecule structure and pore forming process. VCC is secreted as pro-VCC, of approximately 72 kDa. It has a pro-domain at the N-terminal. Proteolytic cleavage generates mature VCC. During the approach to the target membrane, the water-soluble molecules of VCC bind to the target membrane and become a membrane-bound monomer. Subsequently, membrane-binding monomers transform to an intermediate heptamer, the pre-pore. Finally, pre-stem domains reorganize and insert into the lipid bilayer to form a functional channel-VCC pore (Kathuria and Chattopadhyay, 2018).

1.3.2.3 Phobalysin P (PhlyP) – a new small β-PFT

Photobacterium damselae subsp. *damselae* is a pathogen of marine animals, which can also cause wound infections in humans, leading to necrotizing fasciitis and even sepsis. Our group has characterized that Phobalysin P (PhlyP), acronym of "photobacterial lysin encoded on a plasmid", a bacterial small β-PFT, which is a virulence factor of *Photobacterium damselae* subsp. *damselae* (Rivas et al., 2013; Rivas et al., 2015).

Based on the amino acid sequences, we predicted that PhlyP is related to VCC. Studies in our group proved this idea by functional analyses (osmoprotection, morphological observation of pores under electron microscopes and biomechanical properties by demonstrating SDS-stable complexes (Rivas et al., 2015)). Even though PhlyP has many common characteristics with other common small β-PFTs, there are also some differences between them. We compared VCC with PhlyP, to identify functional differences.

Both the PhlyP and VCC toxin monomers have a pro-domain (P), analogous proteolytic activation sites (PAS), a cytolysin domain (C) and a β-trefoil lectin domain (L-βT). However, only VCC has a β-prism lectin domain at the C-terminus which makes the whole VCC monomer has more amino acid residues than PhlyP (Fig. 8a). The I-TASSER server was used to predict the structure of PhlyP. The similarity-score at the channel-forming region is up to 0.99, however the score of the entire monomer is lower because of the β-prism lectin domain in VCC (Fig. 8b). Taking the known spatial structure of VCC as a template to build a model of the PhlyP channel using MODELLER, indicated that PhlyP has a smaller amino acid residue serine (S) at the narrow channel point instead of tryptophan (W) in the corresponding position of VCC. This would make channel of PhlyP a little wider than of VCC. Moreover, there are fewer charged amino acids in the pore-forming region of PhlyP than in VCC (Fig. 8c and d) (von Hoven et al., 2017). In order to get recombinant Pro-PhlyP, the gene encoding pro-PhlyP was amplified by PCR. Products were purified and cloned into pTrcHisA before transforming Shuffle Express competent *E. coli* cells. Ni-NTA agarose was used to affinity purify His-target pro-toxin from *E. coli* cell lysates. Using anti-His6 antibody, Western blot was employed to estimate the concentration of pro-PhlyP taking His6-tagged pro-VCC as a standard (Fig. 8e) (Rivas et al., 2015). Alignment at the amino acid sequences level of pro-PhlyP and pro-VCC shows 50% homological identity (Fig. 9). Notably, the predicted pore channel formed by VCC is slightly narrower than the PhlyP pore size, as the narrow point of the VCC pore is composed of a heptad of tryptophan residues-W318, while the same position in PhlyP is a slimmer serine -S341 (De and Olson, 2011; Rivas et al., 2015).

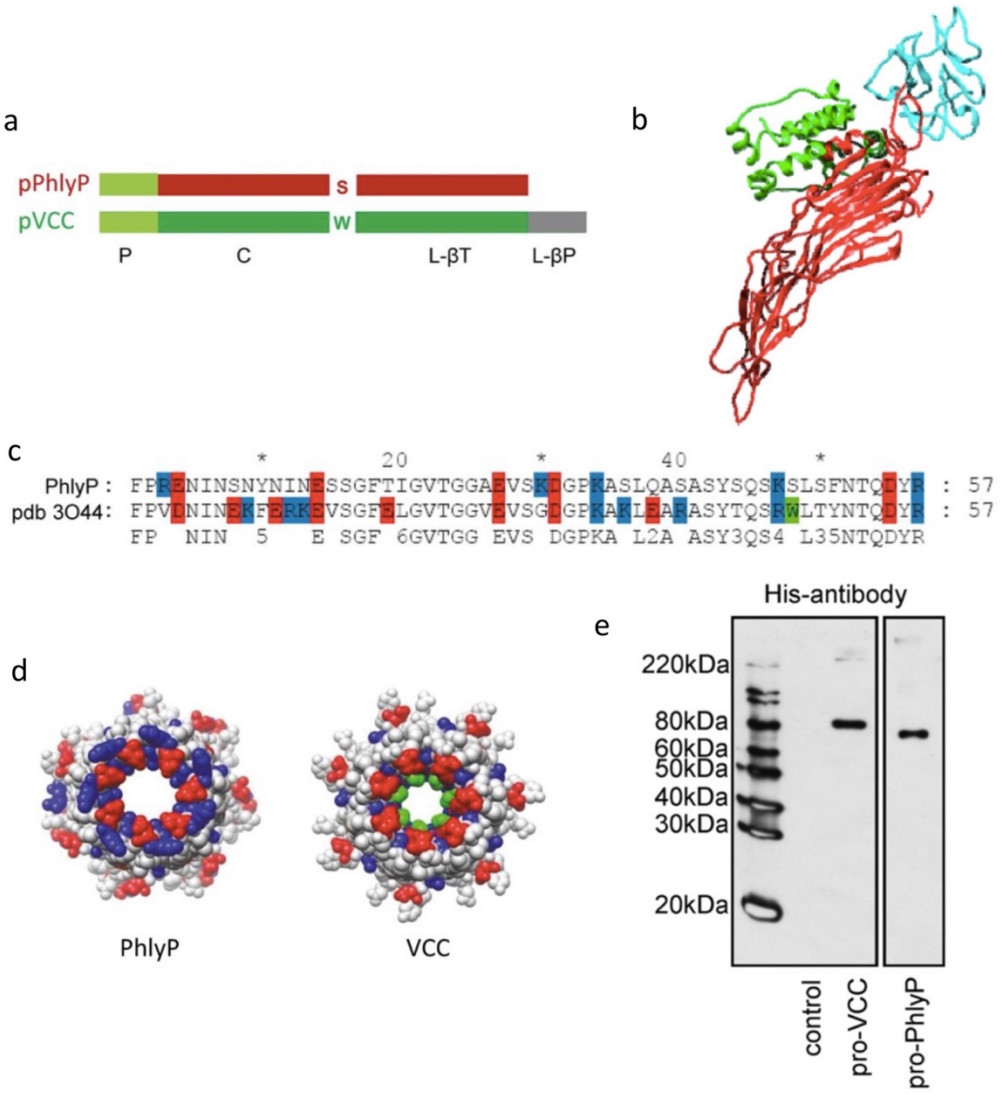

Figure 8: The predicted secondary structure of PhlyP. a, Both the PhlyP and VCC toxin monomers have a pro-domain (P), analogous proteolytic activation sites (PAS), a cytolysin domain (C) and a β-trefoil lectin domain (L-βT). Only VCC has a β-prism lectin domain at the C-terminus. **b**, Secondary structure of PhlyP molecule according to the similarity comparison by I-TASSER. **c** and **d**, Space fill representation of heptameric pore complexes of PhlyP and VCC shown from cytosolic side. Note heptad of tryptophan (green) narrowing the lumen of the VCC pore. **e**, Purified N-terminally His6-tagged pro-VCC and pro-PhlyP were analysed by western blotting with anti-His antibodies (Rivas et al., 2015; von Hoven et al., 2017).

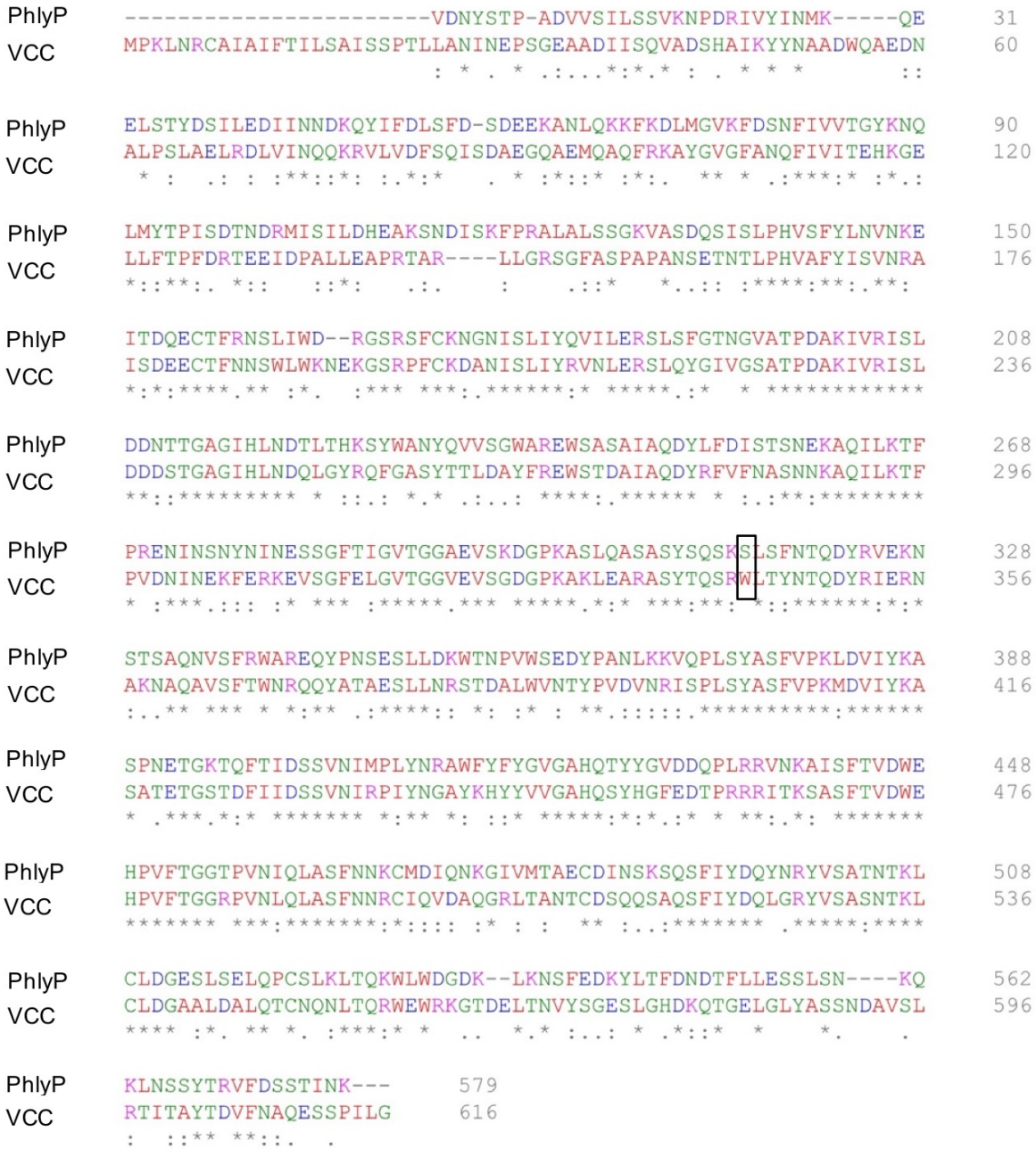

Figure 9: Comparison between protein sequence of PhlyP and VCC toxin. Alignment at the amino acid sequences level of pro-PhlyP and pro-VCC shows up to 50% homological identity. The box in black denotes the residue forming the channel narrow point of VCC pores (W), and the presumably corresponding residue in PhlyP (S).

1.4 Early consequences of PFT-attack

A consequence of pore formation by PFTs is membrane permeabilization and uncontrolled, sometimes long-lasting fluxes of water, ions and molecules through this non-gated toxin pore that disorders the substance balance between intra- and extracellular environments. Continued failure of ion homeostasis will ultimately change the cellular osmotic pressure and result in cell swelling, shrinking and rupture (Bischofberger et al., 2012; Kennedy et al., 2009). At high doses of PFTs, PFTs can cause cell death through rapid necrosis, programmed necrosis, apoptosis or pyroptosis. However, various biochemical pathways activated in host cells may minimize or repair injuries at low dosage of toxins, which can sometimes rescue target cells (Brito et al., 2019).

The exchanges of substances, especially the fluxes of Ca^{2+}, K^+ and ATP are the primary effects of PFT-induced membrane permeabilization. The fluxes between inner and outer sides of the PM and their final concentrations strongly influence the host cell response. Fluctuations of cellular ion concentrations are monitored by host cells to detect the volume changes and then trigger regulatory volume decrease or increase (Hoffmann et al., 2009). The activation of Na^+/K^+- ATPase triggered by the volume changes, which can exchange intracellular Na^+ and extracellular K^+ by ATP consumptions, has been identified in the host responses to α-toxin. On one hand, this consumption can aggravate the further loss of ATP by leakage through membrane damage and inoperable mitochondria (Baaske et al., 2016; Gierok et al., 2014; Walev et al., 1993). On the other hand, the decrease in the ATP / ADP ration caused by the loss and consumption of ATP activates AMP-activated kinase (AMPK) by phosphorylation. The activated AMPK functions as an energy sensor to trigger more downstream signal pathways that affect cellular metabolism, e.g. autophagy (Hardie et al., 2012; Kloft et al., 2010).

The egress of cytosolic ATP to the extracellular environment can trigger P2X receptors, which opens channels, allowing potassium efflux and calcium influx (Jiang et al., 2012; Locovei et al., 2007; Miller et al., 2011). This highlights the potential importance of secondary signalling pathways that decide the fates of the host cells.

The primary damages and responses after PFT attack depends on toxin concentrations, -species, and characteristics of pores (size, conductance). Besides the dramatic ATP loss, the attacks by PFTs can also lead to sustained Ca^{2+} influx and K^+ efflux in cells. However, Ca^{2+} influx shows different dynamics depending on the type of PFT. CDCs can form stable, non-selective pores that cause massive Ca^{2+} influx and K^+ efflux, while toxins from RTX family can only make temporary pores that allow either Ca^{2+} influx or K^+ efflux depending on different pore conformations (Fiser et al., 2012; Hotze and Tweten, 2012; Linhartova et al., 2010; Osickova et al., 2010). Hence, Ca^{2+} influx here induced by RTX causes ion fluctuations rather than continuous increase (Uhlen et al., 2000). Interestingly, some CDCs also trigger Ca^{2+} influx oscillations, which does not seem to correspond with their larger pore forming properties (Babiychuk et al., 2009; Gekara et al., 2007). It is worth addressing whether any intracellular calcium comes from intracellular Ca^{2+} store and if, in low concentration, any CDCs behave like RTXs to form transient pores rather than large stable ones.

Calcium influx plays extremely important roles in membrane repair. Upon CDC-induced membrane permeabilization, Ca^{2+} triggers the formation and release of blebs that contain damaged membranes with the help of annexin proteins. These proteins are activated by free Ca^{2+} and form an embolism to separate the blebs from the rest of healthy membranes. By releasing the blebs through this annexin-embolism mechanism, the pores made by CDC are removed (Babiychuk et al., 2011). Alternatively, the membrane damages induced by SLO result in the rise of intracellular Ca^{2+} concentration soon afterwards, which can trigger secretory lysosomal exocytosis. Lysosomes merge with plasma membranes to release acid sphingomyelinase(ASM). Sphingomyelins on the PM can be transformed by ASM to ceramides thus enabling the host membrane to swallow the region containing the SLO pore via caveolar endocytosis. Internalized SLO would be fed into the endosomal degradative pathway (Fig. 10) (Idone et al., 2008; Tam et al., 2010).

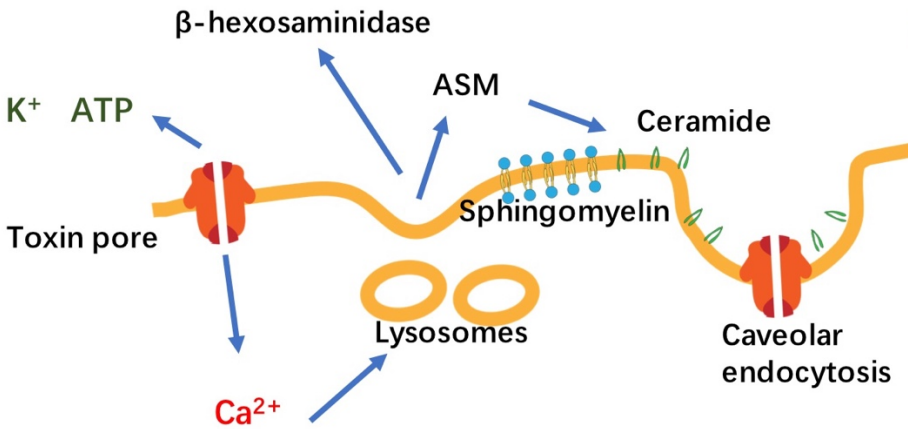

Figure 10: A schematic diagram of cellular repair induced by SLO pore forming. The pore-forming damages on the target membranes induced by SLO result in the rise of intracellular calcium concentration soon afterwards. This increase of cellular Ca^{2+} triggers a series of exocytosis and endocytosis activities. Many lysosomes containing acid sphingomyelinase (ASM) are generated after the activation of exocytosis and merge into healthy membrane to release the enzyme. Sphingomyelins on the PM can be cleaved by ASM and to yield ceramides thus enabling endocytosis of the localized region wrapping the toxin pore.

The calcium influx induced by PFTs not only plays roles in calcium-dependent repair, but also takes part in many other physiological activities in the host cells. In particularly, experiments demonstrated that calcium was an activator in protease signalling calpains (Bumba et al., 2010; Kennedy et al., 2009; Soong et al., 2012), thus inhibiting physiological functions of the mitochondria (Braun et al., 2007). Furthermore, *Bordetella* adenylate cyclase toxin transports adenylate cyclase (AC) enzyme into the target cells by pore forming thus regulate the signalling molecule cAMP. The extracellular calcium influx can activate the calpain proteins. With the association of cellular lipid rafts, talin proteins are cleaved in a calpain mediated way to promote pore forming, as the presence of talin can disturb the insertion process of the toxin (Bumba et al., 2010). However, calpastatin, the cellular endogenous inhibitor of calpain, is one of the indirect downstream targets of caspase-1. This reminds us the extreme complexity of signalling pathways responded to PFTs (Soong et al., 2012).

Some of the cellular signal pathways are activated to keep membranes intact or to reduce the destructive ability of PFTs, while some others are triggered to enhance their PFT toxicities incomprehensively. In particular, Akt/PKB protein kinase, a

serine/threonine kinase, is a critical protein group involved in many important physiological activities including cell metabolism, transcription and survival (Song et al., 2005). Aerolysin extracted from *Aeromonas*, *S. aureus* α-hemolysin from *Staphylococcus aureus*, and the HlyA from *E. coli* can perforate the target membranes and lead to free calcium influx thus inhibiting Akt (Wiles et al., 2008). The relevant research found that this inactivation of Akt happened through the failure of cellular phosphatases (Wiles et al., 2008). Moreover, studies revealed that the dephosphorylation induced by *listeria monocytogenes* in Histone H3 led to a decrease of cellular transcription activities (Hamon et al., 2007).

PM damage induced by PFTs such as SLO, LLO, VCC and *E. coli* haemolysin lead to massive decreases of intracellular potassium which triggers a “quiescence-like state” in cells characterized by transient block on translation initiation, autophagy, and the formation of lipid droplets (Gonzalez et al., 2011; Kloft et al., 2010). Also, Monalysin, secreted by *Pseudomonas entomophila*, results in protein synthesis arrest in gut (Chakrabarti et al., 2012; Opota et al., 2011). Translational control is a major contributor to the rewiring of gene expression observed in target cells of *S. aureus* α-toxin (Clamer et al., 2015), which may help the host cells to keep cellular metabolic stability. Autophagy recycles intracellular compounds as new building materials by catabolising cytosolic elements (Smets et al., 2010). It has been proposed to also contribute to the host cells’ survival by clearing up toxin pore structures (Gutierrez et al., 2007), but experimental evidence is lacking. Autophagy appears to help host cells to survive depending on the time required for recovery of membrane integrity. When the recovery process was quite slow, such as in the case of LLO, autophagy played a helpful role. However, when recovery was rapid, autophagy was not as beneficial as in slow-repair (Gonzalez et al., 2011). Lipid droplets in the “quiescence-like state” may serve as energy stores during attack by PFTs. Similar to the lipid droplets induced by starvation in yeast, all eukaryotic cells investigated possess some active devices to store lipid (Willison and Johnston, 1985). This formation of lipid droplets occurs even in the quiescence period, and is independent of the unfolded protein responses pathway (Schuler et al., 1996), but may depend on MAPK signalling ways (Gonzalez et al., 2011). Studies showed that the transient arrest in protein anabolism did not dependent on MAPK or caspase-1 pathways, nor were they related to UPR (Gonzalez et al., 2011; Ron and Walter, 2007). However, the protein synthesis arrest depends on the

phosphorylation of GCN2 kinase and its target, eukaryotic initiation factor alpha (eIF2α) (Kloft et al., 2010). The duration of protein synthesis arrest corresponds with the time required for cellular potassium recovery (Gonzalez et al., 2011).

PFTs activate the P38 MAPK signal pathway in all known cases (Bischofberger et al., 2012). However, besides the P38, the JNR and ERK are also activated by PFTs (Gonzalez et al., 2011; Kao et al., 2011). It has been proved that the MAPK signal pathway has definitely positive effects on cell survival when responding to PFTs (Huffman et al., 2004). Experiments with α-hemolysin showed that the P38 took part in the membrane recovery from damage and this was confirmed with aerolysin (Gonzalez et al., 2011; Husmann et al., 2006). Massive potassium efflux induced by PFTs can also trigger the activation of the nod-like receptor family pyrin domain-containing 3 (NLRP3). The NLRP3 inflammasomes participate in the activation of caspase-1, thus initiating the relevant cellular activities (Gurcel et al., 2006). Moreover, inflammatory cytokines caused by PFTs, such as interleukins 1β and 18, are liberated from pro--forms by caspase-1 to initiate inflammatory responses (Dunne et al., 2010). It has also been shown that the activation of caspase-1 not only induces inflammation, but also leads to pyroptosis in the host cells triggered by *S. aureus* (Soong et al., 2012). At the same time, *S. aureus* hemolysin and aerolysin can activate caspase-2 in epithelial cells (Imre et al., 2012), which promotes cell apoptosis in a strict potassium efflux dependent manner. Down-regulating the expression of caspase-2 can inhibit the cellular apoptosis in responses to PFTs (Imre et al., 2012).

Gene expression can be affected by PFTs. α-toxin at concentrations of 40–160 ng/ml functions on monocyte and epithelial cells and results in large release of IL-8, which happens through the activation of the NF-κb signal pathway (Dragneva et al., 2001). Gene expression is regulated by transcription factors and can be influenced by the modification of histone proteins in PFT attacked cells. Particularly, toxins from pathogenic *listeria monocytogenes* and other bacteria in the same family have been reported to lead to considerable dephosphorylation of Histone H3 and H4. This dephosphorylation of histone proteins affects gene expression and even influences some immunity gene translations (Hamon et al., 2007). PFTs can activate sterol regulatory element-binding proteins (SREBP) in a potassium-dependent way, which indirectly targets caspase-1 (Gurcel et al., 2006). The activation of SREBP can

increase the cellular survival responses from PFTs (Gurcel et al., 2006). Meanwhile, the decrease of SREBPs expression can lead to the host cell being more vulnerable to apoptosis (Im and Osborne, 2012). This ability of SREBPs to promote survival from PFTs has been proposed to be most likely due to the repair of damaged membranes (Gurcel et al., 2006). However, this assumption is in conflict with the observation that cellular recovery from α-toxin attack does not depend on transcription or translation (note that SREBP is a transcription factor) (Valeva et al., 2000; Kloft et al., 2012)

That aerolysin can trigger the activation of SREBPs and leads to the generation of lipid droplets indicates that the cell-autonomous defense against PFTs involves major changes in lipid metabolism (Gurcel et al., 2006; McCoy et al., 2010; Wiles and Mulvey, 2013). Additionally, loss of potassium leads to the arrest of global translation, activation of the MAPK pathway and histone H3 dephosphorylation (Bischofberger et al., 2012). Briefly, potassium efflux out of cytosol induced by PFTs is not only a consequence of pore formation, but also an important trigger for the cellular responses against PFTs.

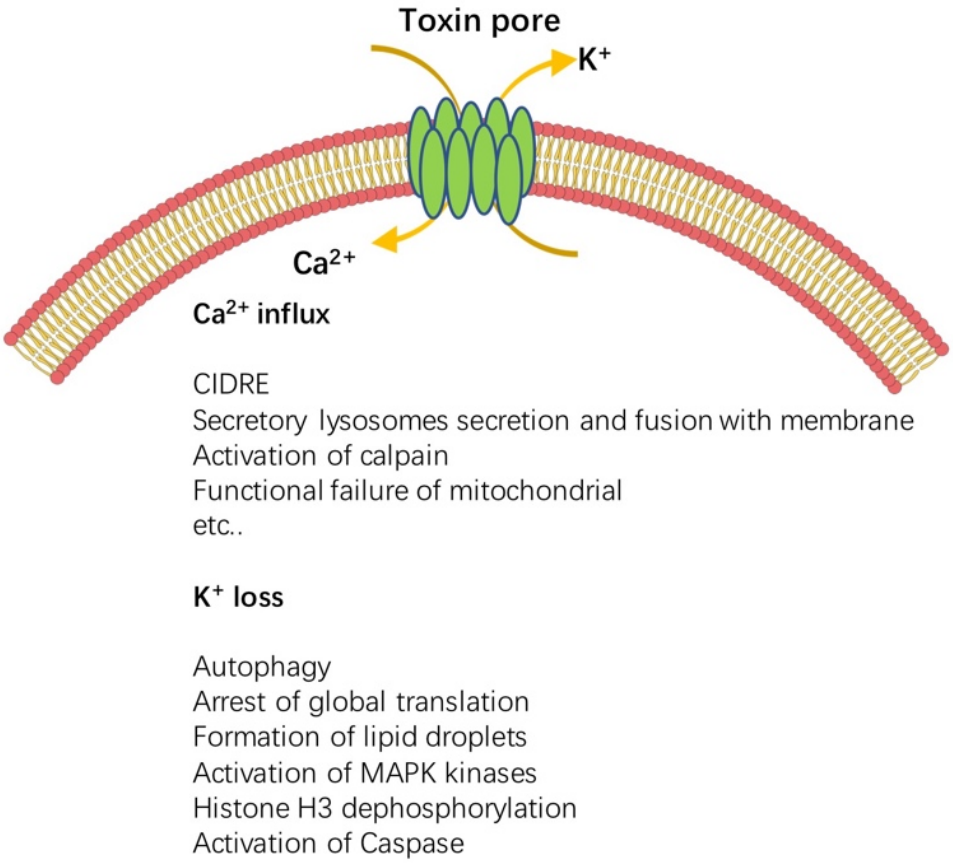

Figure 11: Cellular responses against PFTs. Calcium and potassium ions are the main triggers of cellular responses to PFTs (Bischofberger et al., 2012).

1.5 The fate of target cells

PFTs make non-gated pores in the PM, which could simply kill the target cells. In reality, the fate of both the bacteria and the target cell are far from being this simple, and the struggle between them is complicated (Dal Peraro and Van Der Goot, 2016a). As powerful weapons of bacteria, PFTs may clearly lead to cell death, but this is not the only possible outcome for a target cell.

1.5.1 Cell death

PFTs can lead to cell death in several ways. In particular, high levels of toxins may lead to cell death in rapid lytic ways because of the uncontrolled water entry through toxin pores. At relatively high concentrations of PFTs, the target cells can undergo rapid necrosis, which is usually characterised by failure of mitochondria due to the massive loss of ATP and potassium. Low concentrations of PFTs can lead to relatively slower programmed cell death, such as necroptosis or pyroptosis, the latter being a highly pro-inflammatory death mechanism. PFTs may also trigger non-inflammatory cell deaths such as apoptosis or through excessive and autophagy, which on the other hand be helpful for pathogen eliminations and cellular recovery. At sub-lethal concentrations, PFTs change cellular normal physiological functions, probably to assistant bacterial growth and survival in a host. The specific type of cell death that occurs depends on toxin concentrations, species and the host cell-types (Gonzalez-Juarbe et al., 2015; Kitur et al., 2015; Kitur et al., 2016; LaRocca et al., 2014; Mathur et al., 2019).

Recombinant α-toxin from *clostridium septicum* can make large diffusion pores on the target membranes, which mostly have open constructions. It causes fast potassium efflux and ATP release thus trigger rapid necrosis. Necrosis induced by this recombinant toxin features with permeability to propidium iodide (PI), no DNA fragmentation and no activation of caspase proteins (Knapp et al., 2010). Studies in potassium-rich medium showed significant delay of rapid necrosis, which revealed that cellular potassium decrease was the early cue (Knapp et al., 2010). The fast necrosis

here occurred through the activation of calpains and cathepsins from lysosomes, in comparison with apoptosis reported before that is triggered by other small PFPs (Kennedy et al., 2009). The detrimental decrease of ATP and potassium caused by PFTs are the direct stimulus to the rapid necrosis.

Reportedly, PFTs trigger pyroptosis, a caspase-1 dependent pro-inflammatory cell death (Mathur et al., 2019). Caspase-1 can be triggered by many stimulants. In PFTs cases, the massive loss of intracellular potassium induced by membrane damage can trigger the generation of inflammasomes that can activate caspase-1. Actually, caspase-11 can also activate pyroptosis which mostly responded to gram-negative bacteria toxins (Lamkanfi and Dixit, 2014). Although they share many common features with necroptotic cell death, such as cytosolic swelling and membrane rapture, pyroptosis is different than other modes of cell death both in morphology and mechanism (Bergsbaken et al., 2009; Lamkanfi and Dixit, 2014). Particularly, the prominent feature of pyroptosis is that it is caspase-1/11 dependent strictly. Caspase-1/11 act as enzymes to process the precursors of IL-1β and IL-18 into mature inflammatory cytokines, activate gasdermin D by separating the N-terminals to form large membrane pores, that resulting in leakage of intracellular contents including pro-inflammatory cytokines and rapid membrane rapture (Bergsbaken et al., 2009; Kovacs and Miao, 2017). PFTs from *B. cereus* can activate the generation of NLRP3 inflammasomes, the secretion of IL-1β and IL-18, and cell lysis through pyroptosis, which are triggered by both toxin pores and caspase 1/11-dependent membrane pores (GSDMD inner-membrane channels) (Mathur et al., 2019). GSDMD protein is one member of the GSDM family that has been identified as the effector of pyroptosis. The molecular structure of GSDMD in humans consists of an N-domain and a C-domain connected by a linker (Ding et al., 2016; Liu et al., 2016). The N-domains are the parts which form pores at membranes after activation. In the pore formation process, the linker is cleaved by caspase-1/11 thus to release the N-domain from the C-domain to merger into the PM and oligomerize to form a GSDMD pore (Aglietti et al., 2016; Ding et al., 2016; Liu et al., 2016). These non-selective inner-membrane channels are of 10–15 nm wide with 16 monomers, which are large enough to release small proteins including mature cytokines. At the same time, massive water and sodium influx lead to cellular volume increase, cellular ionic gradients decrease, swelling, membrane rapture and finally cell death (Kovacs and Miao, 2017).

Necroptosis is one mode of programmed necrosis with high pro-inflammatory characteristics that destroys eukaryotic cell membranes, thus playing important roles in the activation of the immune system (Kaiser et al., 2008). In the process of necroptosis, receptor-interacting serine-threonine kinases 1 (RIP1) is activated though the interaction with tumor necrosis factor (TNF) receptors, toll-like receptors (TLRs) and some other signals from extracellular space. By binding with RIP3, necroptosomes were formed by phosphorylation (Kaiser et al., 2008). The effector proteins of necroptosis are MLKL. After the phosphorylation by RIP 3, the N-domains of MLKL merge into the PM and oligomemerize into a cation selective membrane inner channel (Zhang et al., 2018). Necroptosis is strictly dependent on RIP1, RIP 3 and MLKL. Any suppression of RIP1, RIP 3 and MLKL can subvert cell necroptosis (Kaiser et al., 2013; Wang et al., 2007). α-toxin of *S. aureus* triggers cell necroptosis in macrophages thus playing roles in lung damage. Any way to block necroptosis can save lung macrophages and weaken the disease severity, yet necroptosis is harmful to the host cells in lung infections and limit inflammation (Gonzalez-Juarbe et al., 2015; Kitur et al., 2015; Kitur et al., 2016). Later studies reported that necroptosis was the principle manner of macrophage death treated by pathogens of PFTs producing. The triggering factors of necroposis includes membrane damage, the massive loss of cellular inner homeostasis, the failure of mitochondrial and the production of reactive oxygen species (ROS) (Gonzalez-Juarbe et al., 2015).

Helicobacter pylori vacuolating toxin A (Vac A) is a good model for studying of cell death as it can cause cell death in both programed necrosis and typical apoptosis pathways. Exposure of human gastric epithelial cells to VacA toxin results in cell death that is independent on caspase activation, but with the appearances of cell swelling, intracellular ATP decrease and the release of pro-inflammatory proteins (Radin et al., 2011). Programmed necrosis induced by *Staphylococcus aureus* α-toxin results in many typical features such as cell swelling, cytoplasmic vacuolation, cellular ATP decrease, membrane damage and the production of pro-inflammatory proteins (Essmann et al., 2003). Apoptosis is also activated in response to VacA. VacA merges into cells and accumulates in endosomes independent of clathrin pathway and finally internalizes into the inner membrane of the vacuoles to form hexametric oligomers with a favouritism of chloride anions. When the vacuoles move close to mitochondria, a

major part of VacA can merger into the inner membrane of mitochondria and most likely form similar channels there. Pore forming causes the loss of mitochondrial membrane potential, the interference with metabolism, and the activation of apoptosis (Rassow, 2011).

Autophagy is a specialized, regulated intracellular catabolic mechanism that responds to cellular stress or starvation usually. By the degradation of organelles, autophagy acts as a disposal and recycling pathway to provide survival possibilities in some special conditions, such as cell stress and nutrient deprivation. The distinguishing feature of autophagy is the formation of autophagosomes, which are intercellular vesicles that are surrounded by double membrane-bilayers. It is believed that autophagy evolved as a survival pathway in response to starvation. PFTs can also trigger autophagy, including α-toxin of *S. aureus*, VCC and *E. coli* haemolysin (He and Klionsky, 2009; Kloft et al., 2010), and the triggering mechanism by PFTs indicate that starvation and energy shortage play a role. Initially, two cellular pathways were reported to participate (Kloft et al., 2010). The first one is by AMP-activated protein kinase (AMPK). Membrane perforation leads to massive reduction of the cellular ADP/AMP-ratio, which activates AMPK. Activated AMPK triggers autophagy by inhibiting target of rapamycin-complex 1 (TORC1). The second mechanism is the phosphorylation of eukaryotic translation initiation factor 2-alpha (eIF2α) by general control nonderepressible 2 (GCN2 or EIF2AK4) and protein kinase R (PKR, also termed EIF2AK2). GCN2 is conserved between yeast and man. It works as a nutrient sensor and can be activated by uncharged tRNAs. Phosphorylated GCN2 causes global translational arrest and functions as a trigger of autophagy in response to starvation. PKR, which is involved in autophagy activation in viral infection, was reported to also play a role in the accumulation of autophagosomes in cells treated by *S. aureus* α-toxin (Kloft et al., 2010). Previously, it has been shown that autophagy was helpful for the host defence against VCC (Saka et al., 2007), and it has been speculated that autophagy serves to destroy the PFT. However, experimental evidence for digestion of VCC is lacking and for the related *S. aureus* α-toxin, it has been shown that pore complexes are not degraded. Therefore, autophagy may actually serve to maintain metabolic homeostasis. Autophagy helps cell survival when the recovery process is quite slow, while for rapid recovery processes, autophagy was not as beneficial as under slow-repair conditions (Gonzalez et al., 2011).

1.5.2 Membrane repair and survival

The ability to repair membranes after damage is a fundamental mechanism to maintain homeostasis (McNeil and Steinhardt, 2003). Early studies on membrane repair of oocytes after mechanical damage have been shown that sequential mechanical wounds can be removed repeatedly only with the presence of extracellular calcium (Chambers et al., 1961). The major conclusion of these studies was that repair depends on the influx of calcium into cells. Later, it was reported that cultured human fibroblasts recovery from the membrane damages caused *Staphylococcus aureus* α-toxin (Thelestam and Mollby, 1983). This finding demonstrated that target cells can also survive damage by toxins forming circumscribed pores lined by protein. During the following decades, observations were verified for several other toxins and mechanisms were elucidated.

Plasma membrane perforation induced by PFTs may cause calcium influx and potassium efflux. Rapid and effective repair of large lesions (by CDCs, mechanical lesions or LASER-induced damage) is highly calcium dependent and may involve a variety of mechanisms including blebbing, shedding, endocytic degradation and exocytosis of outward vesicles. The influx of free extracellular Ca^{2+} considered an indispensable trigger of PM repair and can also activate protective cytoskeletal remodelling. However, long-lasting influx causing high levels of intracellular Ca^{2+} is extremely harmful to cells, as it can disturb cellular signal pathways and finally lead to cell death. Therefore, the cellular Ca^{2+} influx and the final intracellular Ca^{2+} level after membrane damage are key factors determining cell fate (Brito et al., 2019).

The recovery mechanism triggered by calcium entry induced by PFTs is called calcium influx-dependent repair-mechanisms (CIDRE). The membrane protrusions in SLO-treated human embryonic kidney cells, which usually forms when the membrane is damaged, covers the toxin pore domains and sequentially become larger in the direction against the cell body to form blebs. At the same time, the annexin protein, a calcium binding protein, constitutes a complex analogous to a bolt to cut off this protrusion at the root of the blebs, thus leaving the blebs out of the cell body (Babiychuk

et al., 2011; Keyel et al., 2011). Annexin proteins quickly translocate to membrane lesions according to their different sensitivities to calcium. In particularly, annexin 2 and 6, which are highly sensitive to cellular calcium, were identified to early recruit to the PM damage sites and locate in the blebs, and in vesicular induced by SLO or PLY toxins. The translocation and accumulation of low calcium-sensitive annexin 1 and 5 to membrane damage locations usually occurs later, indicating the lower chance of membrane recovery, because of the high toxic cellular calcium level (Potez et al., 2011; Wolfmeier et al., 2016). However, the speculation that cells are protected against PFTs by annexin 1 was proved by the detection of annexin 1 in membrane blebs and the increased susceptibility to CDCs of annexin 1-inhibited HeLa cells (Brito et al., 2019; McNeil et al., 2006). Moreover, annexins were enriched in the high density structures under PLY toxin pores, which resemble annexin 5 in the two-dimensional arrays that occurred in the membrane when damaged by laser (Brito et al., 2019; Carmeille et al., 2015; Wolfmeier et al., 2016). These observations suggest that annexins protected host cells by clogging PFTs pores, avoiding calcium accumulation and diffusion to the whole cell.

Blebbing is a universal response to many agents that cause PM damage, including PFTs. Interestingly, some studies showed that blebbing that occurred during PFT attacks might be because of the innate characteristics of particular membrane domains which respond to toxins accumulation and binding, rather than to the permeabilization damage from PFTs (Keyel et al., 2011; Skocaj et al., 2016). Large membrane blebs are formed in PLY or SLO treated cells to create a limited space with higher calcium level insider compared to the rest of the intracellular space (Babiychuk et al., 2011; Wolfmeier et al., 2015). These blebs can protect the host cells to some degree from the deleterious calcium increase and leakage of intracellular contents. When treated with PFT ShlA from *S. marcescens,* gut epithelial cells of drosophila formed membrane protrusions resembling blebs that contained damaged organelles. Moreover, ShlA-deficient strains can lead drosophila to enduring more intensified damage, thus promoting the idea that blebs response played a key role in maintaining membrane integrity and restricting host damages (Brito et al., 2019; Lee et al., 2016; Martin et al., 2014). ESCRT was identified to play a role in the process of membrane deformation and scission, such as MVB biogenesis and viral budding. The PM shedding intermediated by ESCRT-III was completely verified in membrane damage induced by

laser (Jimenez et al., 2014). In PFTs context, the ESCRT-III component CHMP4B was found to be distributed in the PM treated with LLO, the abundant ESCRT assembly and disassembly subunits were found in the vesicle released by host cells exposure to CDCs (Brito et al., 2019; Wolfmeier et al., 2016).

Upon activation of exocytosis by PFTs peripheral lysosomes merge with the PM to mend membrane lesions, reduce membrane stress, and are involved in spontaneous recovery of lipid-based membrane damage (Brito et al., 2019; Togo et al., 2000). At the same time, acid sphingomyelinase (ASM) enzymes carried by these lysosomes are released into the extracellular environment after fusion with the PM (Corrotte et al., 2012; Draeger and Babiychuk, 2013). Sphingomyelin in the outer leaflet of the plasma membrane can be transformed by ASM to ceramide thus enabling the cell membrane to swallow the localized region by wrapping the damage pore of SLO to form the structure of caveolar, which is referred to the endocytosis pathway (Idone et al., 2008; Tam et al., 2010). ASM- or caveolin-deficient cells are not able to recovery from SLO-induced damage (Schoenauer et al., 2019; Schuchman, 2010; Tam et al., 2010). Although, the mechanism of endocytosis used to remove PFT pores and the internalization of toxin pores by caveolar need more visualized evidence. Moreover, the internalized active toxin pore might attack the endosome membrane resulting in the release of toxins to the cell cytosol. This endocytosis mechanism that internalizes the damage pores into multivesicular bodies (MVB) has been seen in many host responses to different PFTs (Chen et al., 2017; Corrotte et al., 2012; Husmann et al., 2009). Internalized PFTs can be degraded after the fusion of MVB and lysosomes or re-released to the extracellular environment through exosomes pathway (Husmann et al., 2009). Recent studies showed caveolin-1 and GTPase regulators associated with focal adhesion kinase-1 (GRAF1) contributed to the recovery from PFTs pores, both on the membrane repair and inner cellular environment homeostasis (Babiychuk et al., 2008; Bianco et al., 2009; Nygard Skalman et al., 2018). Notably, exocytosis can promote membrane shedding and the ceramide produced from ASM can help annexin 1 binding to the PM. This means, in the cell recovery from PFTs, all the repair pathways like annexin clogging, membrane shedding, lysosomes exocytosis, and endocytosis of toxin can play complementary roles in a manner that profits each other to against their common enemy (Babiychuk et al., 2008; Bianco et al., 2009). For example, endocytosis contributes to the elimination of SLO pores by CIDRE. The

permeabilization on the PM by SLO results in rapidly influx of calcium, which triggers lysosomes production to merge into the damaged membrane. The fusion of endolysosomes with membranes lead to the release of ASM into the extracellular environment, which transforms sphingomyelin on the PM to ceramide thus producing massive endosomes containing the structure of toxin pores. SLO pores are arranged into the compartment of endosomes before being digested by internalization mechanism (Corrotte et al., 2012; Idone et al., 2008; Tam et al., 2010).

Rapid Ca^{2+} influx dependent repair does not take place with *Staphylococcus aureus* α-toxin. The unsuccessful activation of rapid Ca^{2+} dependent repair by α-toxin might be because of insufficient calcium influx, stable structure of the α-toxin pore, or some other unknown reasons. Recovery of *Staphylococcus aureus* α-toxin damaged membranes may need hours. Endocytosis is essential for this slow repair response to α-toxin, but it is independent of free calcium influx. Uptake of α-toxin is comparably slow and requires dynamin. Interestingly, the undegraded α-toxin is released by the host cells packed in toxosomes, a kind of exosome (Husmann et al., 2009). The fate of α-toxin toxosomes is not known. However, the basic process of toxosome formation has been later confirmed for anthrax toxin and the authors demonstrated that toxosomes may spread to other cells. Recent research proved that the recovery from α-toxin involved p38 MAPK (Husmann et al., 2006; Kloft et al., 2009) . That membrane repair may occur after attack by a small β-PFT has been confirmed for aerolysin and a role of autophagy, and the phosphorylation of eIF2α has been demonstrated for there as well (Gonzalez et al., 2011). K^+ efflux is the critical activator of p38 and of eIF2α-kinase GCN2 (Kloft et al.,2009; Kloft et al., 2010). These findings have been reviewed (Bischofberger et al., 2012; Brito et al., 2019). Although it has been shown that p38 was indispensable for the cellular recovery from *S. aureus* α-toxin, it was dispensable for keratinocyte repair after SLO-attack (Husmann et al., 2006). However, activation of p38 was seen with virtually all PFTs investigated up to now (Brito et al., 2019).

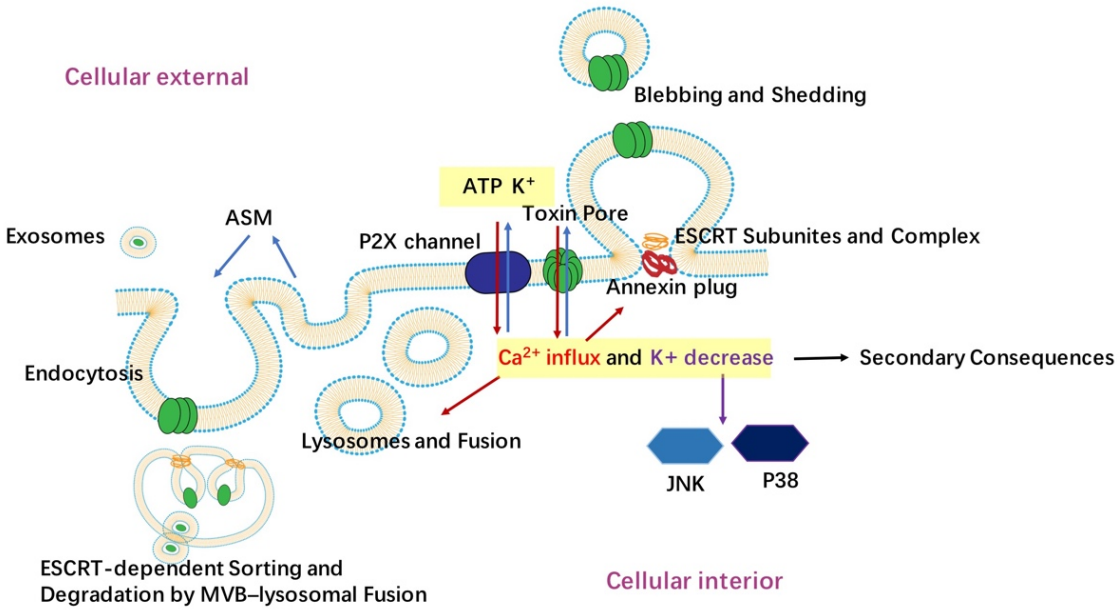

Figure 12: Multiple mechanisms promoting cell survival. The perforation damages and secondary membrane channels induced by PFTs allow massive Ca^{2+} influx and K^+ efflux, which in turn trigger many mechanisms to protect the host cells. Annexin protein, one calcium binding protein, constituted a complex like a bolt to cut off this protrusion at the root of the blebs, thus letting the blebs containing the pore leave the cell body. ESCRT has been identified to play role in the process of membrane deformation and scission. Lysosomes merge into the PM to mend membrane lesions and reduce membrane stress. Sphingomyelin can be catalysed by ASM and transform to ceramide thus enabling the cell membrane to swallow the localized region wrapping the damage toxin pore to form the structure of caveolar. Internalized PFTs can be degraded after the fusion of MVB and lysosomes or re-released to extracellular environment through exosomes pathway. The K^+ efflux can activate the MAPK pathways, especially P38, to compose a widely conservative defence mechanism fighting against the PM pore formation.

1.6 Significance, open questions and aim of the present study

PFTs are important virulence factors of bacteria, and many pathogenic bacteria can produce at least one PFT. Damage of plasma membranes may serve to access nutrients, promote bacterial growth, escape from host immunity, or introduce other virulence factors into cells. Despite decades of research, numerous questions regarding the mechanisms of pore formation and the role of PFT during infection remain. The consequence of PFT attack is not only a function of the PFT's properties itself, but is co-determined by membrane repair responses of target cells. Therefore, it is important to understand the mechanisms of membrane repair. Over the last 15 years,

repair of large lesions, including mechanical lesions and those inflicted by CDC-type PFT, like SLO, has been studied in detail. Unfortunately, the mechanisms emerging from these studies are frequently summarized under the label “membrane repair”. This is misleading, because evidently, studies on CDC fall short of explaining membrane repair in the case of *S. aureus* α-toxin and aerolysin (members of a large family of PFT), because cellular defence against these small PFTs does not depend on extracellular calcium.

One of the major open questions at the beginning of these studies was why small β-PFTs are not subject to “canonical”, i.e., calcium-influx dependent repair. We considered that either the general structural difference between CDCs and small β-PFTs could be responsible, or different conductivity for calcium. Therefore, the first aim of the present work was to contribute data to differentiate between these two possibilities. To this end, PhlyP and VCC, two similar small β-PFTs, were used here for comparative experiments, because homology-based modelling suggested that PhlyP-pores might be somewhat wider than VCC-pores, and possibly have increased conductance for calcium.

The second aim of the present work was to address the question, whether secondary events (in particular secondary membrane damage) might contribute to the net effect of PFT-attack. This question was raised by the long standing observation that α-toxin seems to form small pores or large pores depending on the concentrations of toxin (large pores being permeable for calcium) (Walev et al., 1993). The nature of the different lesion types is unclear. The proposed involvement of P2X7 channels during PFT-dependent damage suggested that cellular channel forming proteins might be involved, and the recent characterization of gasdermin and MLKL as cellular pore forming proteins suggested these proteins as potential candidates. Unlike CDC, small β-PFT like α-toxin are suitable to analyse the role of secondary membrane damage because they restrict the flux of ions, vital dyes, or cytosolic markers. Consequently, they are suitable to detect secondary lesions which are permeable for these marker molecules.

2 Materials and methods

2.1 Materials

2.1.1 Medicals and materials

Table 1: Medicals and materials used in this study

Name	Company
ANTI-FLAG M2 (mouse, F3165)	Sigma-Aldrich Chemie GmbH, Germany
Anti-GSDMD (rabbit, G7422)	Sigma-Aldrich Chemie GmbH, Germany
ATP Bioluminescence Assay kit CLS II	Roche, Germany
BIO-Rad Protein Assay,	Bio-Rad, Germany
BSA, albumin fraction 5 ≥98%, powdery bovine	Roth GmbH, Germany
Blebbistatin	Sigma-Aldrich Chemie GmbH, Germany
Culture plates -12 well	Greiner Bio-one, Germany
Cell culture microplate-96 well	Greiner Bio-one, Germany
Calcium chloride, dried powder	Roth GmbH, Germany
Chloramphenicol	SIGMA-Aldrich Chemie GmbH, Germany
Cremophor	SIGMA-Aldrich Chemie GmbH, Germany
Coverslips	Thermo Scientific, Germany
Culture bottles, Cellstar Tissue Culture Flasks 250ml,	Greiner Bio-one, Germany
Cell culture Medium DMEM + Gluta MAXTM-I,	Gibco (Invitrogen TM), UK

Cell culture Medium DMEM/F-12 + Gluta MAXTM-I,	Gibco (Invitrogen TM), UK
Centrifuge tubes, 15 ml and 50 ml	Cellstar, Greiner Bio-one, Germany
Cell culture black microplate	Greiner Bio-one, Germany
DMSO (dimethyl sulfoxide for molecular biology)	Roth GmbH, Germany
Desipramine	Sigma-Aldrich Chemie GmbH, Germany
Ethanol ≥ 99.5%, Pure	Roth GmbH, Germany
EGTA (ethylene glycol-bis(β-aminoethyl ether)-N,N,N′,N′-tetraacetic acid)	Roth GmbH, Germany
Fluo-8 AM	Santa Cruz Biotechnology, Inc. Germany
FCS (Fetal Calf Serum)	Life technology, inc., Germany
Glass Pasteur pipettes, 150 mm	VWR International, Germany
Glycine, ≥ 99%	Sigma-Aldrich Chemie GmbH, Germany
HEPES, (4-(2-hydroxyethyl)-1-piperazineethanesulfonic acid), 1M	Sigma-Aldrich Chemie GmbH, Germany
Hoechst stain	Molecular Probes, USA
HBSS (Hanks' Balanced Salt Solution)	Sigma-Aldrich Chemie GmbH, Germany
HCL (Hydrogen chloride)	Merck, Germany
Magnesium chloride ≥ 98.5%, anhydrous	Roth GmbH, Germany
2-Mercaptoethanol	Roth GmbH, Germany
4-methyl-umbelliferyl-N-acetyl-β-D-glucosaminide	Sigma-Aldrich Chemie GmbH, Germany
MEM (NEAA), non-essential amino acid	Sigma-Aldrich Chemie GmbH, Germany

Mono Q column	GE Healthcare, Germany
NaOH (Sodium hydroxide)	Merck, Germany
Ni-NTA Agarose	Qiagen, Germany
Parafilm	Pechiney Plastic Packaging, Inc., USA
Paraformaldehyde	MERCK, Darmstadt, Germany
PCR clean tubes, 5 ml	Eppendorf, Germany
Penicillin	Life technology, Inc., Germany
PI (Propidium iodide)	Sigma-Aldrich Chemie GmbH, Germany
Pipettes, 10 µl, 10 ml and 25 ml	Cellstar, Greiner Bio-one, Germany
KCl (Potassium chloride)	Merck, Germany
KH_2PO_4 (Potassium dihydrogen phosphate)	Merck, Germany
PPADS	Santa Cruz Biotechnology, Inc., Germany
Probenecid	Sigma-Aldrich Chemie GmbH, Germany
QuikChange II XL Site-Directed Mutagenesis Kit	Agilent Technologies, Germany
Rotiphorese Gel 30	Roth GmbH, Germany
Schuffle Express competent *E.coli* cells	New England Biolabs, Germany
Na_2HPO_4 (Sodium phosphate dibasic)	Roth GmbH, Germany
NaCl (Sodium chloride)	Roth GmbH, Germany
Na_2SO_4 (Sodium sulfate), Suprapur®	Merck, Germany
Na_2HCO_3 (Sodium bicarbonate)	Merck, Germany
Suramin-sodium	Santa Cruz Biotechnology, Inc., Germany
Streptomycin	Life technology, Inc., Germany
Triton X-100	Roth, Germany

Trypsin, 0.5% Trypsin-EDTA (10x)	Gibco (InvitrogenTM), UK
Tweezers	Plano GmbH, Germany

2.1.2 Equipment

Table 2: Equipment used in this study

Name	Company
Bunsen burner, Fire-boy eco	Integra Bio Science, Germany
Biolumat 9600 instrument	Berthold, Germany
Cell culture incubator	Binder, Germany
Centrifuge, max. 8K, GS-6	Beckman Coulter GmbH, Germany
Electron microscope EM 109	Carl Zeiss GmbH, Germany
Epifluorescence microscope, Axiovert 200M	Carl Zeiss GmbH, Germany
Freezer -20° C Liebherr Premium	Liebherr, Germany
Freezer -20° C Bosch economic-super	Bosch, Germany
Freezer -70° C, Hera freeze	Heraeus Instruments, Germany
Incubator of bacterial culture	Heraeus Instruments, Germany
Laser scanning microscope, Zeiss 510 Meta-Microscope	Carl Zeiss GmbH, Germany
Libra, Mettler P5	Mettler-Toledo GmbH, Germany
M401 flame photometer	Sherwood Scientific Ltd, UK
Nanodrop, ND1000 spectrometer Peqlab	Biotechnologie, Germany
Neubauer chamber, Neubauer improved	Roth GmbH, Germany
Libra, precision balance 1201 MP2	Sartorius AG, Germany
Phase contrast microscope	Wilovert Will, Germany
pH meter, WTW pH320	WTW, Germany

Pipetus®-junior	Hirschmann Laboratory, GmbH, Germany
Refrigerated Centrifuge, GPKR Centrifuge	Beckmann Coulter, Germany
Shaker Incubator	GFL (Gesellschaft für Labortechnik) GmbH, Germany
Shakers	Edmund Buehler, Germany
Shaker incubator, controlled environment incubator shaker	New Brunswick Scientific Co. Inc., USA
Spectrophotometer, Ultrospec 2100 pro, UV-Visible	Amersham Biosciences, GE-Healthcare, Germany
Sterile bench, MicroFlow, biological safety cabinet	Astec, Bioquell, UK
Scale, Mettler P5	Mettler-Toledo GmbH, Germany
Transfection device, Nucleofector® II LONZA	Amaxa Biosystems, Germany
TriStar LB941 Multimode Microplate Reader	Berthold Technologies, Germany
Ultracentrifuge, OptimaTM LE-80K	Beckman Coulter GmbH, Germany
Voltage source, Desatronic 500/400	Desage, Germany
Water bath	Köttermann GmbH & Co KG, Germany
Water bath vibrator, Certomat WR waterbath	B. Braun Biotech International, Germany

2.1.3 Software

Table 3: Software used in this study

Name	Company
Adobe Illustrator CS6	Adobe Inc., USA

AxioVision Release 4.8.2	Carl Zeiss GmbH, Germany
DNA star	DNASTAR, Inc., USA
Photoshop CS6	Adobe Inc., USA
EndNote X7	Thomson Reuters, Canada
Microsoft® Office 2015	Microsoft Corporation, USA
LSM Image Browser, Release 4.2	Carl Zeiss GmbH, Germany

2.1.4 Liquid and buffer

Table 4: Liquid and buffer used in this study

Name	Quota
Ampholyte solutions	4 ml Bio-Lyte 3/10 ampholyte in 56 ml sterile water
Base buffer	20 mM Tri-HCl (pH 7.5), 250 mM Sucrose, 1 mM $CaCl_2$, 1 mM $MgCl_2$, in distilled water
Binding buffer	50 mM NaPO4, 300 mM NaCl, 10 mM imidazole, 1 mg/ml lysozyme, 4 mM Pefabloc, pH 8.0
1% BSA (Albumin fraction V)	0.17 µM BSA in PBS
3% BSA (Albumin fraction V)	0.5 µM BSA in PBS
Choline buffer	129 mM Choline-Cl,

	0.8 mM $MgCl_2$, 1.5 mM $CaCl_2$, 5 mM Citric acid, 5.6 mM Glucose, 10 mM NH_4Cl, 5 mM H_3PO_4, pH 7.4 (NaOH)
Cremophor (Macrogol-35-glycerol-Ricinoleate) stock solutions	0.1 % (w/v) Cremophor, in sterile water
Dialysis buffer	20 mM Tris, 20 mM NaCl, 24 h at 4°C
ECPs of PhlyP storage solutions	25 mM $CH_2(COOH)_2$, 250 mM NaCl, 50% (v/v) Glycerol pH 5.5
Electrophoresis buffer	25 µM Tris, 0.2 M Glycine, 3.5 µM SDS in distilled water
30% Ethanol Solution	30% (v/v) EtOH ≥ 99.5% in distilled water
50% Ethanol Solution	50% (v/v) EtOH ≥ 99.5% in distilled warter
70% Ethanol Solution	70% (v/v) EtOH ≥ 99.5% in distilled water
Fluo-8 AM stock solutions	100 µM Fluo-8AM in DMSO
HaCaT cell culture medium	10% (v/v) FCS, 10 mM HEPES, 100 units /ml penicillin, 100 µg/ml streptomycin in 500 ml DMEM/F-12+GlutaMAXTM-I

Hoechst (Maximum stock solution)	16 µM Benzimide H 33342 in distilled water
Hoechst / PBS	3.3% (v/v) of stock solution in PBS
Linear gradient of ion chromatography (pro-PhlyP)	0-1.0 M NaCl, 50 mM malonic acid, pH 5.5, totally 15 ml
Linear gradient of ion chromatography (pro-VCC)	20 mM -500 mM NaCl in 20 mM Tris, pH 8, totally 20 ml
MEF cell culture medium	10% (v/v) FCS, 10 mM HEPES, 100 units / ml penicillin, 100 µg/ml streptomycin in 500 ml DMEM + GlutaMAXTM-I
PBS solution	0.14 M NaCl, 2.7 µM KCl, 9.9 µM Na_2HPO_4, 1.8 µM KH_2PO_4, pH 7.4 (NaOH) in distilled water
Precipitation buffer	50% (v/v) ECPs suspensions, in 3.3 M ammonium sulphate.
Probenecid stock solutions	2 µM probenecid, in sterile water
Rinsing buffer	0.85% (v/v) NaCl, in sterile water
Sodium citrate-phosphate buffer	200 mM Na_2HPO_4, 100 mM citric acid, in sterile water

Stop solutions	2 M Na_2CO_3 1.1 M glycine in sterile water
TBST solution	50 µM Tris, 0.15 M NaCl, 0.1% (v/v) Tween, in distilled water
Transfer buffer	48 µM Tris, 39 µM glycine, 13 µM SDS, 20% (v/v) Methanol in distilled water
Western blot loading buffer	65 mM Tris 10% (v/v) glycerol 5% (v/v) 2-mercaptoethanol 2% (w/v) SDS bromophenol blue
20 mM Tris-HC	20mM Tris pH 7.5 (HCl) in distilled water
0.5 M Tris-HCl buffer	0.5M Tris pH 9 (HCl) in distilled water
1 M Tris-HCl buffer	1M Tris, pH 7.4 (HCl), in distilled water
0.1% Triton X-100 in PBS	0.1% Triton X-100 (v/v), pH 7.4, in PBS
0.5 % Triton X -100 in Choline buffer	0.5% Triton X-100 (v/v) in Choline buffer.
1x Trypsin solution	10% (v/v) 10x trypsin-EDTA in PBS

2.2 Methods

2.2.1 ATP-measurements

With the concentration of 1–2×10^4 / well in total 200 µl culture medium, HaCaT cells were seeded in 96-well plates and cultured over night before incubation with toxins. After incubation for different times and specific toxins of different concentrations, HaCaT cells were washed and then exposed to triton (0.5% Triton X-100) for lysis and ATP detection reagent Bioluminescence Assay kit CLS II (Roche). Following mixing by shaking on a Vortex machine, cellular ATP in the cells were measured and recorded in a Biolumat 9600 instrument.

2.2.2 Single Site directed mutagenesis of pro-PhlyP and pro-VCC

The production of mutants pro-PhlyP S/W and pro-VCC W/S were achieved by exchanging the single amino acid (S in pro-PhlyP and W in pro-VCC) using the QuikChange II XL Site-Directed Mutagenesis Kit form Agilent Technologies. The mutations were introduced by PCR amplification. For pro-PhlyP S/W, pTrcHisA-pro-PhlyP was taken as template and the primer pair 5`-aactctataatcttgtgtattaaaagataaccattttgattgactataactagcactagcttg-3´ and 5`-caagctagtgctagttatagtcaatcaaaatggttatcttttaatacacaagattatagagtt-3´ was added to before PCR amplification (72 °C, 5-minute extension, 18 cycles). The same PCR method was used for the construction of pro-VCC W/S with template pQE30-pro-VCC and primer pair 5`-aagttatacccagagtcgcagcttaacctacaacacacaag-3´ and 5`-cttgtgtgttgtaggttaagctgcgactctgggtataactt-3´. Parental plasmids with no mutated target gene was removed by DpnI enzyme thus ensuring that all remaining plasmid was the product of mutagenesis. These were then transformed into Ultra competent XL10-Gold cells for amplification and culture. Next, mutated plasmids were isolated from transformed clones and identified by custom DNA sequencing (StarSeq) of both strands. Plasmid DNA were transformed and expressed in NEB SHuffle Express competent *E. coli* (C3028).

2.2.3 Using Fluo-8 AM to measure changes of cellular Ca^{2+}

The changes of host cellular Ca^{2+} concentration induced by PFTs were measured by the instrument TriStar LB 941 from Berthold Technologies. Free cellular Ca^{2+} binding with Fluo-8 AM caused fluorescence signal increases that can be detected by fluorescence reading instrument. Fluo-8 AM (from Santa Cruz Biotechnology Inc.) were kept in dark -20 °C and taken out only before experiments. In the loading process, Fluo-8 AM was light-avoided. The fluorescence measurement was operated under the protocol of instrument TriStar LB 941 from Berthold Technologies.

HaCaT cells were seeded in 96-well black cell culture microplates and cultured at 37 °C over night. Each well had HaCaT cells 3×10^4 in totally 200 µl culture medium. Before measurement, HaCaT cells were incubated with a dye mixture including 100 µM Fluo-8 AM, 0.1% cremophor (w/v) and 2 mM probenecid at 37°C for 30 min. The Fluo-8 AM dye mixture was mixed thoroughly by shaker oscillation. After incubation with Fluo-8 AM dye mixture, HaCaT cells were washed twice gently with medium. The loading of toxins was implemented through the injector of instrument. Suitable filter was chosen on the TriStar LB941 instrument with 485 nm of excitation and 535 nm of emission at central wavelength. Measurement results were ordered to record every 5 seconds in total 3 min. Experiment data were exported in excel format and analysed in Microsoft office 2007. HBSS as blank negative control and SLO 2,5 µg/ml as positive control were injected at the same time always. Anther control group was the supernatant of HaCaT cells treated by toxins, which were always negative results to tell that the increase of fluorescence signal was strictly reported the intracellular Ca^{2+} changes but not the leakage of Fluo-8 by cell lysis.

2.2.4 Assessment of PFTs-induced PI influx by fluorescence microscopy

The extracellular PI entry triggered by PFTs were assessed and analysed by fluorescence microscopy. Cells were seeded in 6-well culture plates with glass slips inside and cultured over night to get well adhesion and growth. PFTs of specific concentrations incubated the target cells for indicated time. After that, toxin-treated

cells were washed 2 times with PBS. PI of 50 µg/ml was loaded to cells for 1 min. After fix with PFA of 2% for 10 min, cells were then exposed to Hoechst 33342 to stain cellular nuclei and washed 2 times afterwards before mantled by coverslips.

Experimental samples were visualized with fluorescence microscopy Axiovert 200 furnished by Plan Apochromat 100x/1.4 aperture lens in the wide view field. For each experimental group, 100 events were counted and analysed.

2.2.5 Cell transfection and microscopy imaging of GSDMD

The cDNAs of GSDMD was inserted into a modified pCS2 vector with 3 x Flag tags at N-terminal (pCS2-3flags-hGSDMD). This vector was generated and offered kindly by Prof. Dr. Shao from Chinese Academy of Sciences.

HaCaT cell were seeded in 6-well culture plate (1 x 10^6 /well) with glass coverslips inside and cultured overnight before experiments. The cells were transfected with pCS2-3flags-hGSDMD vector through Amaxa transfection system following the manufacturers' instructions. After that, the cells were cultured overnight in 37 °C again. Before experiments, the samples were pre-incubated with or without inhibitors.

The cells were then exposed to indicated toxins for indicated time. After toxin treatment, the cells were washed 3 times with PBS before the fixation procedure. 2% PFA were used here to fix samples for 15 min at room temperature. Two times of wash with PBS were followed. After that, the cell samples were permeabilized with 0.1% triton X-100 in PBS for 10 min. This step was required to make access for antibody to detect the proteins inside. Following fixation and permeabilization, the samples were incubated with primary antibody ANTI-FLAG M2 (mouse, F3165, Sigma) and Anti-GSDMD (rabbit, G7422, Sigma) for overnight at 4°C. After incubation with primary antibody, samples were washed with PBS and incubated with AlexaFluor® conjugated secondary antibodies for 1 h at room temperature. Samples on coverslips were placed and fixed on glass slid by using liquid glue and then visualized using Zeiss Axiovert 200M epifluorescence microscope assembled with Plan-Apochromat 100x / 1.40 aperture

lens. Digital images were exported out with Zeiss Axiocam and processed with AxioVision.

2.2.6 Cellular K^+ measurement after PFT-attack by flame photometry

The loss of cellular K^+ is an important sign of primary damage by PFTs and the replenishment of this ion is a hallmark of recovery of membrane integrity. The cellular K^+ level after PFT-attack here was quantified by flame photometry (Gonzalez et al., 2011; Husmann et al., 2006). HaCaT cells were seeded one night before in 6-well plate and cultured over night. After treatment with specific toxin of indicated concentrations, cells were washed with K^+ free choline buffer 2 ml and 3 times at different time points before exposure of 2 ml choline buffer (including 0.5% Triton X-100) to lysis at least for 30 min at room temperature on a shaker. The liquid after lysis were collected to 5 ml clean PCR tubes and analysed in a M401 flame photometry. The operation of the M401 instrument was according to the supplier's instructions.

2.2.7 β-Hexosaminidase active Assay

The analysis of β-Hexosaminidase was performed by TriStar LB 941 instrument from Berthold Technologies. Briefly narrated here: cells were seeded one night before experiment in 12-well plates and cultured over night. Before experiment, culture medium was removed and identified toxin of specific concentration was added. At different incubation time points, supernatant 350 µl were collected and placed on ice. After the collection of all samples, 50 µl of 6 mM 4-methyl-umbellyferyl-N-acetyl-β-d-glucosaminide in sodium citrate-phosphate buffer of pH 4.5 were added. All samples were placed in 37°C environment for 15 min. After incubation, all reactions were stopped by addition of 100 µl stop-solutions including 2 M Na_2CO_3 and 1.1 M glycine. 100 µl reaction solutions from each sample were analysed under TriStar LB 941 multimode reader instrument with set up of 355 nm of excitation and 460 nm of emission, 3000 of lamp energy, 0.1 ms of counting time. Digital data were exported in excel format and analysed by excel office software. Detailed description see (Rodriguez et al., 1997).

2.2.8 Cell culture

Both HaCaT and MEF cell lines were cultured with DMEM medium while DMEM/F-12 + GlutaMAXTM-I (Gibco) were used for HaCaT cell culture and DMEM + GlutaMAXTM-I (Gibco) were used for MEF cells. FCS of 10%, HEPES of 10mM, penicillin of 100 units/ml and streptomycin of 100 µg/ml were added to DMEM medium. Cells were cultured in cell-culture bottles in incubator and stabilised at 37°C with stable concentration of CO_2 5%. Growth status of cells must be monitored everyday and spilt once or twice every week based on their growth situation. Both HaCaT and MEF cell lines were growing adherently on bottom of culture bottles. Before experiments, cells were separated from bottles by using trypsin for 3–5 min at 37°C. To do this, cells were washed 2 times with PBS before the adding of trypsin of 0.05% in 2 ml. Optical microscope was used to observe the detachment process. The detachment process was ended by adding DMED medium 5 ml or 10 ml. Cells were later transported from bottles to a new 15 ml sterile tube and centrifuged at 1000 r/min for 5 min. After centrifugation, cells were re-suspended in 10 ml fresh medium again. 2 ml medium with cells were taken into one new culture bottle with 20 ml fresh medium for culture again in incubator. The rest 8 ml were calculated and seeded in cellular culture plates according to indicated experiments protocol.

2.2.9 Toxins preparation

Toxins used in this thesis included extracellular productions of *Photobacterium damselae* subsp. *damselae* (ECPs); recombinant pro-VCC and pro-PhlyP toxins; mutant of pro-VCC (pro-VCC W/S), and mutant of pro-PhlyP (pro-PhlyP S/W). These materials were kindly prepared by Martina Meyenburg in our lab.

Pro-VCC W/S and pro-PhlyP S/W were generated in the frame of this thesis by QuikChange II XL site-directed mutagenesis kit from Agilent Technologies (principles, some details and results are described in the Results section).

The procedures to produce pro-PhlyP and ECPs were as published before. For ECPs: *Photobacterium damselae* subsp. *damselae* were cultured on LB plates equipped with

cellophane membrane. After culture of 60 h at room temperature, the cellophane membranes were washed with 2 ml rinsing buffer. All supernatant samples were adjusted the optical density to 1 at OD600 and then centrifuged to remove bacteria. Subsequently, all samples were purified by membrane filter with pore size of 0.2 μm. The further purification was performed by isoelectric focusing (IEF, 230–550 V, 15 W; 4 h; 6–8°C) and ion chromatography (0.4 ml/min). ECPs of *Photobacterium damselae* subsp. *damselae*. were sorted out by adding precipitating buffer and then centrifuged. The pellets were later exposed to Bio Rad ampholyte solutions before separation with IEF (Hemolytic activity concentrated at pH 5.5 to 6.5). Collected samples were mixed with binding buffer at ration of 1:5 (v/v) and then added to Mono S column. Fractions were collected and stored in -70 °C. pro-VCC was used as standards to measure the relative concentrations of pro-PhlyP by SDS-PAGE with silver stain.

The expression of recombinant pro-toxin of *Vibrio cholera* cytolysin was described before (Olson and Gouaux, 2005). Thanks to Olson for providing the PQE-30 vector carrying pro-VCC gene. Here slightly depict: Origamin B cells transfected with PQE30-pro-VCC gene vector were grown on LB culture plates. IPEG were used to trigger the production of pro-VCC. After growth, cells were harvested through centrifugation. Binding buffer was later used to dissolve bacteria pellets. Bacteria suspension samples were then treated with ultrasonication for lysis and disruption. Filters with 0.2 μm pore size and Ni-NTA agarose from Qiagen were introduced to filter and purify samples. More details about purification steps were described at Qiagen's purification system protocol. Before loading samples on Mono Q column (Ion chromatography), all fractions were pooled with highest concentrations and were purified by dialysis buffer. After loading, flow rate was adjusted at 0.5 ml/min. The eluted samples were pooled again with highest toxicity activities and 50% (v/v) glycerol were added before storage (−20°C). Here by this procedure, the purity can get to 99% and the concentration was 1 mg/ml measured by densitometric analysis of SDS-PAGE gel stained by Coomassie and Bio-Rad proteins assays respectively.

The expression of pro-PhlyP was achieved by building a recombinant vector carrying the pro-PhlyP gene (*hly*A_P). The gene of pro-PhlyP was amplified through PCR by using *Photobacterium damselae* subsp. *damselae* as templates under the catalysis of

Taq DNA polymerase of high fidelity from Kapa (Rivas et al., 2015). Amplified DNA samples were then purified and digested with BamHI restriction enzymes. After digestion, target gene samples were cloned into vector pTrcHisA at BamHI site to consist a pTricHisA-pro-PhlyP recombinant gene vector. pTricHisA-pro-PhlyP gene vectors were then transformed into shuffle Express competent *E. coli* cells were from New England Biolabs (NEB). More procedure details were obtained at NEB protocol. His6-tagged proteins were then purified by Ni-NTA agarose and the purification were assessed by densitometric analysis of SDS-PAGE gel stained by Coomassie. Concentrations were measured by western blot with pro-VCC as standards. Primers are: *Phlyp*- Forward (5′ -AACTATTCTACACCTGCAGA) and *PhlyP*-Reverse (5′ -TTAACCCCAAATGAGCTAAT).

2.2.10 Western blot

Cells were lysed and mixed with loading buffer with an equal volume before heated at 95°C for 5 min. Protein samples then were loaded into wells of the SDS-PAGE gel (10%). Molecular weight marker was loaded in a new well. Specific protein samples were separated in the gel for 1–2 h before transferred onto nitrocellulose membrane. After blocking at room temperature with 5 % BSA or 5 % skim milk in TBST for 1 h, membrane with separated protein samples were incubated with first antibody for 1 h or overnight at 4°C. After that, membrane was washed three time with TBST and mixed with an HRP-conjugated second antibody for 1 h at room temperature. Membrane was washed three times again with TBST. The target proteins were measured by enhanced chemiluminescence assay (ECL) kit (Roche Applied Science), and exposed to the emitted light on X-ray film.

2.2.11 Statistics

Three independent experiments are needed at least for each single data figure. Error bars here tells the variation of standard errors from each group statistical means. Student's *t*-test with 2-sides and ANOVA were used to analyse the significance of difference of mean values between two statistics groups. The significance of variation is reported here: * means P value < 0.05; ** means P value < 0.01; *** means P value < 0.001.

3 Results

Part I: Evidence for differential ability of small β-PFT to activate calcium-influx dependent membrane repair (CIDRE)

3.1 Membrane permeabilization by PhlyP

A notable observation during initial characterization of PhlyP was that this toxin made cells permeable for propidium iodide (PI) while VCC did not (Fig. 13a from Rivas et al. 2015). This led us to investigate whether PhlyP and VCC can lead to similar loss of cellular K^+ after toxin attack. To this end, HaCaT cells were treated with purified PhlyP and the lysates were measured in a M401 flame photometer, which was equipped with a potassium filter. The experiment showed that cellular K^+ concentration in the PhlyP group dropped significantly, down to ~10% of the initial level after 10min (Fig. 14a), and the results in the VCC group were similar (Fig. 14b). It was not unexpected, that both PhlyP and VCC induce large decreases of cellular K^+, but because the PhlyP pore appears to have a slightly wider channel than the VCC pore (see cartoon Fig. 13b), we decided to investigate the kinetics of K^+ loss induced by these two related toxins in more detail.

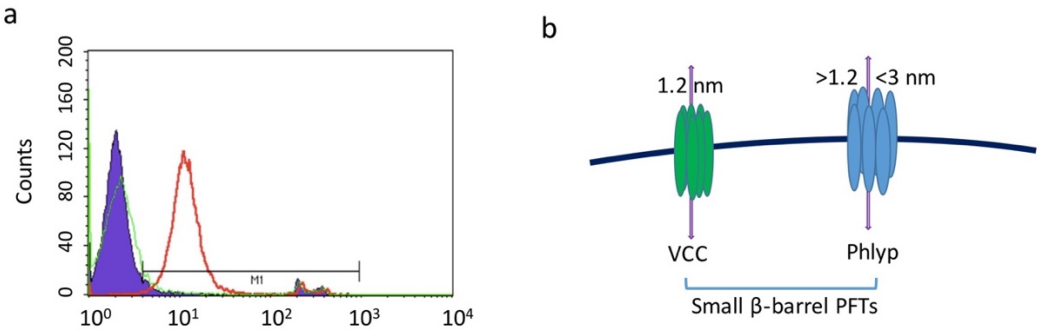

Figure 13: Only PhlyP-attacked cells allow PI influx. a, HaCaT cells in suspension were incubated with PhlyP (100 ng/ml) for 4 min before PI (50 g/ml) was added. Samples were analysed by flow cytometry after 1 min incubation at 37°C. FL3H, fluorescence intensity for PI; counts, number of events per channel. Fluorescence intensity of was indicated on X-axis. Red line, PhlyP; green line, VCC; filled area, untreated cells (Rivas et al., 2015); for contributions see Appendix 2. **b,** PhlyP pores have slightly wider channels than VCC pores.

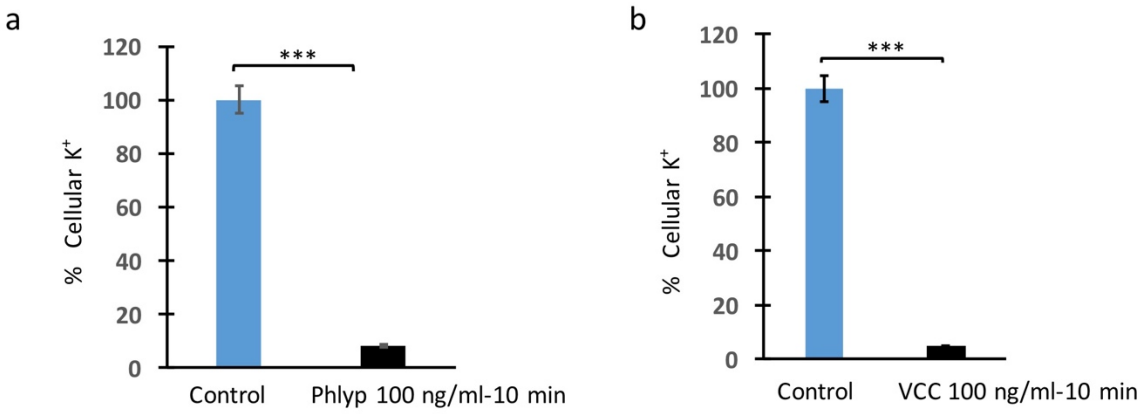

Figure 14: PhlyP and VCC both induce massive loss of K^+. a and **b**, PhlyP and VCC induce strong cellular K^+ decrease. Both toxins affected HaCaT cells in suspension for 10 min at 100 ng/ml before cellular K^+ concentration was measured by flame photometry with lysate cells. Values in b and c represent percentages of the results for untreated controls; mean values ± standard errors (SE) are shown ($n \geq 3$). Statistical significance was calculated with Student's *t*-test.

3.2 PhlyP triggers rapid loss of cellular potassium

To investigate time- and dose-dependent cellular K^+ loss after permeabilization by PhlyP and VCC, purified VCC was used to treat HaCaT cells. Cellular K^+ concentration was measured at various time points. The cellular K^+ level was continually decreasing under the attack of VCC during 60 min of incubation, and reached less than 40% of initial K^+ level within 20 min (Fig. 15b). Although both PhlyP and VCC can lead to significant loss of cellular K^+, the PhlyP-triggered efflux of K^+ happened more rapidly.

The recovery of cellular K^+ concentration after membrane damage is the hallmark of membrane resealing. In order to investigate the cellular K^+ restoration after PhlyP and VCC attack, HaCaT cells were treated with PhlyP and VCC briefly before re-cultured in medium without toxins (Fig. 15a). After incubation with PhlyP for 10 min, the cellular K^+ level in HaCaT cells was reduced to around 10%, but after re-culture for 2 h without toxin, cellular K^+ level increased to approximately 90%. The loss of cellular K^+ after treatment with VCC was similar to PhlyP. After 10 min, host cellular K^+ fell to less than 10%. However, even after re-incubation with culture medium for 2 h, the K^+ level did not recover (Fig. 15c).

Cellular recovery after PhlyP attack was also supported by microscopy data obtained by colleagues, who used extracellular products of P. damselae subsp. damselae (ECPs) to treat HaCaT cells before the cells were stained with PI. Cells were washed and re-cultured in medium for 1h before being staining with PI. Influx of PI happened within 8 min and the membrane was resealed again within 60 min (Fig 15d).

To further observe the time-dependent recovery of cellular K^+ in 24 h after treatments of PhlyP and VCC, HaCaT cells again were treated a second with PhlyP and VCC. Thereafter, the cells were re-cultured in medium for 24 h. It is obvious to see from the results that cellular K^+ level increased immediately following the re-culture in medium after PhlyP attack (at 15 min incubation in culture medium, the K^+ level was back up to ~50%). In 1 h after re-culture, the cellular K^+ concentration went up to ~90% compared with control group (Fig. 15e). After 24h, the K^+ level decreased again and maintained approximately ~70% (Fig. 15f). This loss from 90% to 70% might be caused by cell death (although the membranes were repaired, some target cells did not survive). In contrast, the loss of cellular K^+ triggered by VCC happened more slowly than by PhlyP, and after cells were re-cultured in medium, the cellular K^+ level remained low until cell death (Fig. 15g).

The data indicated that the small differences at the channel-forming regions of these two related small β-PFTs, PhlyP and VCC, brought significantly different kinetics of the changes of cellular K^+. To summarize, the pore-forming on target membranes by both PhlyP and VCC lead to major losses of cellular K^+. However, the loss triggered by VCC was slower yet gradually worsened beyond the level attained by PhlyP, and could not be restored. Although PhlyP caused strong loss of cellular K^+, the host cells recovered quickly after toxin removal, which indicated membrane resealing. Considering that PhlyP can result in PI (MW:668.4) influx, we speculate that it could make membranes permeable to Ca^{2+} as well, which led us to investigate cellular Ca^{2+} changes after the attack.

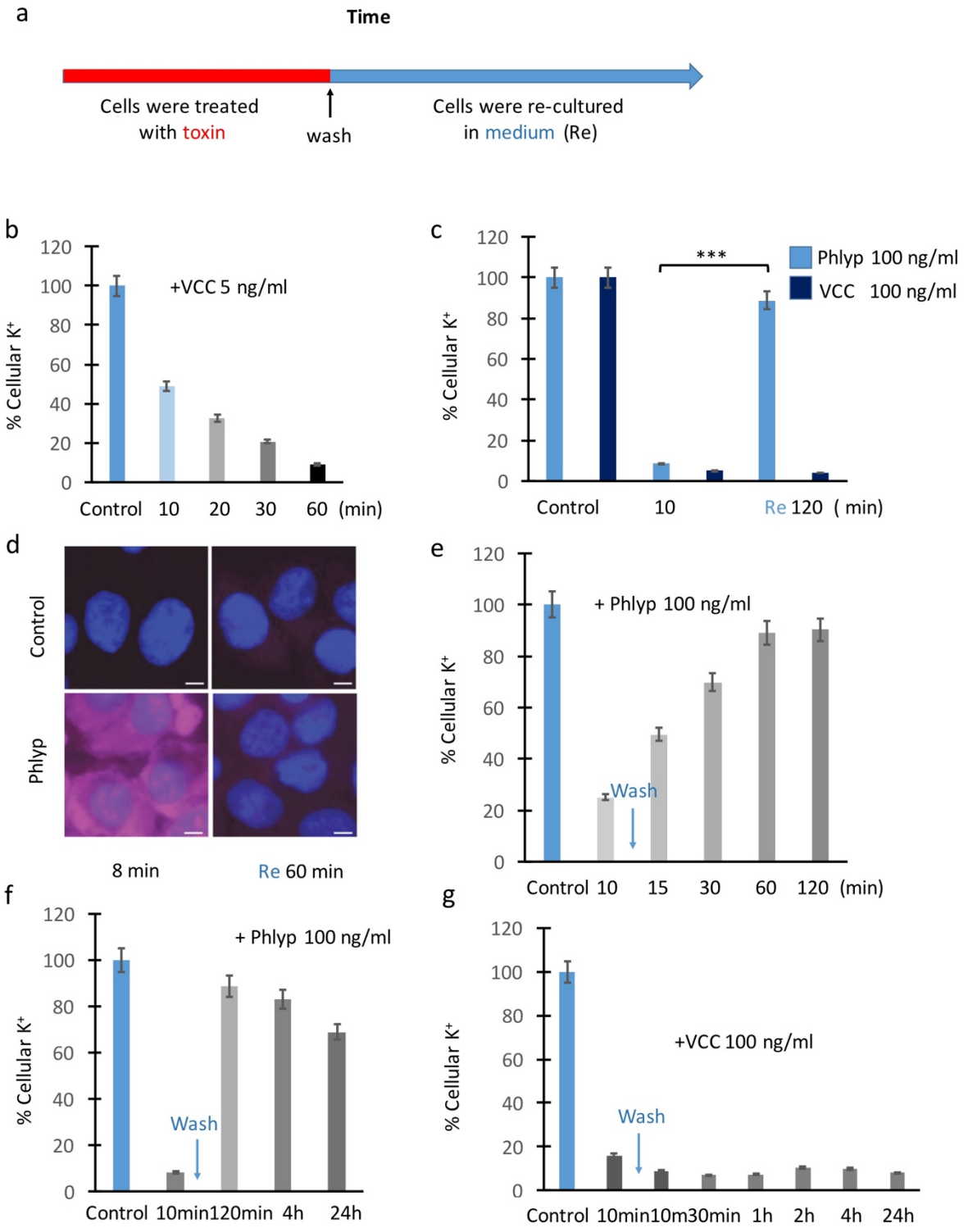

Figure 15: PhlyP triggers rapid but reversible loss of K^+ from HaCaT cells, while VCC induces slow, but irreversible loss of K^+. a, The procedure of cell treatment. Cells were first treated with a specific toxin for times indicated in figures. After washing, cells were re-cultured in medium. **b,** Cellular K^+ levels drop after VCC attack. Adhered HaCaT cells were incubated with VCC at 5 ng/ml before cellular K^+ concentration was measured after toxin treatment, wash and incubation for various periods of time. **c,** HaCaT cells were incubated with PhlyP and VCC at 100

ng/ml for 10 min respectively. After that, the cells were washed and re-incubated in medium again. Cellular K^+ concentration was measured by flame photometry in cell lysates 2 h later. **d,** ECPs containing PhlyP (extracellular productions of *P. d.* subsp. *d.* strain AR119) were used to treat HaCaT cells for 8 min at 37°C. The cells were stained with 50 µg/ml PI and Hoechst 33342. After washing, the cells were re-incubated in culture medium for recovery without ECPs. The non-toxigenic strain (Ø) was used as the control group. Representative pictures are shown here. Scale bar = 10 µm (von Hoven et al., 2017); for contributions see Appendix 2. **e,** Time-dependent cellular K^+ level after attack by PhlyP over 2 h. HaCaT cells were treated with PhlyP 100 ng/ml for 10 min before cells were re-cultured in medium again. Cellular K^+ concentration was measured by flame photometry in cell lysates after different times. **f,** Time-dependent cellular K^+ recovery over 24 h after PhlyP treatment. HaCaT cells were exposed to PhlyP 100 ng/ml for 10 min before cells were re-cultured in medium again. Cellular K^+ concentration was measured at 2 h, 4 h and 24 h. **g,** Time-dependent cellular K^+ recovery over 24 h after VCC treatment. HaCaT cells were exposed to VCC 100 ng/ml for 10 min before cells were re-cultured in medium again. Cellular K^+ concentration was measured at 10 min, 30 min, 1 h, 2 h, 4 h and 24 h. Values represent percentages of the results for untreated controls; mean values ± standard errors (SE) are shown ($n \geq 3$). Statistical significance was calculated with Student's *t*-test.

3.3 The kinetics of PhlyP and VCC-dependent Ca^{2+} influx is different

Whether a Ca^{2+} influx occurs in PhlyP-treated cells is relevant because cells can set up an efficient repair mechanism after attack by SLO, which is strictly Ca^{2+} influx dependent (Idone et al., 2008). Therefore, HaCaT cells treated with SLO served as a control group. This toxin triggered a notable rise of Fluo-8 AM fluorescence intensity, which indicates free Ca^{2+} increase (Fig. 16a). Extracellular products (ECPs) of *P. damselae* subsp. *Damselae* (ECP 306, i.e., mature PhlyP) were used to treat HaCaT cells after pre-incubation with Fluo-8 AM. There was a significant increase in fluorescence, while the non-toxigenic strain (TM) ECP group did not induce such a response (Fig. 16b). This result was important in that it revealed that extracellular products of a non-toxigenic strain do not elicit significant changes of the Fluo-8-signal, and that a functional *hlyA* gene (encoding pro-PhlyP) in that genetic background is sufficient to induce a massive increase of the signal.

These results were supported by experiments of others in our group, where purified PhlyP was used to treat HaCaT cells, which were pre-incubated with Fluo-8 AM.

Sequential images from video-microscopy showed that intracellular Ca^{2+} concentrations rise, causing strong fluorescence signals after 20 s. This is accompanied with blebbing of the plasma membrane, as shown in the images of (Fig. 16c).

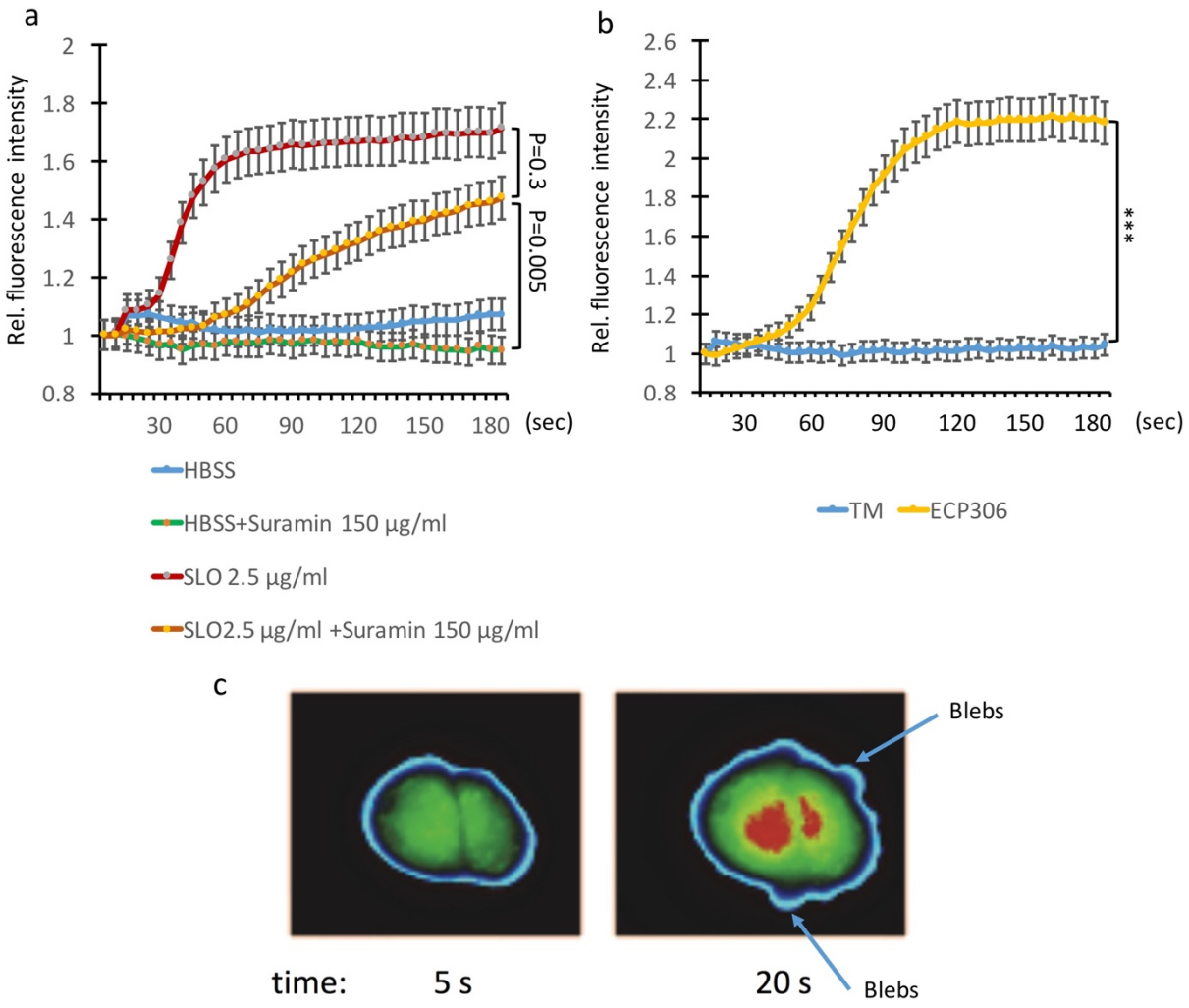

Figure 16: PhlyP (ECPs) triggers significant influx of Ca^{2+} similar to SLO, and activates the formation of blebs. a and **b,** Cells were loaded with Fluo-8 AM for 30 min and exposed to SLO (2.5 µg/ml), PhlyP (ECPs), fluorescence intensity was recorded at intervals of 5 s for a period of 3 min. **c,** HaCaT cells were pre-incubated with Fluo-8 AM before exposure of PhlyP 100 ng/ml. Sequential images from microscopy are shown here. False-colour means the intensities of the fluorescence signal: red represents high intensity, blue represents low intensity. Blebs are noted with arrows (von Hoven et al., 2017); for contributions see Appendix 2. Values represent percentages of the results for untreated controls; mean values ± standard errors (SE) are shown ($n \geq 3$). Statistical significance was calculated with Student's *t*-test.

The data indicates that PhlyP can trigger influx of Ca^{2+}, like SLO, which could account for the recovery of cellular K^+. Therefore, we conducted dose-response experiments on HaCaT cells to see changes of cellular Ca^{2+} concentrations dynamically after exposure of PhlyP or VCC. With toxin dose increase, the Fluo-8 AM fluorescence intensity values in the PhlyP-treated group were higher, and the increase was faster (Fig. 17a). In the VCC group, there was a lag period of nearly 60 s before the onset of increased fluorescence and the speed of signal increases was slower (Fig. 17b). Although both PhlyP and VCC triggered significant fluorescence signal increases, they required different time to initiate the increase and to reach maximum levels. This prompted the questions, 1) whether the signal increases triggered by PhlyP and VCC are caused by different mechanisms, and 2) what these mechanisms might be. We hypothesized that PhlyP might induce influx of extracellular Ca^{2+} through toxin pores, whereas VCC-induced increases of intracellular Ca^{2+} might be due to an influx through some cellular channel. Reportedly, P2 purinoceptors are involved in host cellular responses against PFTs and take part in regulation of Ca^{2+} influx (Michel et al., 1996; Schoenauer et al., 2014; Skals et al., 2011). Suramin is a broad spectrum inhibitor of P2X7 receptors. Here, we employed suramin to see whether it could influence Ca^{2+} influx triggered by PhlyP or VCC. Suramin moderately reduced the amplitude of PhlyP-triggered signal rises. Importantly, the increase of the fluorescence signal was not completely blocked (Fig. 17c). Similar results were also apparent in SLO-induced Ca^{2+} influx experiments (Fig 16a). In striking contrast, the VCC-triggered fluorescence increase was fully prevented by suramin (Fig. 17d).

That the Ca^{2+} signal increase by VCC can be blocked by suramin, suggested that the Ca^{2+} influx occurred through some targets of suramin, such as P2 receptors-protein-coupled receptors or associated channels. However, the Ca^{2+} influx triggered by PhlyP and SLO was significant and only moderately inhibited by suramin (Fig. 16a and 17c). Even though PhlyP belongs to the family of small β-PFTs, it appeared to be able to trigger Ca^{2+} influx independent of suramin-sensitive mechanisms. It became of interest to test if suramin and Ca^{2+} influx have an effect on cellular K^+ recovery after PFT-induced damage.

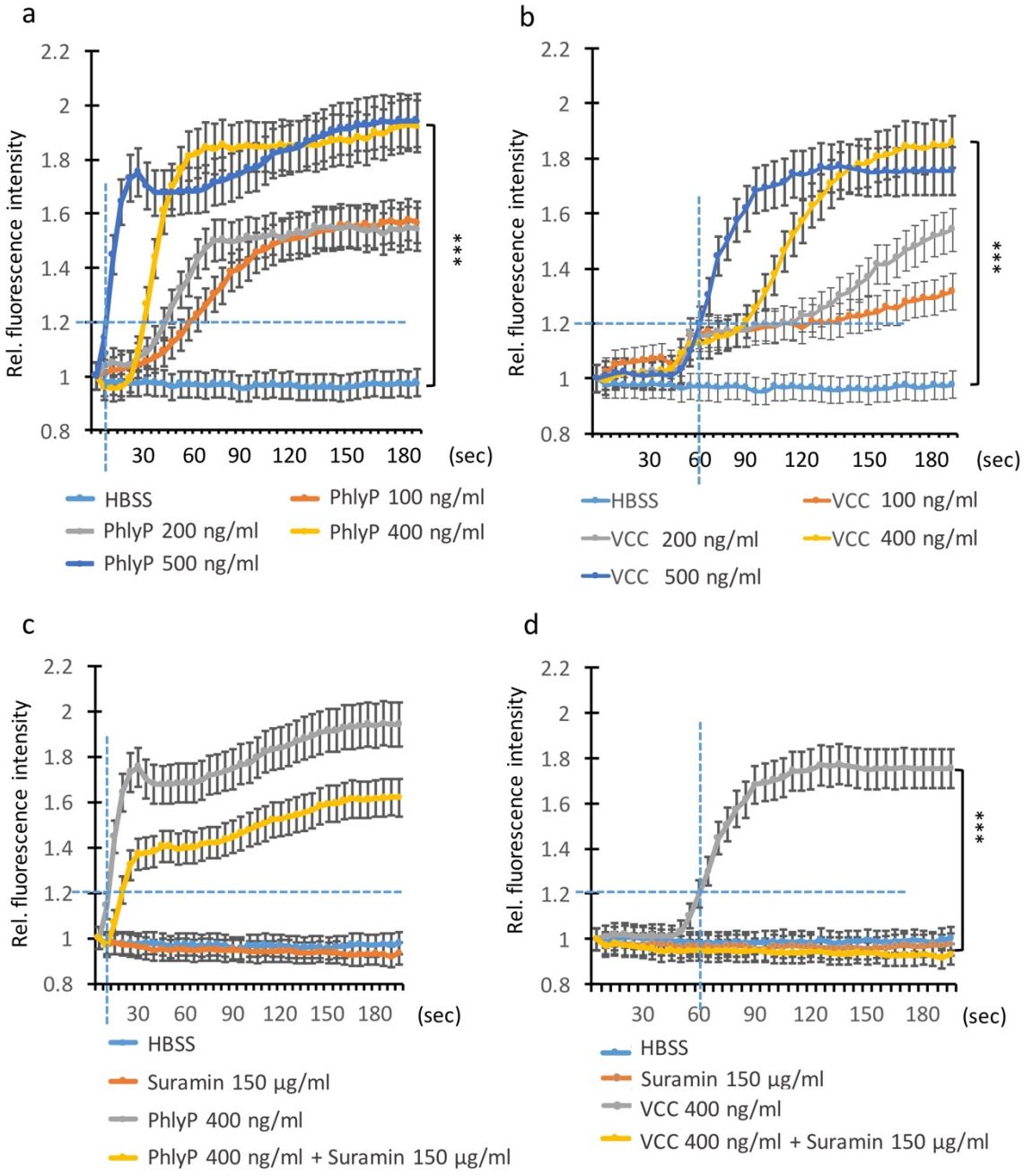

Figure17: PhlyP and VCC behave differently in toxin-induced cellular Ca^{2+} influx. a and **b,** Rapid, dose-dependent changes of intracellular Ca^{2+} concentration induced by PhlyP or VCC. HaCaT cells were pre-incubated with Fluo-8 AM before being exposed to various doses of toxins. Fluorescence intensity was recorded at intervals of 5 s for a period of 3 min. **c** and **d,** Cells were pre-treated or not with 150 µg/ml suramin. After that, Fluo-8 AM was loaded for 30 min with or without this inhibitor before the exposure of PhlyP or VCC (400 ng/ml). Fluorescence intensity was recorded every 5 s over 3 min. The blue dashed horizontal line demonstrates the threshold chosen to compare delayed time (intersection of x-axis and the red dashed vertical line). Data are percentages of the values for untreated groups; mean values ± SE are shown ($n \geq 4$). Statistical significance was calculated with Student's *t*-test.

3.4 Calcium influx after pore formation by PhlyP and VCC influences cellular potassium recovery

In order to investigate if cellular Ca^{2+} influx can influence cellular K^+ recovery after membrane permeabilization induced by PhlyP, HaCaT cells were treated with PhlyP before being re-cultured in medium with low Ca^{2+}- content (calcium free basal media containing only 1% FCS) for recovery of 2 h. The cellular K^+ level was measured in cell lysates. The results suggest that Ca^{2+} was required for cellular K^+ restoration in PhlyP-attack cell group (Fig. 18a).

Because suramin influenced Ca^{2+} influx induced by PhlyP and VCC experiments were performed to test potential effects of suramin on cellular K^+ replenishment. Suramin led only to a moderate inhibition of cellular K^+ recovery triggered by PhlyP (P= 0.02), but there was no obvious influence in the VCC group (Fig. 18 b and c). This suggests that P2XRs and associated pannexin channels are unlikely to be decisive for repair of the PhlyP pore.

Recovery of cellular K^+ is an indicator of plasma membrane repair after permeabilization by PFTs, and Ca^{2+} is an indispensable factor of cellular K^+ recovery after PhlyP attack. This led us to investigate whether downstream signalling pathways of Ca^{2+} dependent mechanisms involved in repair of large membrane pores, such as SLO pores, are involved in the membrane recovery from PhlyP attack.

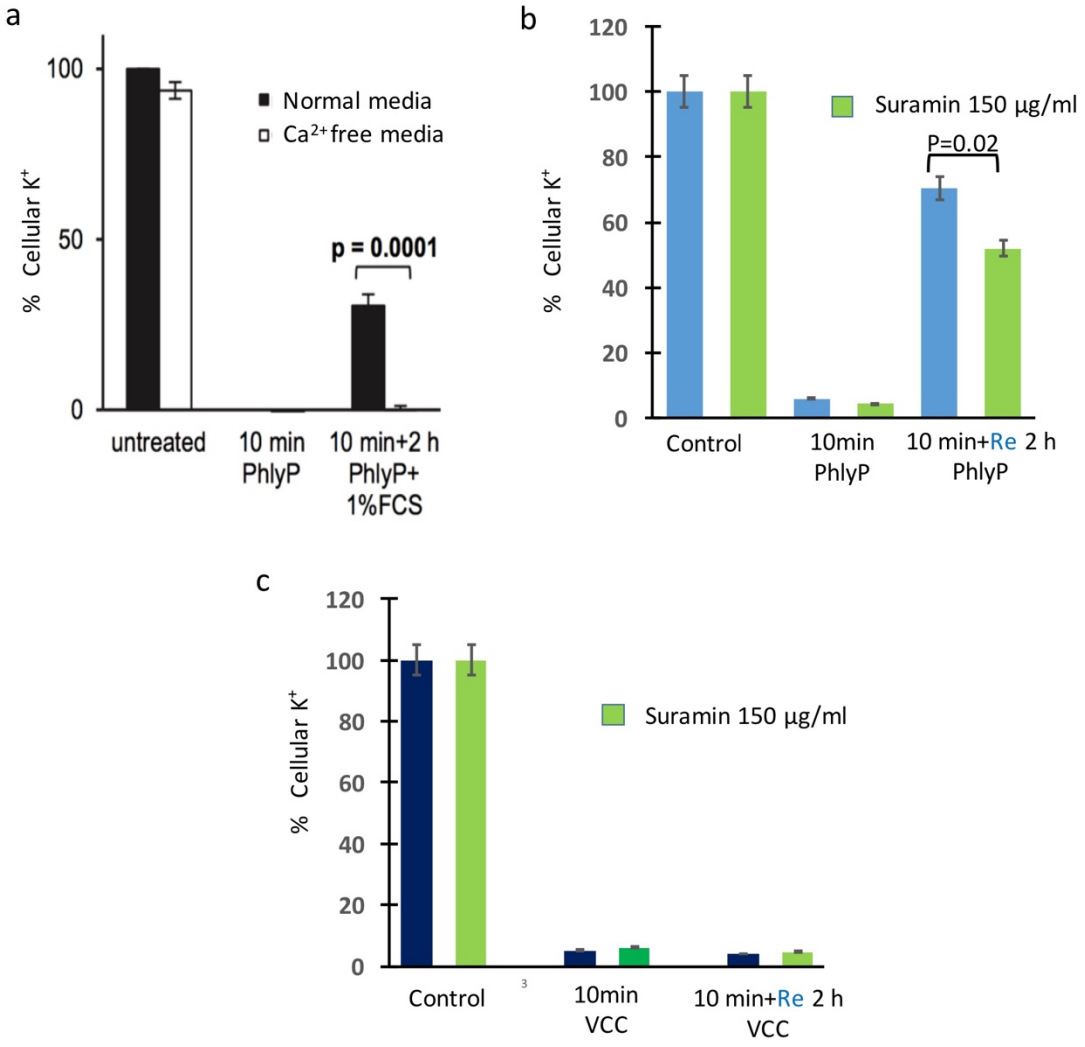

Figure 18: Ca^{2+} influx is indispensable for cellular K^+ recovery triggered by PhlyP. a, the cellular K^+ levels do not restore after PhlyP attack in Ca^{2+} depleted medium. HaCaT cells were cultured in normal or Ca^{2+} free medium with 1% FCS. After exposure of PhlyP 100 ng/ml for 10 min, the cells were washed and re-cultured in medium. K^+ concentration was measured by flame photometry in cell lysates (von Hoven et al., 2017); for contributions see Appendix 2. **b** and **c,** the recovery of cellular K^+ levels after PhlyP and VCC attack is not affected by suramin. HaCaT cells were pre-incubated or not with suramin 150 µg/ml for 30 min. After that, the cells were exposed to PhlyP and VCC 100 ng/ml for 10 min in medium with or without suramin. Toxins were removed and cells were re-cultured in medium with or without suramin for 2 h. The cellular K^+ concentration was measured by flame photometry in cell lysates. Data are percentages of the numbers for untreated groups; mean values ± SE are shown ($n \geq 4$). Statistical significance was calculated with Student's *t*-test.

3.5 PhlyP, but not VCC, triggers efficient lysosomal exocytosis

It is known that damaged cellular plasma membranes can fully recover after exposure to PFT, including SLO (Thelestam and Möllby, 1983; Walev et al., 2001). The efficient repair following membrane attack by large PFT, such as SLO, is strictly Ca^{2+} dependent (Walev et al., 2001; Stanisstreet, 1982; Morgan et al., 1986; Keefe D et al., 2005; Idone et al., 2008). Various down-stream mechanisms, such as exocytosis and endocytosis, are involved in Ca^{2+} dependent membrane repair. Here lysosomes serve as exocytic vesicles to fuse with the plasma membrane. This fusion reduces membrane stress and promotes endocytosis by releasing acid sphingomyelinase (ASM) followed by production of ceramide. The release of β-hexosaminidase and exposure of luminal Lamp-1 on the membrane surface are hallmarks of secretory exocytosis (Reddy et al., 2001). A schematic representation model of wounded membrane repair in response to large pore-forming protein SLO, is presented here (Fig. 19).

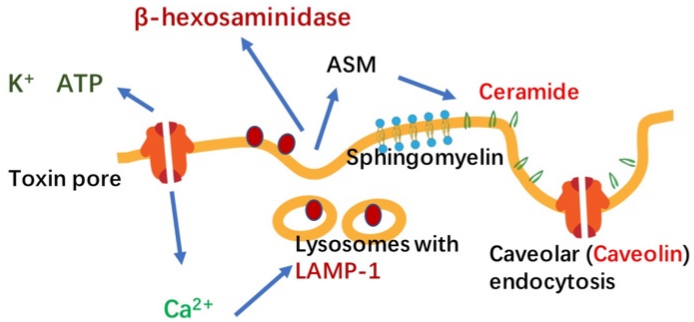

Figure 19: The current model of SLO-induced Ca^{2+}-dependent membrane repair mechanism. SLO-pores cause rapid Ca^{2+}-influx that trigger both exocytosis and endocytosis. The fusion of lysosomes with damaged membrane release β-hexosaminidase and ASM, which promotes endocytosis by formation of ceramide.

As β-hexosaminidase is released during lysosome exocytosis, the levels of β-hexosaminidase in culture supernatants can be used to measure lysosomal exocytosis (Rodríguez et al., 1997). Here, we used SLO treatment as a positive control group. As expected, SLO induced notable release of β-hexosaminidase out of HaCaT cells (Fig. 20a). After that, ECPs with mature PhlyP included were used to treat HaCaT cells. This treatment triggered significant β-hexosaminidase production, just like SLO did (Fig. 20b). Next, we compared β-hexosaminidase release after PhlyP and VCC treatment. At the same concentrations, PhlyP triggered strong β-hexosaminidase production

while VCC did not (Fig. 20c). No β-hexosaminidase release after VCC treatment was recorded, regardless of how high the levels of VCC were in cultures (Fig. 20d). As no release of lactate dehydrogenase (LDH) is caused by PhlyP (see Rivas et al. 2015) or SLO under the conditions of this experiment, β-hexosaminidase production reports exocytosis of lysosomes, not lysis of cells.

Further evidence that PhlyP, but not VCC activates a "classic" Ca^{2+} dependent membrane repair response is the appearance of the lysosomal marker protein Lamp-1 at the target cells membrane surface, as shown by others in our group. MEFwt cells were exposed to PhlyP or VCC and stained Lamp-1 was detected by fluorescence microscopy in PhlyP-treated cells; this was different from the VCC treated group (Fig. 20e).

SLO attacks epithelial cells resulting in rapid Ca^{2+} entry through toxin pores. This is the main trigger to activate lysosomal exocytosis and acid sphingomyelinase (ASM) release. ASM at the outside layer of the target PM will transform sphingomyelinase to ceramide. Ceramide triggers internalization of wounded membranes via caveolar endocytosis. Therefore, Ca^{2+} triggered exocytosis of lysosomal ASM is considered indispensable for repair of large membrane pores (Corrotte et al., 2013). In order to investigate whether ASM is involved in the case of membrane repair after attack by PhlyP, we used desipramine (DPA), an inhibitor of ASM, which has been demonstrated to impair membrane resealing in the case of SLO (Tam et al., 2010). After exposure to toxin, HaCaT cells were re-cultured in medium to induce cellular K^+ recovery. Results showed, DPA had no influence on cellular K^+ loss after VCC treatment (Fig. 21a). More importantly, DPA had no significant effect on the initial loss of K^+ caused by PhlyP, but it reduced replenishment of cellular K^+. The effect was more pronounced when DPA was combined with blebbistatin, a compound which inhibits membrane blebbing (von Hoven et al.,) (Fig. 21b).

The role of ASM was verified by others in the group who investigated if ceramide, the product of ASM-catalysed break down of sphingomyelin, is indeed produced after PhlyP attack. MEFwt cells were treated with or without PhlyP and VCC, and cells were stained with ceramide antibody. Fluorescence microscopy pictures showed cells were

mostly ceramide positive in PhlyP-treated group, while no fluorescence signal was detected in VCC-treated group (Fig. 21c).

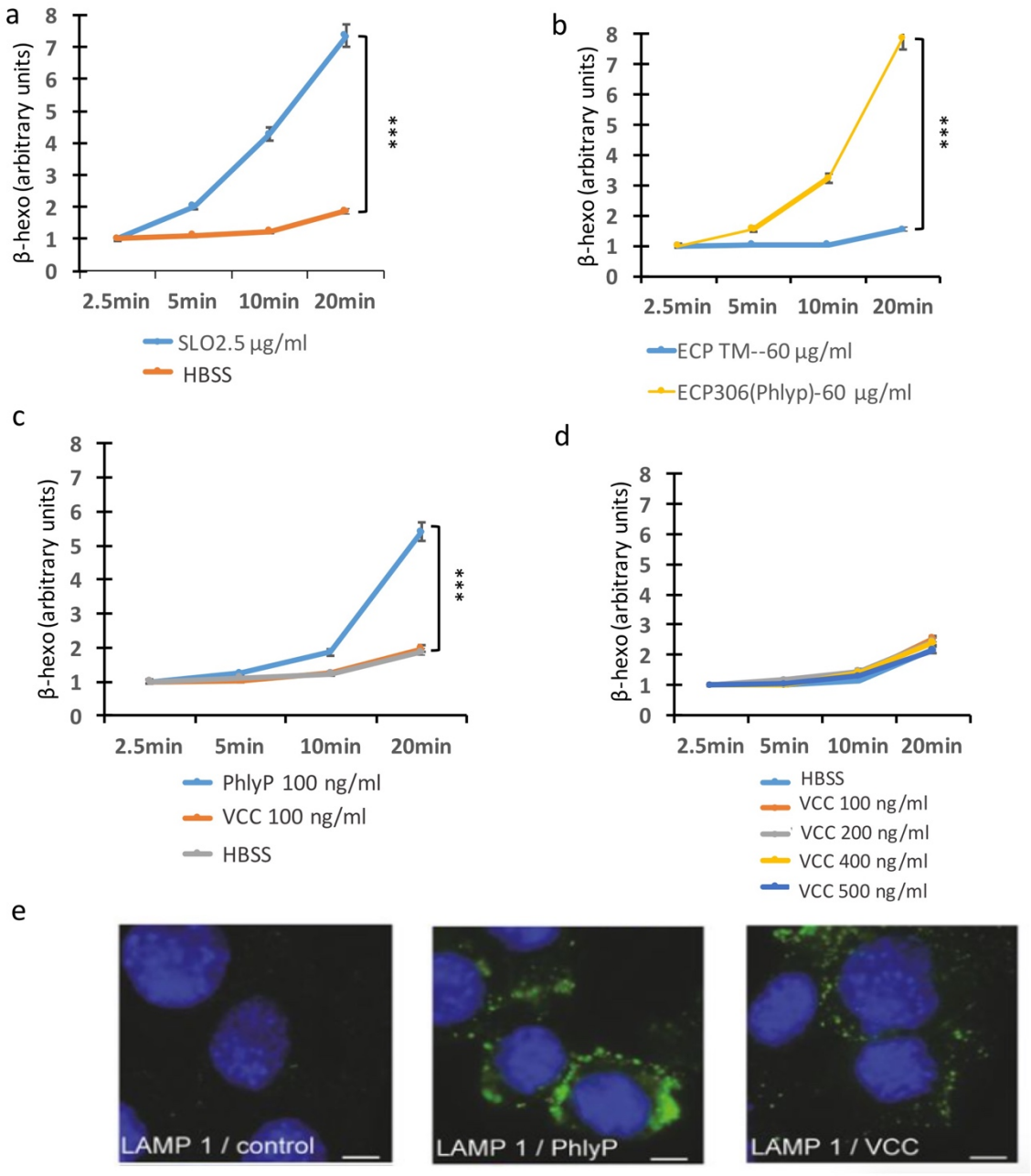

Figure 20: PhlyP, but not VCC, activates secretory exocytosis. a, SLO triggers the release of β-hexosaminidase. HaCaT cells were exposed to SLO 2.5 µg/ml in HBSS at 37°C for various times before measurement of β-hexosaminidase in supernatants. The control group was treated with only HBSS. **b**, PhlyP triggers the release of β-hexosaminidase. HaCaT cells were exposed to ECP of a nontoxigenic strain (TM) and AR306 (PhlyP containing) in HBSS for various times before measurement of β-hexosaminidase in supernatants. **c,** PhlyP attack can induce strong release of β-hexosaminidase, but not VCC. HaCaT cells were exposed to PhlyP and VCC 100 ng/ml in HBSS

at 37°C for various times before measurement of β-hexosaminidase in supernatants. The control group was treated only with HBSS. **d,** the dose-dependent experiment of VCC induced β-hexosaminidase production. The experiment was performed as described in the legend to panel b except that various concentrations of VCC were used. **e,** Lamp-1 proteins are activated by PhlyP, not VCC. MEFwt cells were treated with PhlyP or VCC 100 ng/ml for 10 min at 37°C. After that, cells were stained for LAMP-1 and cellular nuclei. Scale bar = 10 μm (von Hoven et al., 2017); for contributions see Appendix 2. Data are percentages of the numbers for untreated groups; mean values ± SE are shown ($n \geq 3$). Statistical significance was calculated with Student's *t*-test.

The inhibitory effect of DPA and detection of ceramide supported the idea that PhlyP activates known Ca^{2+}-dependent repair mechanisms. This led to further work to investigate if caveolin as part of the endocytosis machinery was involved in this recovery from PhlyP attack. One pilot study of β-hexosaminidase release trigged by PhlyP in MEFwt and MEFcav$^{-/-}$ was made in the frame of this thesis. It showed that deficiency of caveolin made MEF more sensitive to PhlyP, in that it led to enhanced production of β-hexosaminidase (Fig. 21d). This result supported the idea that caveolin might play protective roles during host cells defence against the small β-PFT, PhlyP.

In a series of experiments conducted by colleagues in our laboratory, MEFwt and MEFcav$^{-/-}$ cells were treated with PhlyP to investigate influx of PI by flow cytometry. The results showed that 27.6% of MEFwt cells were stained with PI in 5 min after PhlyP attack, but later in 15 min, this number went down to 8.6%. Fraction decreased that was telling some damaged cell membrane were resealed and PI was excluded by the cells. After 45 min, three fourths of the MEFwt cells recovered to healthy conditions, which emphasised the strong protective role of caveolin. However, this fraction increased to three fourths of MEFcav$^{-/-}$ cells highly positive for PI (Fig. 21e).

Thus far, evidence had accumulated suggesting that PhlyP, a small β-PFT, can activate membrane repair responses so far seen only in response to large PFTs, such as SLO. Cells were able to elicit a Ca^{2+}-dependent membrane repair mechanism to reseal the wounded PM after pore formation by PhlyP, whereas this did not happen after attack by VCC, another small β-PFTs. The difference in responses of host cellular ion balance, the influx of PI, and the membrane repair triggered by PhlyP and VCC, might be at least in part due to the different channel sizes. We considered the narrow points of the channels of potential relevance for this difference.

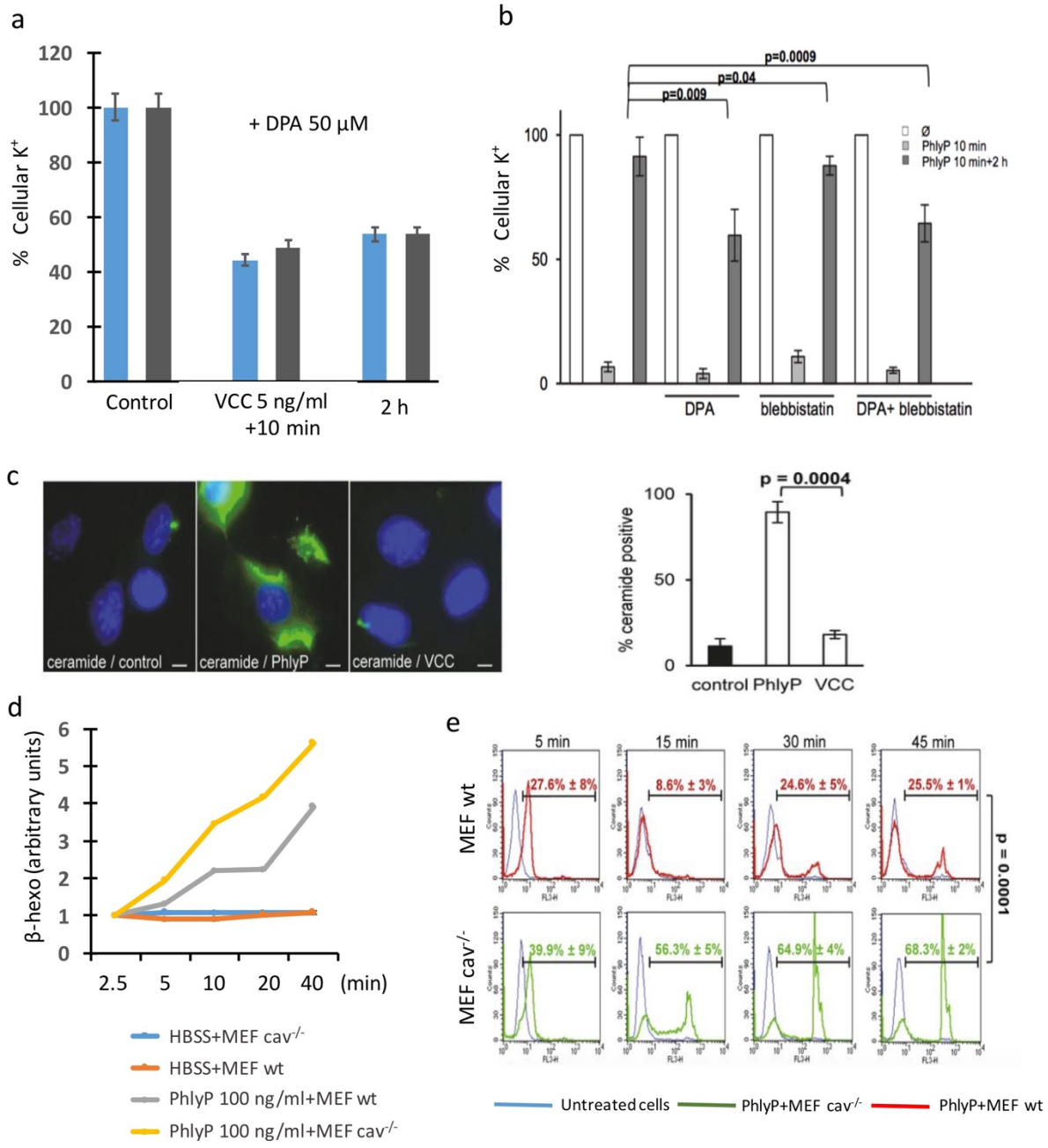

Figure 21: Further evidence for a role of the "wounded membrane response" during cell autonomous defense against PhlyP. a, DPA, inhibitor of acid sphingomyelinase (ASM), does not aggravate the loss of cellular K^+ levels after membrane pore formation by VCC. HaCaT cells were pre-incubated or not with DPA 50 µM for 30 min. After that, cells were exposed to VCC 50 ng/ml for 10 min in medium with or without DPA. The cells were re-cultured in medium with or without DPA for 2 h. Cellular K^+ concentrations were measured by flame photometry in cell lysates. **b**, HaCaT cells were pre-incubated or not with desipramine (DPA), blebbistatin or the combination of DPA and blebbistatin (50 µM, respectively). After exposure of 100 ng/ml PhlyP for 10 min, the cells were re-cultured in medium for 2 h recovery before K^+ concentrations were measured by flame photometry in cell lysates (von Hoven et al., 2017); for contributions see Appendix 2. **c**, MEFwt cells were treated with or without PhlyP or VCC at 100 ng/ml for 8 min. After that, the cells were

stained for ceramide and nuclei. Immunofluorescence microscopy was used to count ceramide-positive cells. Graph representation of data from 150 cells in each group; mean values ± SE are shown (*n* = 3). Scale bar = 10 µm (von Hoven et al., 2017); for contributions see Appendix 2. **d,** A pilot study to test whether caveolin-deficient cells can affect the release of β-hexosaminidase after PhlyP attack (*n*=1). **e,** MEFwt or MEFcav$^{-/-}$ cells were treated with or without PhlyP ECPs (3 µg/ml total protein) for various indicated times. After that, the cells were stained with PI for 1 min before being analysed by flow cytometry. Percentages of PI-positive cells counted by instrument are indicated; mean values ± SE are shown (*n* = 3) (von Hoven et al., 2017); for contributions see Appendix 2. Data are percentages of the numbers for untreated groups; mean values ± SE are shown (*n* ≥ 3 for a-c and e). Statistical significance was calculated with Student's *t*-test.

3.6 Narrowing the PhlyP pore channel and widening the VCC pore channel by mutagenesis

Presumably, PhlyP pores have a smaller amino acid residue serine (S) at their narrow point compared with the larger tryptophan (W) in the VCC pore (von Hoven et al., 2017). The W in the channel narrow point of VCC heptameric pore resembles to the "φ-clamp" structure in the similar heptameric pore formed by anthrax toxin that limits the quantity of passing ions or dyes (Krantz et al., 2005). On the contrary, the S341 residues in the PhlyP toxin amino acid sequence, which are thought to be the narrow point of the PhlyP pore, would form a larger channel narrow point, and therefore pose less resistance to the flux of ions or dyes. Hence, mutagenesis experiments were performed to exchange W318 in the amino acid sequence of VCC and S341 in PhlyP thus producing PhlyP with W (PhlyP S/W) and VCC with S (VCC W/S). Mutation was done using the QuikChange II site-directed kit instructions as described in material and methods part (Fig. 22a). After amplification and extraction, desired plasmid DNA were verified by DNA sequencing. Expression of plasmids was achieved in NEB Shuffle Competent *E. coli.* A schematic diagram of the process of Site-Directed Mutagenesis and the domain structure sketch are shown (Fig. 22b). Genetically modified toxins were used to test the influence of small changes of pore channel width (the swap does not lead to significantly different charge) on cellular Ca^{2+} influx and recovery responses.

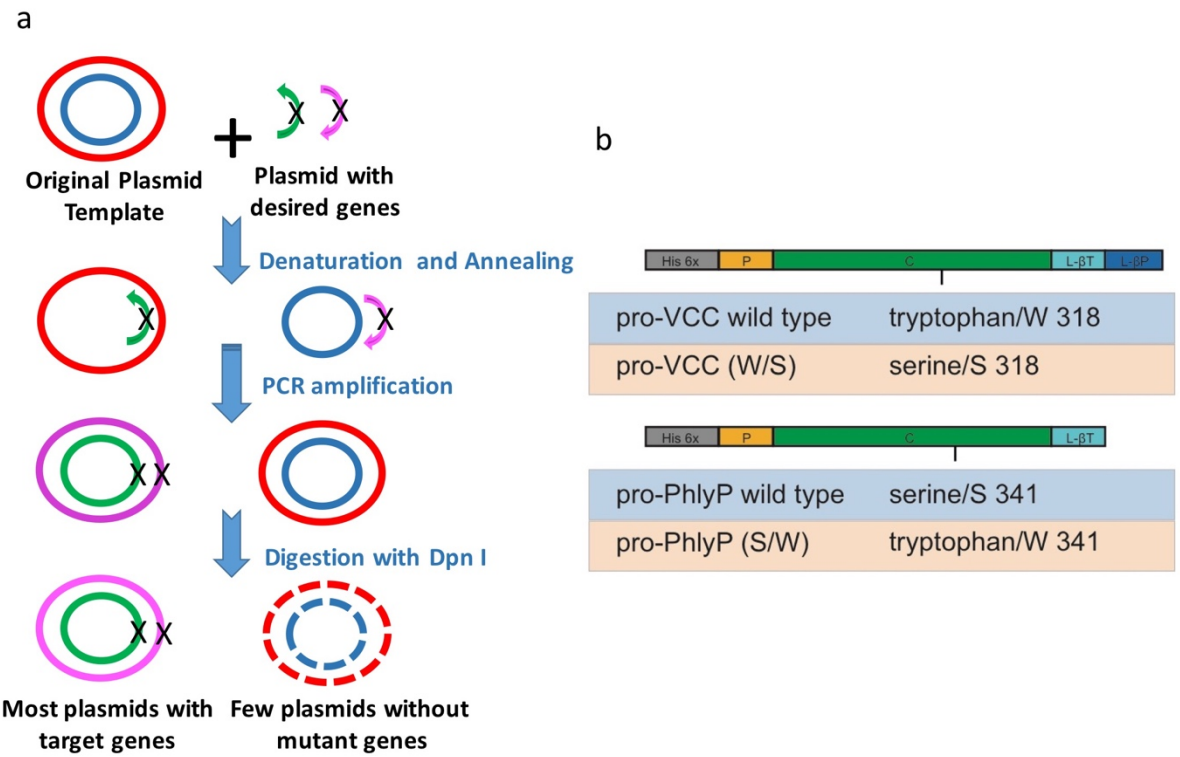

Figure 22: Swapping residues at the narrow point of PhlyP and VCC by mutagenesis. a, A schematic diagram of the principle for Site-Directed Mutagenesis. **b,** The domain structures sketch map of pro-PhlyP, pro-VCC and the mutants pro-PhlyP S/W and pro-VCC W/S. P, prodomain; C, cytolysin domain; L-βT, β-trefoil lectin domain; L-βP, β-prism lectin domain.

3.7 Residues at the pore channel´s narrow points impact Ca^{2+} influx

After the generation of pro-PhlyP S/W and pro-VCC W/S, we investigated the influence on Ca^{2+} influx induced by wild type and mutant toxins. Suramin was used to reduce the effect of P2X receptors. HaCaT cells were pre-incubated with Fluo-8 AM and exposed to either wild type or mutant toxins. Then, fluorescence intensity was measured to record changes of cellular Ca^{2+} levels. Interestingly, though both the wild type pro-PhlyP and mutant pro-PhlyP S/W triggered similar increases in fluorescence signal (probably corresponding to large Ca^{2+} influxes), pro-PhlyP S/W caused a lower rise in fluorescence in the presence of suramin (Fig. 23a and b). Although wild type VCC had the same effect on the increase of fluorescence as mutant VCC, pro-VCC W/S showed significantly higher suramin-insensitive signal rise compared to wild type VCC (Fig. 23c and d).

To sum up, when the channel width of the PhlyP pore is decreased by introducing a tryptophan residue at the channel narrow point (instead of the natural serine), the suramin-insensitive part of enhanced fluorescence intensity decreases substantially. Conversely, when the diameter of the VCC pore channel is widened as in the VCC W/S pore, the suramin-insensitive Ca^{2+} influx increased significantly. These results prompted us to investigate the toxicity and ability of mutants to trigger membrane repair.

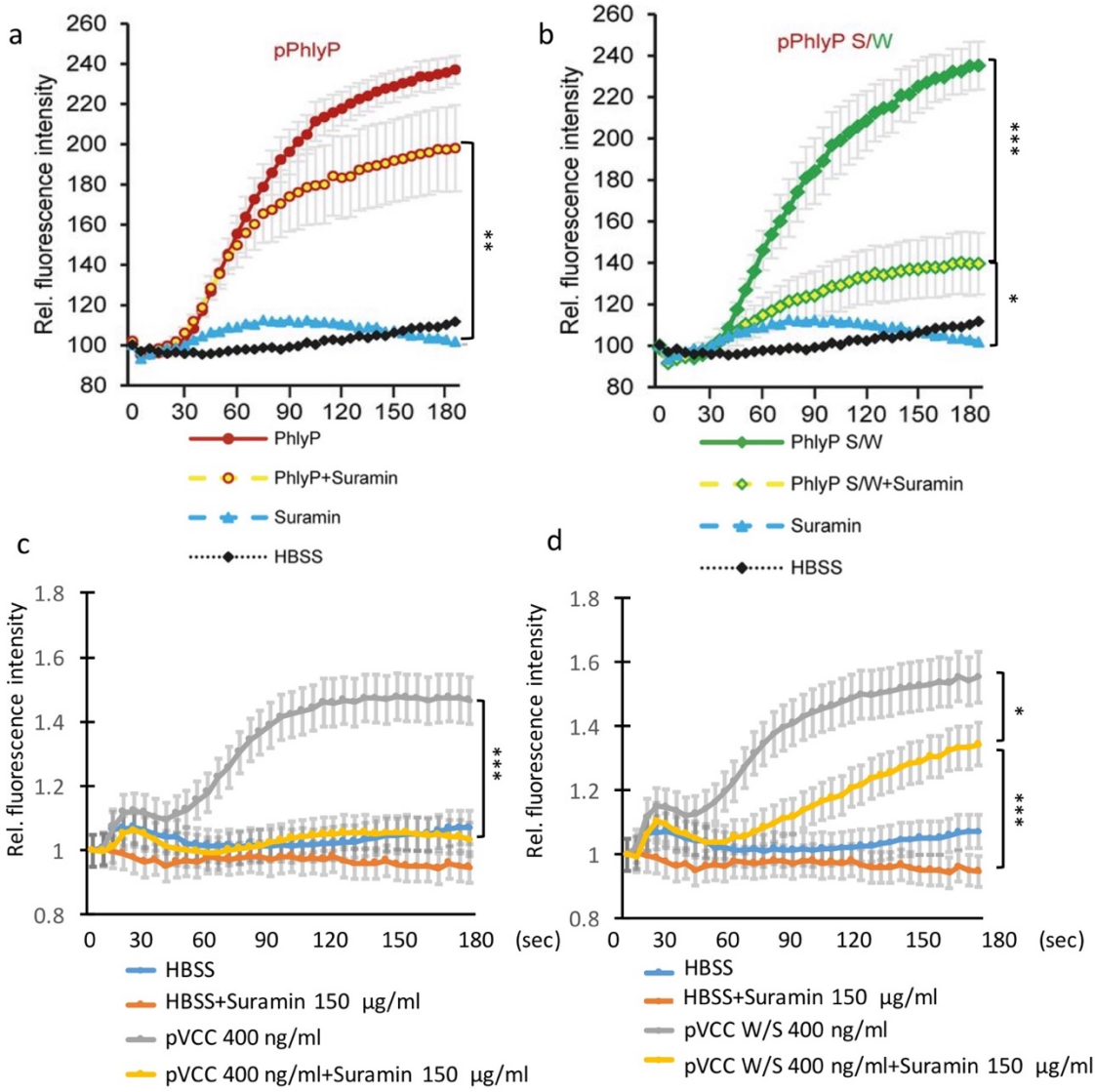

Figure 23: Pore channel changes influence cellular Ca^{2+} influx. a and **b,** pro-PhlyP S/W caused strong increase of cellular Ca^{2+} concentration, like PhlyP, but suramin blocked this effect more than in the pro-PhlyP group. HaCaT cells were treated with or without suramin 150 µg/ml for 30 min before being loaded with Fluo-8 AM. After that, the cells were treated with pro-PhlyP and pro-PhlyP S/W at 400 ng/ml. The fluorescence intensity was recorded every 5 seconds for 3 min (von Hoven et al., 2017); for contributions see Appendix 2. **c** and **d,** VCC W/S mutant permeabilization induced strong Ca^{2+} influx, which could not be blocked by suramin. HaCaT cells were exposed to 150 µg/ml

suramin or not for 30 min before being loaded with Fluo-8 AM in the presence of absence of this inhibitor. After that, cells were treated with VCC (PV1) or VCC W/S (PV3) at 400 ng/ml. The fluorescence intensity was recorded every 5 seconds for 3 min. Mean values ± SE are shown ($n \geq 5$). *P*-values were determined with Student's *t*-test.

3.8 Mutant PhlyP S/W is of lower primary toxicity and triggers weaker recovery responses than wild type PhlyP. VCC W/S is more toxicity than wild type VCC

Single amino acid mutagenesis of pro-PhlyP and VCC had notable effects on Ca^{2+} influx. Then the next question was whether these changes to pore channels also impact primary toxicity and recovery responses. The results indicated that, compared with wild pro-PhlyP, mutant pro-PhlyP S/W decreased the production of β-hexosaminidase, reduced PI influx, and weakened K^+ recovery; while VCC W/S triggered more β-hexosaminidase release and PI-influx than wild VCC. Cell recovery did not happen in either mutant or wild VCC groups (Fig. 24a, b and c). A schematic diagram of the results is shown here (Fig. 24d).

The results are consistent with suramin-insensitive Ca^{2+} influx as a decisive parameter for repair (the assumption being that the increase of cellular Ca^{2+} in response to PhlyP is due to Ca^{2+} influx) VCC W/S induced more suramin-insensitive Ca^{2+} influx, thus leading to more pronounced membrane damage (PI influx) and subsequent β-hexosaminidase release. Pro-PhlyP S/W pores have a narrowed channel and induce less suramin-insensitive Ca^{2+} increase, PI influx and less β-hexosaminidase release. Correspondingly, fewer cells recovered from permeabilization by pro-PhlyP S/W. Wild type pro-PhlyP triggers strongest suramin-insensitive Ca^{2+} influx, thus activating effective cell repair responses. It seems that suramin-insensitive Ca^{2+} influx after toxin attack is the decisive for triggering membrane repair in the case of PhlyP.

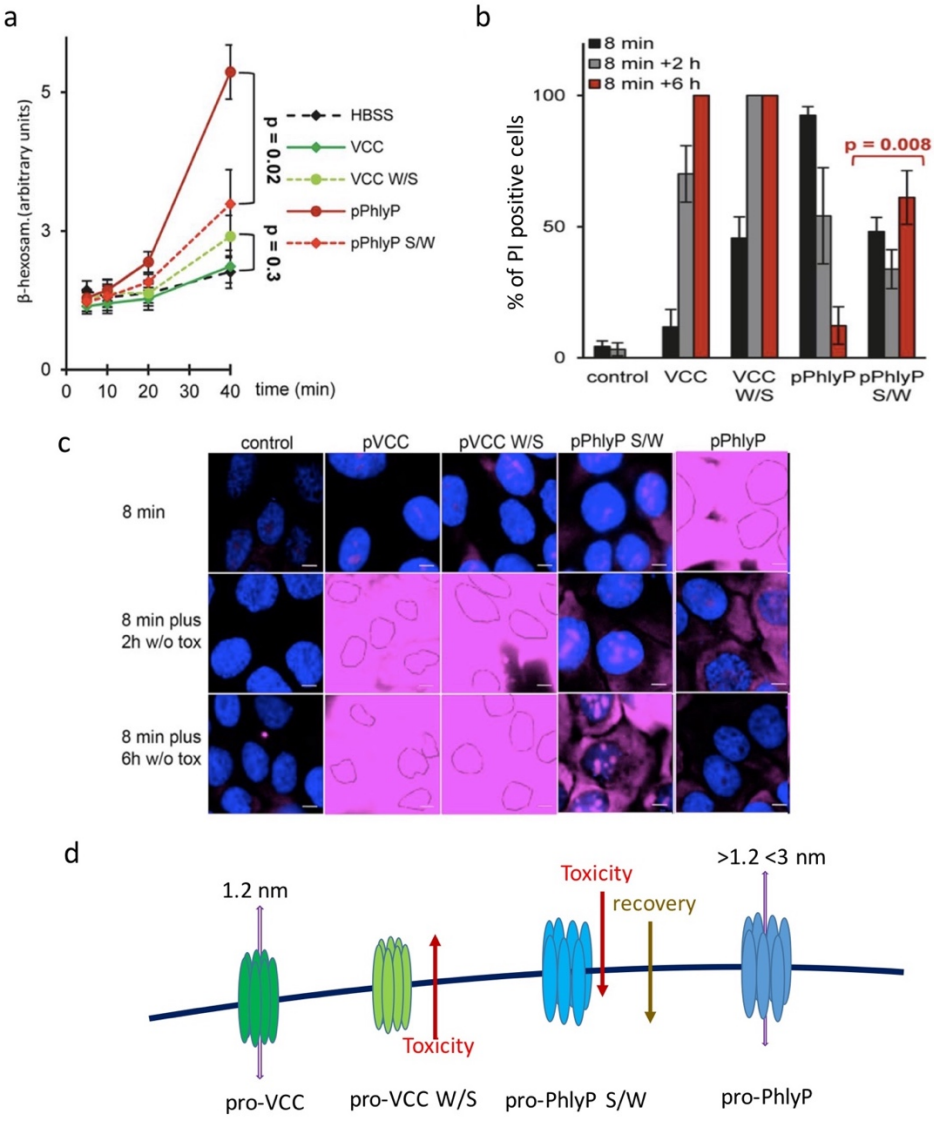

Figure 24: PhlyP S/W: less primary damage and weaker recovery responses than wild type pro-PhlyP toxin. VCC W/S: is more toxic than wild type VCC

a, HaCaT cells were exposed to the indicated toxins (100 ng/ml) for different times and then β-hexosaminidase was examined in supernatants; for contributions see Appendix 2. **b**, PI-positive cells were evaluated and summarized in graph of percentages based on panel C. For each group more than 100 cells were assessed; for contributions see Appendix 2. **c**, HaCaT cells were incubated with pro-VCC, pro-VCC W/S, pro-PhlyP or pro-PhlyP S/W 100 ng/ml respectively for 8 min. After that, 8 min cells were washed and immediately exposed to PI for 1 min. 2 h and 6 h recovery group cells were washed too and re-cultured in normal medium again before incubation with PI dye. Cells were finally fixed and analysed by fluorescence microscopy (von Hoven et al., 2017); for contributions see Appendix 2. **d**, Schematic summary of the relationship between pore channel changes and the influence of pore channel changes on toxicity and cellular recovery response. Mean values ± SE are shown ($n \geqslant 3$). *P*-values were determined with Student's *t*-test.

3.9 A mixture of PhlyP and VCC causes large and rapid Ca^{2+} influx in HaCaT cells, but cells fail to recover

As we can see from the above results, with increases of toxin pore width, suramin-insensitive Ca^{2+} levels rise, and the host cellular recovery responses are getting stronger (from mutant PhlyP S/W to wild type PhlyP). Therefore, the suramin-insensitive part of Ca^{2+} influx plays a crucial role in the activation of Ca^{2+} dependent repair mechanism. Next, we wished to know, whether PhlyP-induced rises of cellular calcium levels could cross-protect cells from a simultaneous attack by VCC; see (Fig. 25a). Combination experiments showed that a mixture of toxins induced sustained loss of cellular K^+ and no recovery, just as VCC did alone (Fig. 25b), though a mixture of toxins brought substantial and rapid Ca^{2+} influx signal rise (Fig. 25c).

These simple combination experiments indicated that a rise of cellular Ca^{2+} concentration sufficient to trigger repair of PhlyP pores, cannot prevent sustained VCC-induced membrane damage. Although it has not been formally excluded in this experiment it appears unlikely that cell populations attacked by one PFT are refractory to the other. Then, the question remains why VCC seems to subvert repair. Looking at the available data, it appears that Ca^{2+} dependent repair mechanism act locally. In other words, only if there is enough Ca^{2+} entry through a toxin pore, it can be removed by the “canonical” Ca^{2+} dependent pathways.

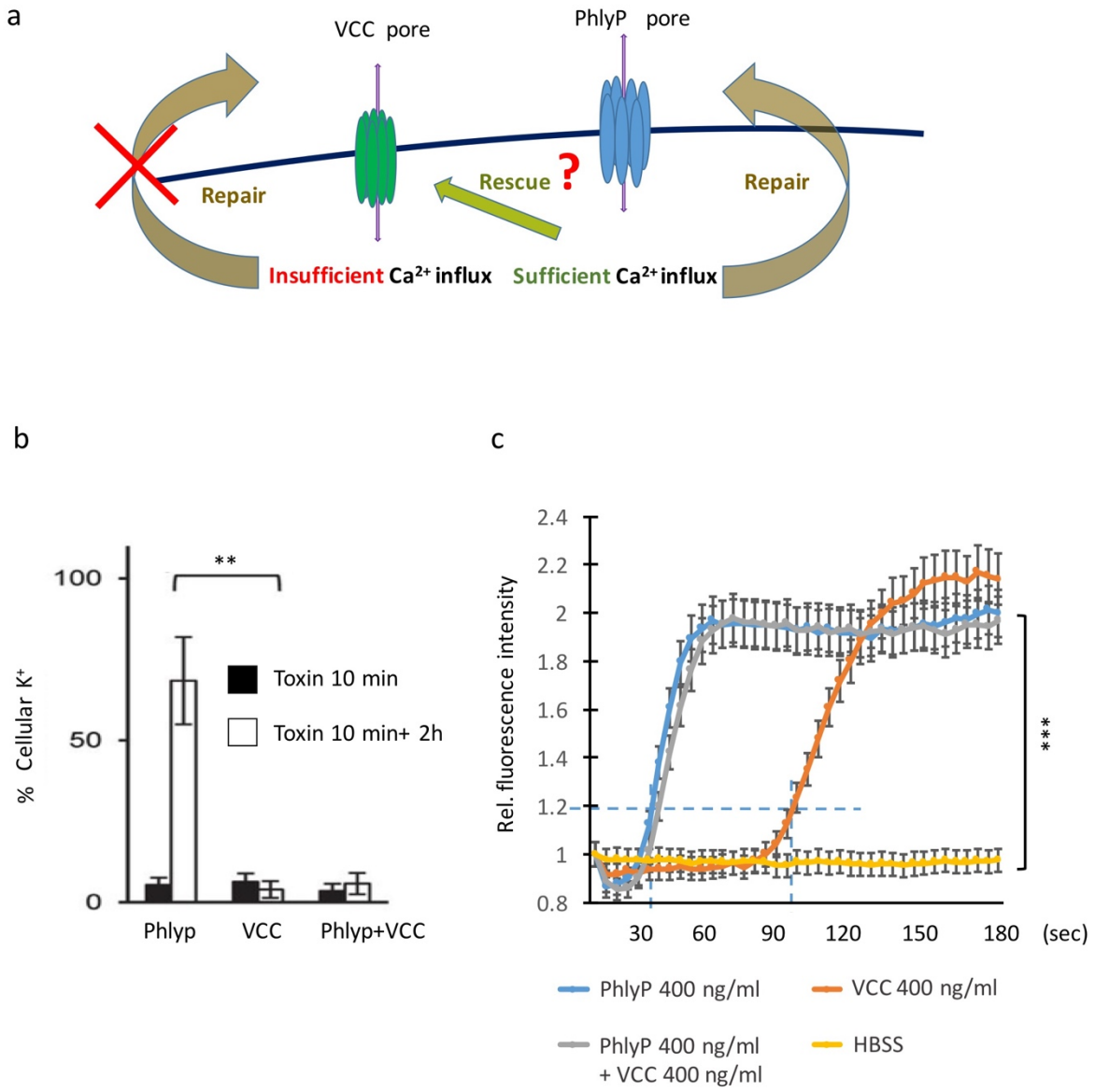

Figure 25: A mixture of PhlyP and VCC toxins induces large and rapid Ca^{2+} influx signals, but fails in K^+ recovery. a, a working hypothesis that Ca^{2+} influx triggered by PhlyP might rescue from simultaneous attack by VCC. **b,** HaCaT cells were treated with either VCC, or PhlyP individually, or a mixture of both toxins (100 ng/ml of each) and incubated for 10 min at 37°C. After that, the cells were washed and cellular K^+ was measured (black bars), or cells were washed and subsequently incubated for 2 h in toxin-free medium before cellular K^+ was measured (white bars); for contributions see Appendix 2 (von Hoven et al., 2017). **c**, membrane pore-forming by the mixture of PhlyP and VCC induced strong Ca^{2+} influx, which behaved like PhlyP alone. HaCaT cells were pre-incubated with Fluo-8 AM for 30 min before exposure to PhlyP, VCC and their mixture. The fluorescence intensity indicates cellular Ca^{2+} levels. Values represent percentages of the results for untreated control groups. The dashed horizontal line indicates the threshold used to compare lag times (intersection of x axis and dashed perpendicular line). Mean values ± SE are shown ($n \geq 3$). *P*-values were determined with Student's *t*-test.

Part II: Secondary membrane damage caused by small PFTs

3.10 The inhibition of MLKL oligomerization does not influence pro-PhlyP toxicity and secretory exocytosis

As shown above, a high concentration of VCC far beyond the lethal threshold can lead to significant Ca^{2+} influx within the order of a minute, which however, does not seem to occur through the VCC toxin pores. This indicates that other membrane channels may be involved. Previously, it has been demonstrated that α-toxin forms small pores or large pores depending on the concentration of toxin (Walev et al., 1993). Massive free Ca^{2+} entry induced by high level of toxins in cells raises the possibility that large pores are involved, and recent developments offer potential clues. Thus, mixed lineage kinase domain-like oligomers (MLKL) form pores at the inner membrane during necroptosis (Chen et al., 2016; Cai et al., 2014).

Considering that PFTs may act as stimulus to trigger necroptosis and lead to cell death, necrosulfonamide (NSA), the chemical inhibitor of MLKL N-terminal domain can be used to test if MLKL pores play a role in toxin attack. In order to see influences on toxin primary toxicity and cellular repair responses induced by NSA, K^+ efflux was measured after treatment of PhlyP with the presence or absence of NSA in HaCaT cells. The results indicated that the NSA group had no difference with control group (Fig. 26a). Thus, MLKL did not modulate PhlyP's ability to disturb membrane integrity.

The release of β-hexosaminidase triggered by PFTs is a hallmark of exocytosis, an important step to the removal of pores and cellular recovery. Therefore, here β-hexosaminidase production was examined after treatment with PhlyP, with or without NSA, in HaCaT cells. Again, NSA did not make any difference (Fig. 26b). These experiments demonstrate that MLKL oligomerization is not necessary for two early changes triggered by PhlyP: loss of potassium and secretory exocytosis (the latter implying that MLKL is also not involved in calcium influx at this point).

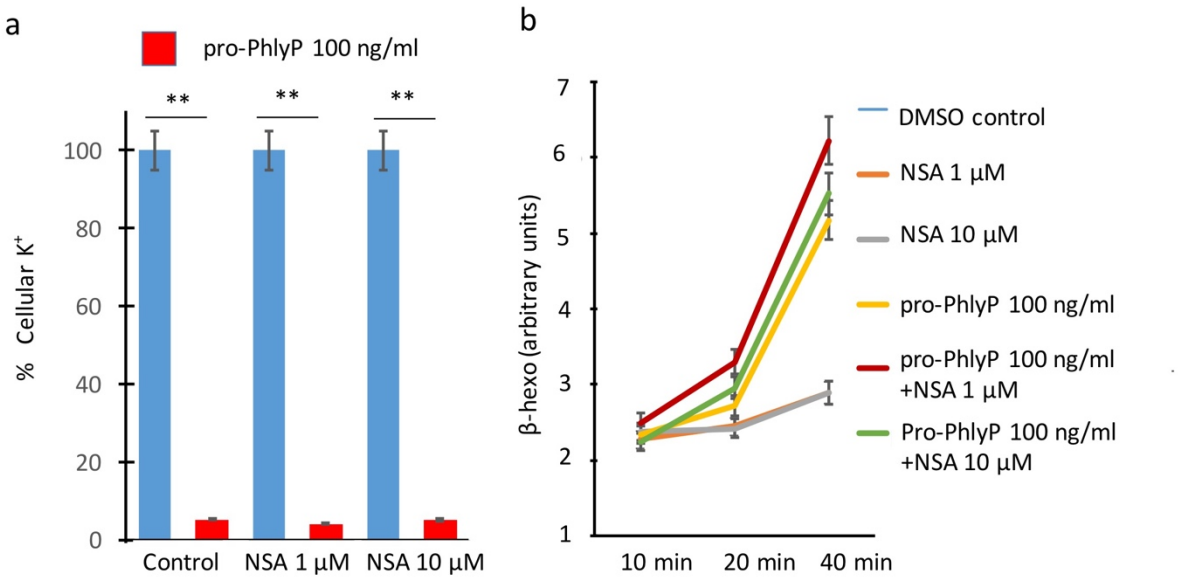

Figure 26: The inhibition of MLKL oligomerization does not influence pro-PhlyP toxicity and the host cellular recovery responses. a, HaCaT cells were pre-incubated with or without NSA for 30 min and then exposed to pro-PhlyP 100 ng/ml for 20 min. After that, cells were washed and lysed before cellular K^+ was measured. **b,** HaCaT cells were pre-incubated with or without NSA for 30 min and then exposed to pro-PhlyP 100 ng/ml in the presence or absence of NSA. Supernatant was collected at the indicated time points before β-hexosaminidase was measured. Mean values ± SE are shown ($n \geq 3$). *P*-values were determined with Student's *t*-test.

3.11 GSDMD channel inhibitor (lanthanides) inhibits primary damage of PhlyP and reduces cellular repair response

Recently, several papers about gasdermin D protein have appeared and made it a highly visible issue because of its functions during pyroptosis. According to Hana M. Russo' s report (Russo et al., 2016), activation of caspase-1 could quickly induce large membrane pores, which are permeable to both cations and anions, and finally lead to swelling, rupture and cell lysis. The function of pore formation was completely dependent on the expression of GSDMD and could be supressed by Lanthanides, which is an active channel inhibitor (Russo et al., 2016). Therefore, we were curious to discover how this widely membrane channel inhibitor (lanthanides) to influence on toxin pore forming, cellular defence responses, and furthermore to estimate whether GSDMD contributes to this PFT attack event. Pro-PhlyP was used to permeabilize the PM of HaCaT cells to observe the dynamic of cellular K^+ levels in the presence or absence of Gd^{3+} and La^{3+}. The results indicated that pro-PhlyP led to cellular K^+ levels

dramatically dropping after 10 min treatment with pro-PhlyP. Contrarily, in the presence of Gd^{3+} and La^{3+}, the cellular K^+ levels showed insignificant decrease after 10 min with pro-PhlyP treatment. Cells were washed and re-cultured in medium for 2 h, the control group K^+ concentration recovered to 90% while the lanthanide groups also showed some recovery (Fig. 27a). In the presence of lanthanides, cellular K^+ loss was more when pro-PhlyP treatment time was extended to 20 min. Cleavage of pro-PhlyP by trypsin aggravates cellular K^+ loss (Fig. 27b), which indicates that lanthanides can delay or weaken the primary damage of PhlyP rather than inhibit it completely (Fig. 27b and c).

Lanthanides influenced the primary damage induced by pro-PhlyP in HaCaT cells. In order to further investigate if lanthanides also affect Ca^{2+} dependent repair mechanism triggered by pro-PhlyP, β-hexosaminidase release was measured after pro-PhlyP incubation for 10 min, 20 min, 40 min with or without Gd^{3+} and La^{3+}. Consistent with the K^+ efflux results, lanthanides completely suppressed the release of β-hexosaminidase (Fig. 26c). Considering that Gd^{3+} and La^{3+} are widely known as inhibitors of large, non-selective, cation-selective membrane channels which have similar ion diameter as Ca^{2+} (Lewis and Spalding, 1998), this outcome was not unexpected. Gd^{3+} and La^{3+} competitively inhibited Ca^{2+} selective passage (pore formed by PhlyP, P2X7 channels or other unknown channels permeable to Ca^{2+}), thus reduced both PhlyP toxicity and cellular recovery responses. At the same time, these results also underscore that lanthanides cannot serve as specific tools to test the activity of GSDMD.

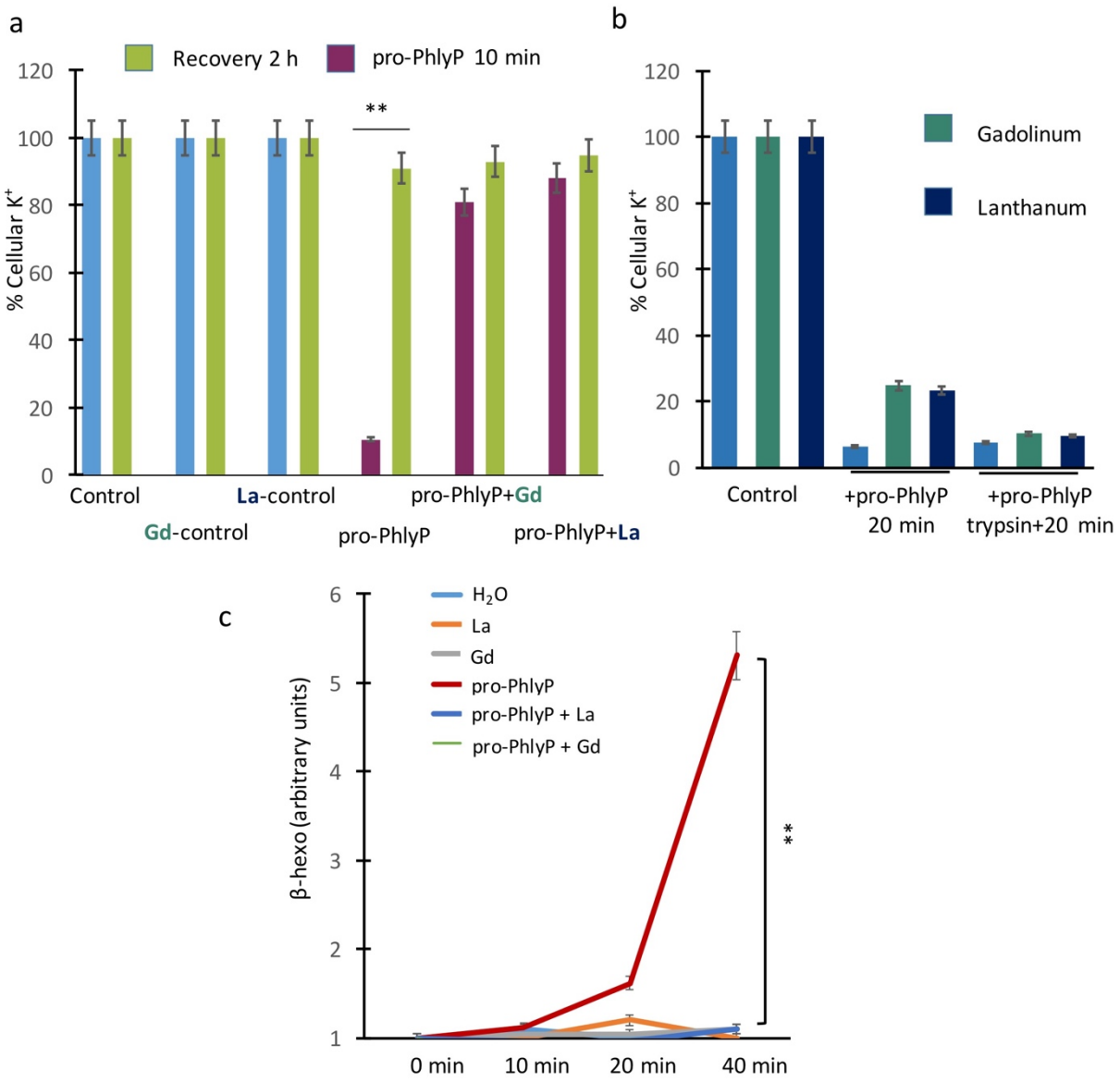

Figure 27: Lanthanides inhibit primary damage by PhlyP and reduce cellular repair responses. a, HaCaT cells were pre-incubated with or without lanthanides for 30 min before being exposed to pro-PhlyP 100 ng/ml for 10 min. After that, cells were washed and re-cultured in medium with or without lanthanides for recovery over 2 h. Cellular K^+ levels were measured immediately or after the 2 h recovery period. **b**, HaCaT cells were pre-incubated with or without lanthanides for 30 min before being exposed to pro-PhlyP or mature PhlyP (trypsin treatment) 100 ng/ml for 20 min. Cells were washed and cellular K^+ levels were measured immediately after the treatment. **c**, HaCaT cells were pre-incubated with or without lanthanides for 30 min before being exposed to pro-PhlyP 100 ng/ml for the indicated times. Cellular supernatant was collected and β-hexosaminidase was measured. Mean values ± SE are shown ($n \geq 3$). *P*-values were determined with Student's *t*-test.

3.12 Caspase inhibitor Z-VAD-FMK dampens the recovery responses to pro-PhlyP without affecting primary toxicity

As the activation and cleavage of GSDMD is strictly dependent on caspase, Z-VAD-FMK (Benzyloxycarbonyl-Val-Ala-Asp (OMe) fluoromethylketone) was introduced here to investigate the activities of GSDMD more specifically. Z-VAD-FMK is a membrane permeable caspase inhibitor, which can reversibly bind to the catalytic site and restrain the activation. In the absence or presence of Z-VAD-FMK, cellular K^+ concentrations in HaCaT cells were measured before or after incubation with pro-PhlyP. The results indicated that cellular K^+ was inexorably lost after pro-PhlyP attack, regardless of presence or absence of Z-VAD-FMK (Fig. 28a). This suggests that Z-VAD-FMK does not influence the primary toxicity of pro-PhlyP.

In order to see cellular repair changes induced by Z-VAD-FMK, β-hexosaminidase release was measured after pro-PhlyP incubation with or without Z-VAD-FMK. The results demonstrated surprisingly that Z-VAD-FMK had partly suppressed the production of β-hexosaminidase. The results after 40 min had significant differences (Fig. 28b). Considering that cellular K^+ replenishment is a marker of membrane repair, Z-VAD-FMK was further used to see its effects on cellular K^+ recovery. After 10 min of treatment with pro-PhlyP and 2 h of recovery, cellular K^+ showed a significantly lower level in the Z-VAD-FMK group than the DMSO control group. These results indicate that the inhibition of caspase by Z-VAD-FMK can lead to less β-hexosaminidase enzyme release, and lower cellular K^+ recovery level, even though the primary toxicity damage was not affected by Z-VAD-FMK (Fig. 28c).

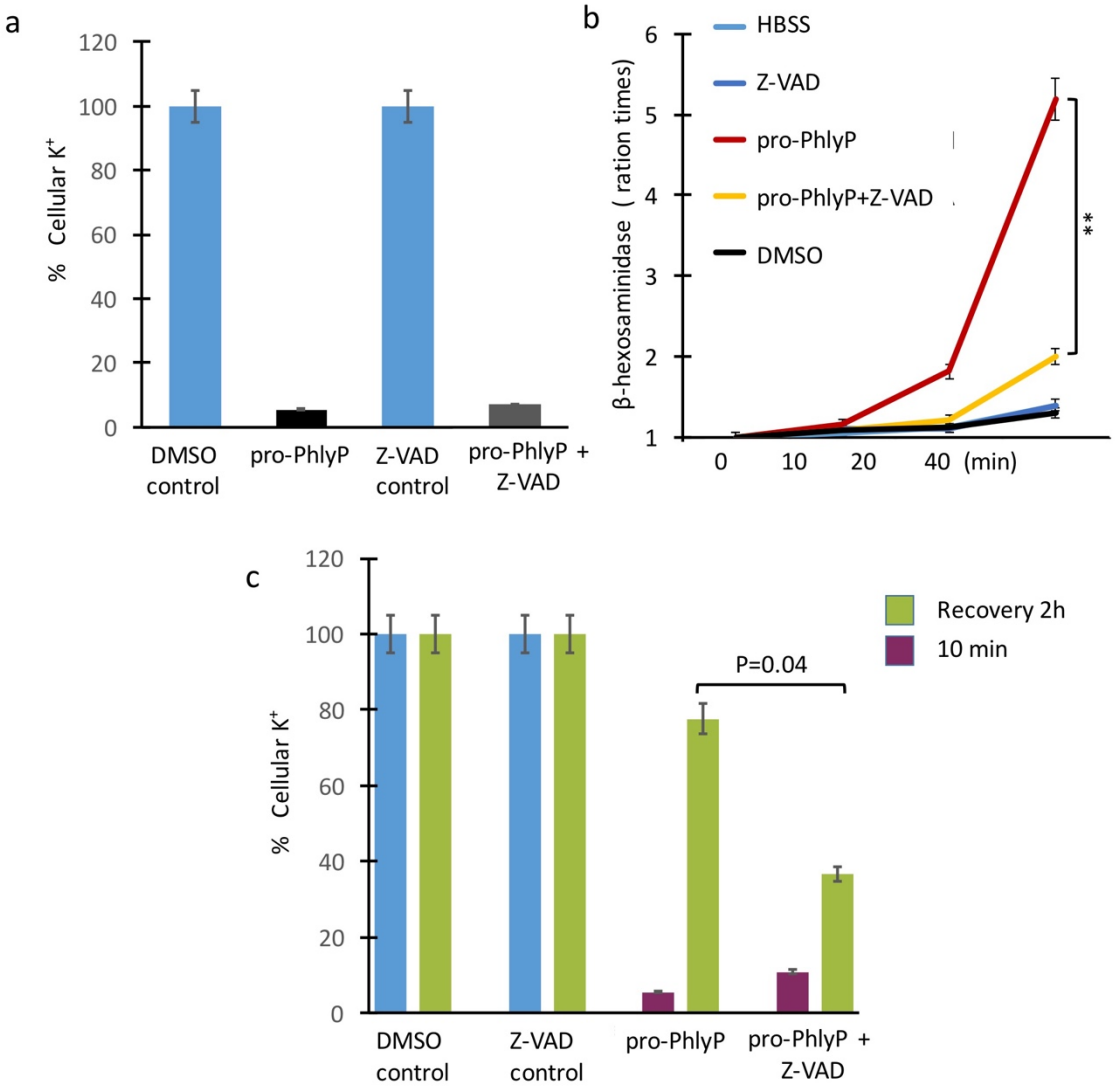

Figure 28: Caspase inhibitor Z-VAD-FMK affects the cellular response to PhlyP. a, HaCaT cells were pre-incubated with or without Z-VAD-FMK 100 µM for 30 min before being exposed to pro-PhlyP 100 ng/ml in the presence or absence of Z-VAD-FMK 100 µM for 20 min. Cells were washed then lysed before cellular K^+ was measured. **b,** HaCaT cells were pre-incubated with or without Z-VAD-FMK 100 µM for 30 min before being exposed to pro-PhlyP 100 ng/ml in the presence or absence of Z-VAD-FMK 100 µM for the indicated times. Cellular supernatant was collected and β-hexosaminidase was measured at the indicated times. **c,** HaCaT cells were pre-incubated with or without Z-VAD-FMK 100 µM for 30 min before being exposed to pro-PhlyP 100 ng/ml in the presence or absence of Z-VAD-FMK 100 µM for 10 min. After that, cells were washed and lysed or re-cultured in medium for a 2 h recovery period before K^+ was measured. Mean values ± SE are shown ($n \geq 3$). *P*-values were determined with Student's *t*-test.

3.13 α-toxin at different concentrations triggers different cellular responses

Earlier studies reported that α-toxin can form pores of different sizes in target membranes depending on toxin concentration (Walev et al., 1993; Jonas et al., 1994). Thus, under low concentrations of α-toxin, a vital dye remained outside the cytoplasm while high concentrations of α-toxin led to influx of the cell-stain. This demonstrates that at least two kinds of lesions are induced by α-toxin, but the nature of these lesions remained elusive. It has been proposed that toxin-pores could be of variable size, depending on toxin concentrations, but we considered the alternative explanation that another, secondary type of lesion might be formed under such conditions, which does not consist of α-toxin. One pilot study of Ca^{2+} influx induced by α-toxin in HaCaT cells showed that at 4 µg/ml of α-toxin, the Ca^{2+} signal began to rise (Fig. 29a). Numerous repeats of above experiments with α-toxin at 0.2, 1, 5, 25 µg/ml documented that signals became stronger with the increase of α-toxin concentration (Fig. 29b). Similar results were also obtained with VCC treated cells (Fig. 17b).

Interestingly, α-toxin at 0.2 µg/ml did not trigger a fast and effective Ca^{2+} influx, but activated p38 MAPK (Fig, 29c), which plays a critical role for recovery after permeabilization by α-toxin (Husmann et al., 2006). Dose-response experiments conducted by colleagues in our group showed that α-toxin at 0.2 µg/ could effectively cause phosphorylation of p38 (but no significant increase of cellular Ca^{2+}), although at a concentration of 25 µg/ml, the phosphorylation of p38 was reduced (Fig. 29c). Unexpectedly, EGTA prevented phosphorylation of p38 only at high concentrations of toxin. This might show that only at those high concentrations of α-toxin (5-25 µg/ml), EGTA could enter cells to prevent Ca^{2+}-dependent steps of p38-phosphorylation. In other words, the experiments may provide another hint at secondary membrane lesions, which are larger than the primary lesions constituted by α-toxin pores.

As we had noticed that Z-VAD-FMK, the inhibitor of caspase, can reduce β-hexosaminidase release induced by pro-PhlyP, we reasoned that GSDMD pores could be candidate secondary lesions which might cause fluxes of Ca^{2+} and PI observed

after treatments with high doses of α-toxin, which at low doses restricts the flux of Ca^{2+}, vital dyes, or cytosolic markers.

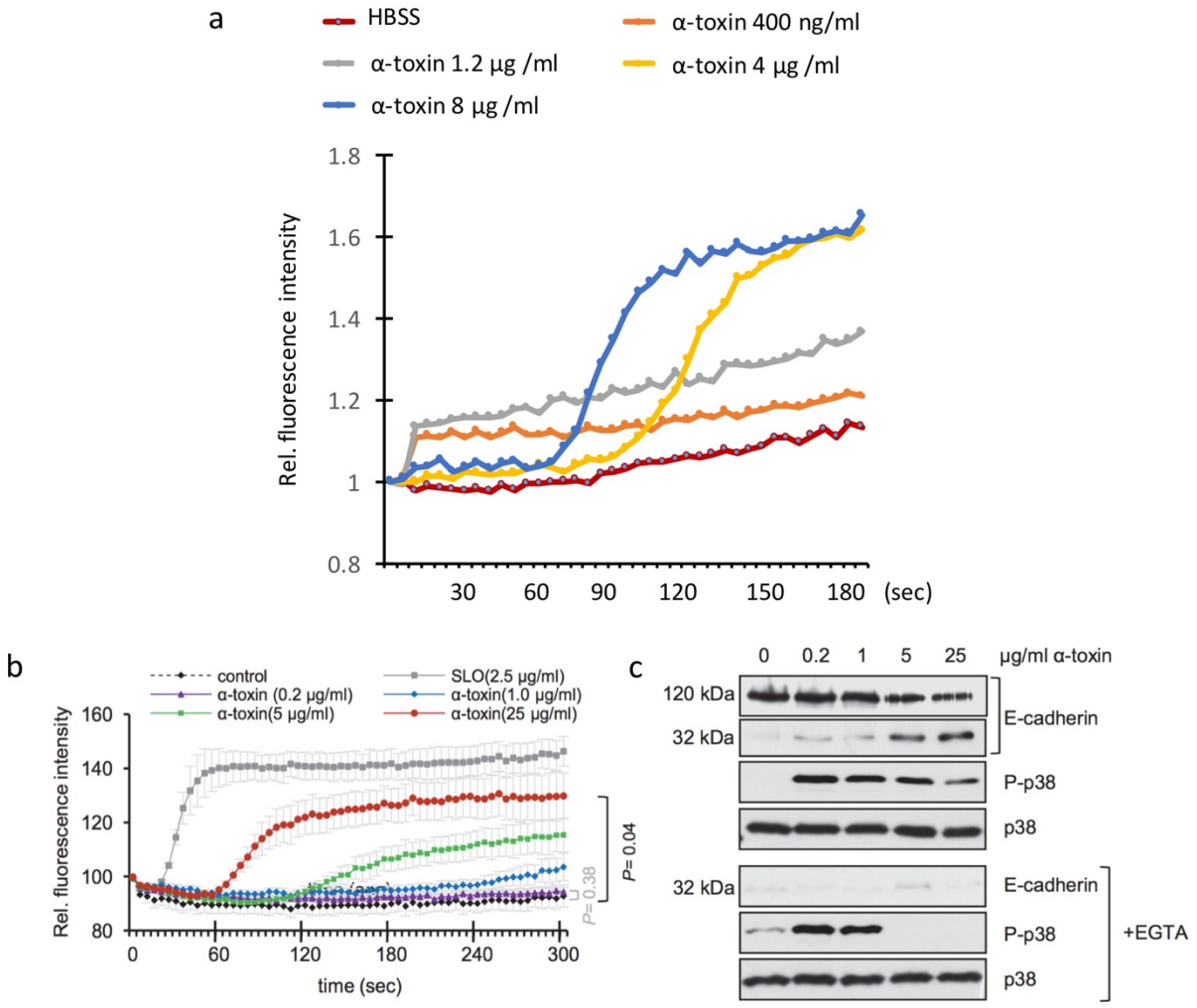

Figure 29: α-toxin triggers different cellular responses at different concentrations. a, HaCaT cells were re-incubated with Fluo-8 AM for 30 min before being treated with α-toxin or HBSS (control group). Fluorescence intensity was measured over 3 min and values were recorded every 5 s (n = 1). **b**, HaCaT cells were treated similarly as panel a, while the concentrations of α-toxin were changed as described in the legend (von Hoven et al., 2016); for contributions see Appendix 2. **c**, HaCaT cell were treated with α-toxin for 1 h with the indicated concentrations in the presence or absence of EGTA. Then relative proteins were analysed by western blot (von Hoven et al., 2016); for contributions see Appendix 2. Mean values ± SE ($n \geq 3$) are shown. *P*-values were determined with Student's *t*-test.

3.14 α-toxin leads to accumulation of GSDMD at the plasma membrane and causes membrane protrusions

Next, we employed microscopy to observe the localization of GSDMD-FLAG fusion-protein after α-toxin treatment in HaCaT. The pCS2 vectors were transfected into HaCaT cells with inserted GSDMD cDNAs (pCS2-3flags-hGSDMD; a kind gift of Dr. Feng Shao). After being cultured in medium with α-toxin, amino-terminally labelled with Alexa 546 (Kloft et al., 2012), for 90 min, cells were washed and incubated with antibodies before being stained with Hoechst and fixed. Analysis and digital images were made by fluorescence-microscopy. Anti-GSDMD antibody was used as first antibody; appropriate secondary antibody controls remained negative. The images show that GSDMD translocates to the plasma membrane in the toxin group, while evenly dispersed in the cytoplasm in the control group (Fig. 30a). Many membrane protrusions were visible in the toxin-treated cells, which were not found in un-transfected cells (not shown).

Then, Z-VAD-FMK was introduced to investigate its potential effect on activation of GSDMD in transfected HaCaT cells under toxin attack. Image analyses demonstrated that only the DMSO control group treated with toxins showed GSDMD translocation to the membranes. The Z-VAD-FMK group and non-toxin group were entirely GSDMD negative (Fig. 30b). Microscopy image results showed that GSDMD was activated and conferred cellular responses to α-toxin (pyroptotic phenotypes).

To see if endogenous GSDMD may be responsible for PI influx at high concentrations of α-toxin, we treated HaCaT cells with various concentrations of α-toxin in the presence or absence of Z-VAD-FMK. Only at 5 µg/ml of toxin, Z-VAD-FMK appeared to reduce the number of PI-positive cells, but the effect was small and remained insignificant (Fig. 30c).

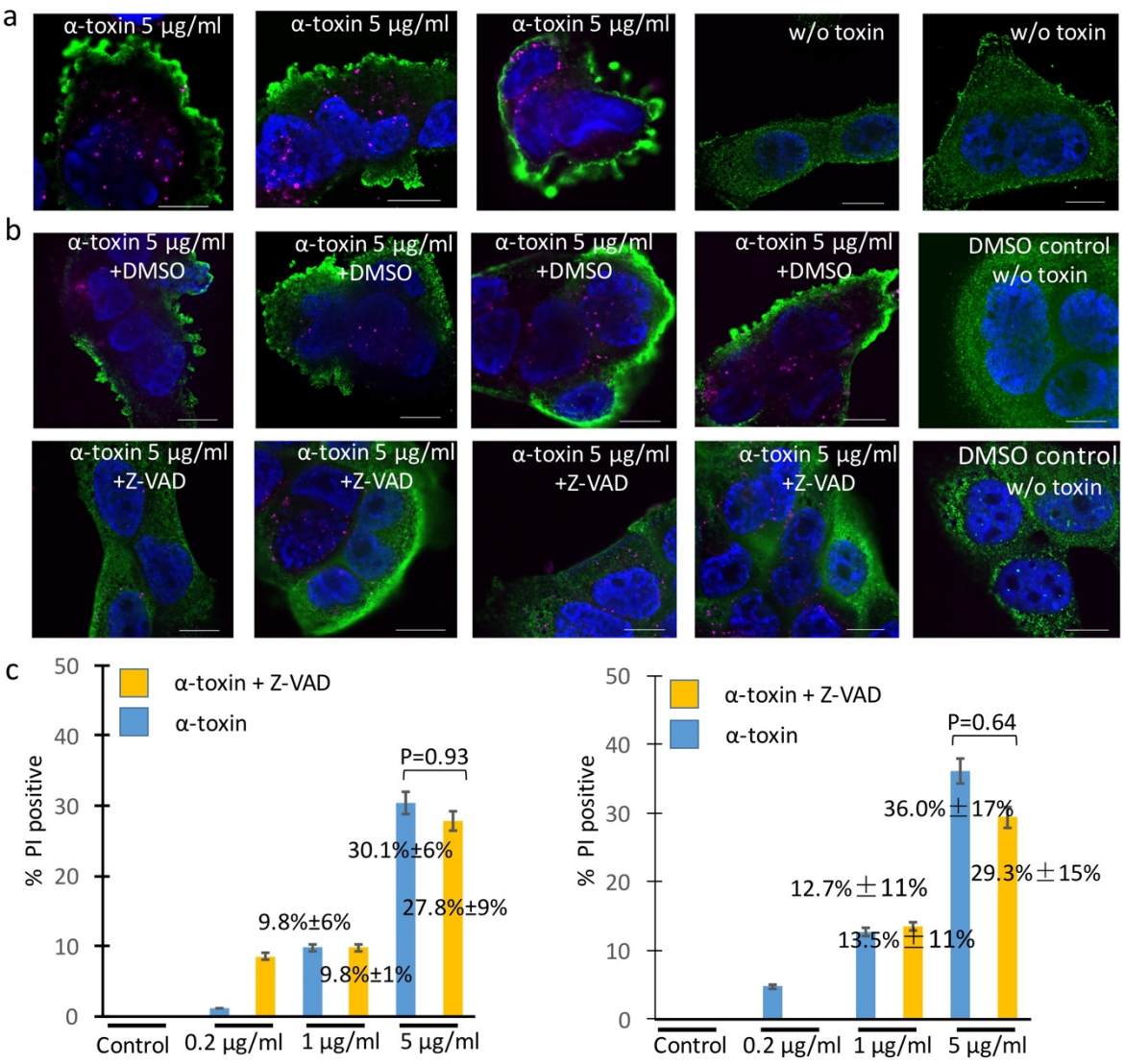

Figure 30: α-toxin triggers accumulation of transfected GSDMD-Flag(3) at the plasma membrane of HaCaT cells, and Z-VAD-FMK inhibits this response. a, HaCaT cells were transfected with vectors and treated with toxins as described in panel a. The first antibody was anti-GSDMD from rabbit. **b,** HaCaT Cells were transfected with pCS2-3flags-hGSDMD vectors before being treated with or without α-toxin at 5 µg/ml for 90 min in the presence or absence of Z-VAD-FMK. 1st antibody: anti-GSDMD from rabbit; 2nd antibody: goat anti rabbit IgG Alexa 488; nuclei were stained with Hoechst; α-toxin were stained with Alexa 546. Scale bar=10 µm. **c**, HaCaT cells were incubated with α-toxin at 0.2, 1, 5 µg/ml for 40 min or 80 min before PI stains incubation for 1 min. The percentage of PI influx positive cells are summarized in the graphs. Mean values ± SE are shown ($n \geq 3$). *P*-values were determined with Student's *t* test.

3.15 Glycine inhibits PI influx induced by α-toxin at high concentrations

Neither MLKL- nor the GSDMD-pores could satisfyingly explain the excessive influx of Ca^{2+} that happened within a short time after incubation of HaCaT cells with high concentrations of α-toxin, thus raising the possibility that membrane rupture was the underlying cause. Here glycine was introduced, which was demonstrated to effectively prevent or postpone membrane rupture (Russo et al., 2016; Estacion et al., 2003), to influence cellular responses triggered by α-toxin. After incubation of cells with α-toxin in the presence or absence of glycine, cellular ATP levels decreased as usual, which indicated that glycine did not prevent membrane damage by the PFT (Fig. 31a and b).

However, glycine significantly inhibited the influx of PI, which was seen when high concentrations of α-toxin were used (Fig. 32), although protection was not complete.

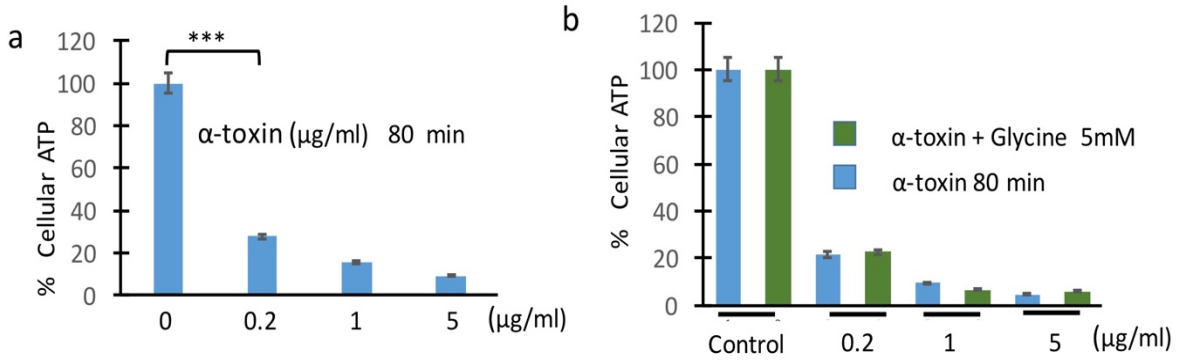

Figure 31: Glycine does not influence cellular K^+ loss triggered by α-toxin. a, HaCaT cells in suspension were treated with α-toxin using the indicated concentrations for 80 min before cellular ATP was measured. **b,** HaCaT cells were pre-incubated with or without glycine 5 mM and treated by α-toxin in the presence or absence of glycine 5 mM for 80 min before cellular ATP was measured. Mean values ± SE are shown ($n \geq 3$). *P*-values were determined with Student's *t*-test.

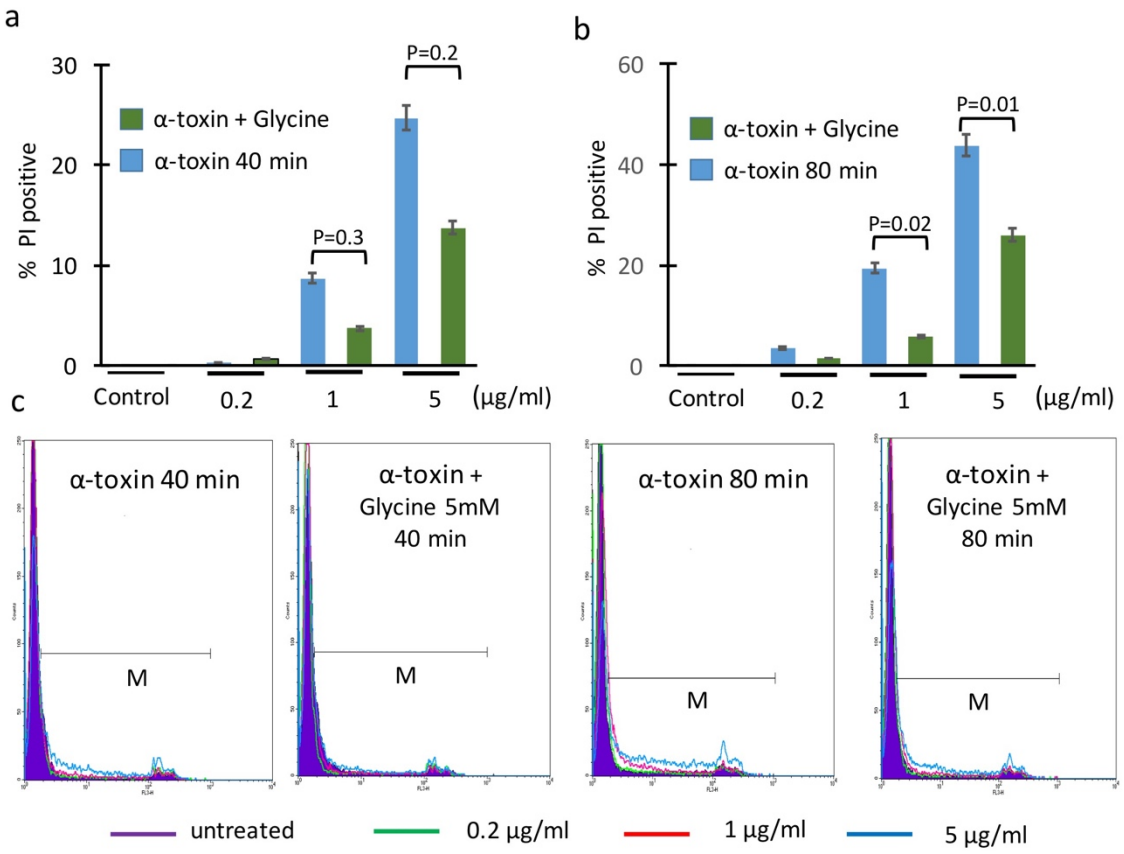

Figure 32: Glycine significantly reduces PI influx induced by α-toxin at high concentrations. **a** and **b**, graphs comparing percentage of PI positive cells for **c**. **c**, HaCaT cells were pre-incubated with or without glycine 5 mM and then exposed to α-toxin with the indicated concentrations for 40 or 80 min in the presence or absence of glycine 5 mM before being stained with PI for 1 min. The Cells were then analysed by flow cytometry. Events marked with cursor M indicated the percentage of PI-positive cells. Mean values ± SE are shown ($n \geq 3$). *P*-values were determined with Student's *t*-test.

4 Discussion

Previous comparative studies led to the unexpected observation that aerolysin and *S. aureus* α-toxin, two bacterial PFT forming small membrane pores failed to trigger rapid calcium-influx dependent membrane repair, while much larger pores formed by CDC type toxins (LLO and SLO, respectively) seemed to be rapidly repaired (Gonzalez et al., 2011; Husmann et al., 2009). For many years, the reason for this "counterintuitive" difference has been unclear (Bischofberger et al., 2012). Major structural differences between CDC and small β-PFTs or low effective pore size, or conductivity for calcium ions were discussed as potential explanations. The data of the present work supports the notion that a small β-barrel pore can induce rapid calcium-influx and repair, provided the channel is sufficiently wide and conductive for calcium: PhlyP, a small β-PFT of *Photobacterium damselae* spp. *damselae* appears to fulfil these requirements, while the orthologous VCC does not.

That PhlyP, compared with the closely related VCC, has a little wider pore channel is suggested by molecular modelling data and conductance measurements (von Hoven et al., 2017). The sum of all available data indicates that this characteristic appears to endow PhlyP with the ability to trigger effective Ca^{2+} influx-dependent repair-mechanisms (CIDRE) in host cells, which so far have only been observed with large PFTs (Bischofberger et al., 2012; Corrotte et al., 2012). In contrast to PhlyP, VCC did not permit recovery of membrane integrity in HaCaT cells. Exploiting the known high resolution pore structure of VCC, site-directed mutagenesis was used here to verify that amino acids at the channel narrow point of PhlyP / VCC modulated influx of free Ca^{2+}, and influenced cellular downstream responses and recovery. The data lead to the conclusion that channel width is a key parameter affecting the ability of a PFT to trigger CIDRE (Fig. 33).

At first glance, this conclusion seems to directly contradict another study concluding that "The pore size formed by PFTs is not the main determinant for cell K^+ recovery". (Cabezas et al., 2017). In that study, the authors showed that membrane permeabilization and recovery after attack by the small α-PFT sticholysin II (St II) in baby hamster kidney cells occurred with similar kinetics as in the case of LLO, although

they form pores of vastly different sizes (Cabezas et al., 2017). In fact, however, the two studies are mutually confirmatory, in that both show that membranes perforated by small PFT pores, formed by toxins such as PhlyP and St II, can reseal. However, as supported by the present data, toxin pores just small enough to limit influx of calcium ions through those pores (e.g. VCC) seem to subvert “canonical” membrane repair via CIDRE (Fig. 33).

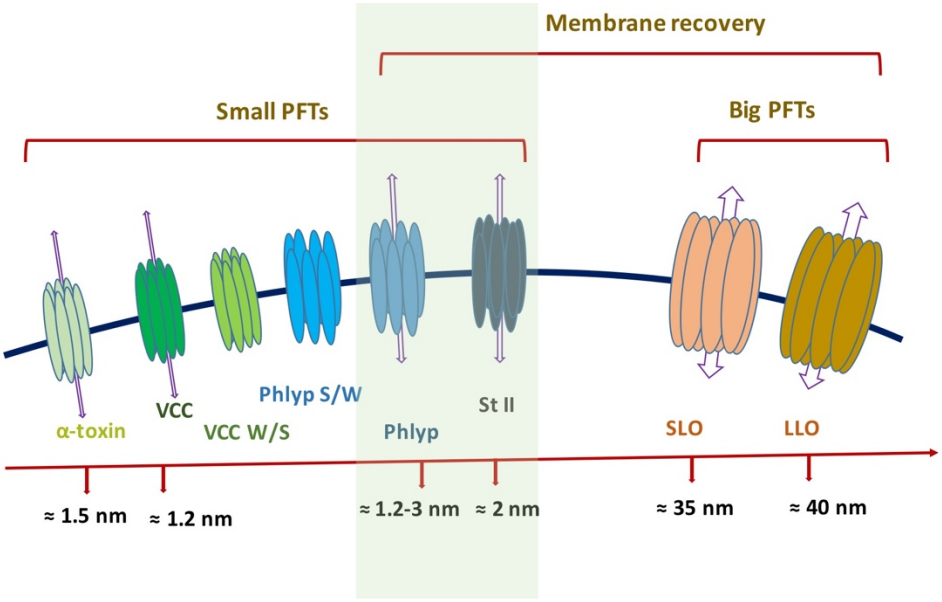

Figure 33: The relationship between PFT channel width and membrane recovery. Depending on the pore size, small-PFT may trigger or subvert membrane recovery. Both Phlyp- and St II-damaged membranes can be repaired. When toxins pores get small, the importance of pore channel width in CIDRE gets obvious.

Host cellular K^+ loss is a marker of membrane integrity that can activate many cellular signal pathways (Dal Peraro and Van Der Goot, 2016a; Bischofberger et al., 2012). PhlyP caused massive and rapid loss of K^+ while the loss of K^+ induced by VCC was comparably slow. It appears that insidious damage, as caused by VCC would be more difficult to recover. Together with the observation that PhlyP-pores are permeable for PI, the different dynamics of cellular K^+ decrease caused by PhlyP and VCC suggests rather non-selective fluxes trough the PhlyP pore which could also favour rapid Ca^{2+} influx. In fact, there was a massive and rapid increase of intracellular Ca^{2+} induced by PhlyP. The effect gets stronger, as the concentration of PhlyP toxin gets higher. The starting point of Ca^{2+} influx signal between different concentration groups are almost the same. On the contrary, the signals of Ca^{2+} influx in VCC treated cells are delayed

and only occur at high levels of VCC, apparently through different Ca^{2+} influx pathways. Corresponding with the different Ca^{2+} influx dynamics (and probably mechanisms), PhlyP pore induced membrane lesions are resealed again whereas VCC subverted membrane recovery. Similar to the repair mechanism triggered by SLO, the recovery after PhlyP treatment involves exocytosis of lysosomes, β-hexosaminidase release, caveolin and endocytosis, which has been proposed to contribute to CIDRE of large PFTs. The data with PhlyP suggests that CIDRE also serves as the priority recovery pathway after PhlyP attack. Although PhlyP activated the MAPK p38 signal pathway, this was not required for recovery from attack by this toxin (von Hoven et al., 2017).

VCC at high concentration triggers significant Ca^{2+} influx signals which turned out to be blocked by suramin. However, cellular free Ca^{2+} in cytosol finally increased substantially by one way or another, whereas it fails to trigger CIDRE. Several explanations are conceivable: 1), VCC toxin in the nanomolar range, at least, is required to trigger Ca^{2+} influx, however picomolar concentrations of VCC are already enough to kill host cells (Moschioni et al., 2002); 2), compared with Ca^{2+} influx induced by PhlyP where only a small fraction was blocked by suramin, Ca^{2+} influx caused by VCC is completely inhibited by this drug. This means that only the suramin non-sensitive part of Ca^{2+} increase induced by VCC could be effective in triggering CIDRE. This could mean that the precise localization of Ca^{2+} influx is decisive: only influx through toxin pores would be able to effectively trigger CIDRE and thus permit removal those pores. The anion selective VCC pore may be hardly conductant for Ca^{2+} but cause major ion perturbations (De and Olson, 2011; Moschioni et al., 2002); 3), different from PhlyP-induced Ca^{2+} influx that occurs quickly, VCC-triggered Ca^{2+} entry is weaker and delayed. It is conceivable that the kinetics of Ca^{2+} entry is simply not vigorous enough to trigger any effective repair mechanism.

The experiment where PhlyP and VCC were co-incubated with HaCaT cells indicated that Ca^{2+} entry sufficient to trigger repair of PhlyP pores probably does not “cross-protect” from simultaneous damage induced by VCC. Further, it is possible that VCC inhibits some downstream mechanisms of CIDRE, such as endocytosis. Previous studies discussed the possibility that the basic structure of CDC family PFT could facilitate rapid repair. However, the present data support the alternative view that sufficient influx of free Ca^{2+} through toxin pores is the main trigger for setting up

effective CIDRE. Thereby, local Ca^{2+} influx may lead to local repair. If damage of the PM is temporally and spatially limited, levels of Ca^{2+} may rise for only short periods and and these increases may remain local. There is almost no free cytoplasmic Ca^{2+} in quiescent cells and cells react upon increasing the intracellular concentration of Ca^{2+} very sensitively. The emerging concept that only Ca^{2+} influx through toxin pores – or possibly in immediate vicinity to pores – will trigger effective CIDRE, requires further verification. Results of mixing experiments with VCC and PhlyP seem to support this concept, but it is possible that they can be eventually explained by other mechanisms (Fig. 25).

When Ca^{2+} entry occurred upon treatment with PhlyP, the intracellular concentration of free Ca^{2+} increased rapidly and activated CIDRE. Other, secondary signalling pathways may play a role, and these pathways could be adaptive, while some others could be detrimental (Bouillot et al., 2018). A deeper understanding of the processes involved after membrane damage by PFT will thus require an analysis of these secondary responses (see Part II).

Although PhlyP and VCC are both small β-PFT, the difference between these two toxins is not limited to channel width and/or conductance. Therefore, we had decided to perform a mutational analysis to swap amino acids forming the (presumed) channel narrow points. Mutant VCC W/S, predicted to have a wider pore channel than VCC, enhanced the primary toxicity on target cells but did not lead to significant release of β-hexosaminidase or other signals of CIDRE. This failure might have been due to the increase of ion fluxes (including Ca^{2+} influx) in target cells through VCC W/S pores. While this was obviously not enough to effectively trigger cellular CIDRE mechanism, it may have been sufficient to enhance toxicity. These results show that the consequences of a tiny modification in small β-PFTs depend on molecular context. The width of the channel´s narrow point is important, but still only one of many factors. The suramin-insensitive part of Ca^{2+} increase may reflect more reliably Ca^{2+} entry through the toxin pore. PhlyP S/W mutant limited the suramin-insensitive Ca^{2+} influx more than PhlyP did, and showed increased toxicity and ineffective repair. In contrast, replacing S of the VCC channel narrow point by W (VCC W/S), slightly increases suramin-insensitive Ca^{2+} entry, but enhances toxicity and subverts repair just like VCC. In other words, the increase of suramin-insensitive Ca^{2+} entry appears insufficient to trigger

effective CIDRE, although disturbances of ion concentrations are severe enough to exert toxicity. Other residues (apart from the one at the channel narrow point) lining the VCC channel will co-determine the flux of ions, and the known anion-selectivity of the VCC pore may further limit calcium influx required for efficient CIDRE.

ATP can activate P2X-receptors. Especially, P2X7 proteins can form larger pores permitting molecules up to 900 kDa to pass through (North, 2002). Proposedly, P2X receptors critically contribute to the lytic effects of PFT (see Introduction). However, the P2X7 inhibitor PPADS directly binds to α-toxin, and therefore disturbs its membrane binding properties (Schwiering et al., 2017). P2X-receptors may play a role as protectors in SLO-intoxicated HEK cells (Schoenauer et al., 2014). To sum up, the role of P2X receptors in the cellular responses to PFTs remains unclear. Studies showed the P2X protein was related with the Ca^{2+} influx through non-selective cationic pore channels (McLarnon, 2005). How this might play a role for the action of small β-PFTs and secondary pathways is unclear. Further, it is unclear how secondary damage contributes to CIDRE in small β-PFTs treated cells.

It is unclear whether the intracellular free Ca^{2+} increase only results from influx of extracellular Ca^{2+} after PFT induced membrane preformation. In fact, a previous study revealed that intracellular Ca^{2+} concentration could rise from intracellular Ca^{2+} stores during small β-PFT triggered membrane damage (Jover et al., 2013). Interestingly, this release of Ca^{2+} from calcium store proved to occur before the formation of membrane pore channels. Calcium store and store operated calcium channels are involved in signalling pathways triggered by SLO (Usmani et al., 2012). However, extracellular calcium is required for repair of SLO-pores or PhlyP pores, although it is not required for recovery from α-toxin or aerolysin. Therefore, we have coined the term calcium influx dependent repair (CIDRE) to emphasize that influx of Ca^{2+} from the extracellular space is required to trigger this mechanism. Our data suggest that an additional requirement for PFT repair could be that the influx of Ca^{2+} has to occur through – or at least next to – the membrane lesion in the PM. Yet, it remains possible that endogenous channel forming proteins are involved.

Two phenomena raised the suspicion that endogenous channels might indeed play a role for the action of small β-PFT, specifically for the entry of Ca^{2+}. First, VCC pores

only allowed the entry of free Ca^{2+} with relatively slow kinetics and only at high (by far supra-toxic) toxin concentrations, but the final levels of intracellular free Ca^{2+} increased significantly. Moreover, this increase proved to be sensitive to P2X channel inhibitor suramin. Second, low levels of α-toxin did not induce increase of intracellular free Ca^{2+} signal but rather high, supracytotoxic concentrations did cause significant Ca^{2+} entry. This is consistent with previous reports that the size of α-toxin induced pore dependent on the concentration of toxin (Walev et al. 1993). Previous studies did not find significant Ca^{2+} or propidium iodide influx, but noticed influx of Na^{+} and efflux of K^{+} or Rb^{+} in the treatment of human peripheral T-cells treated with α-toxin (Walev et al., 1993). The concentration of α-toxin influenced the influx of Ca^{2+}, since high α-toxin concentration led to acceleration of ATP-depletion and determination of Ca^{2+} influx or PI in experiments (Walev et al., 1993). These data are consistent with our present results that low concentration of α-toxin induce pores, which permit the passage of potassium ions leading to a drop of ATP levels, whereas higher α-toxin concentrations permit influx of Ca^{2+}. These two observations pointed to a possible role of secondary mechanisms behind the free Ca^{2+} influx after small β-PFT attack.

Recently, studies reported two types of intracellular channel forming proteins, the lineage kinase domain like pseudokinase (MLKL) and gasdermin D (GSDMD). They are recognized as the effectors of programmed cellular death necroptosis and pyroptosis, respectively (Kovacs and Miao, 2017; Petrie et al., 2019; Wang et al., 2014), which were previously reported to be involved in PFT-induced cell deaths (Kitur et al., 2015; LaRocca et al., 2014; Mathur et al., 2019). Activated MLKL and GSDMD form inner oligomeric membrane-crossing pores, while PFTs form channels from the extracellular leaflet (Ding et al., 2016). The activation of MLKL needs the phosphorylation of receptor interacting protein kinase1 (RIPK1) and PIPK3 successively. Reportedly, α-toxin plays a major role in *S. aureus*-induced necrosis, which was blocked by MLKL inhibition (Kitur et al., 2015; Kitur et al., 2016). In our experiments, NSA, an inhibitor of MLKL oligomerization, affected neither β-hexosaminidase release nor potassium leakage induced by PhlyP. The reason for the apparent discrepancy between our data and those from Kitur et al. are unclear (Kitur et al., 2015; Kitur et al., 2016). Possibly, the different toxins, cell types or read outs were responsible. The issue deserves further studies, in particular because we obtained data with *S. aureus* a-toxin, which indicate that NSA may aggravate the effect

of this PFT, suggesting that MLKL might under certain conditions exert a protective effect (von Hoven et al. 2019).

GSDMD is a member of the gasdermin family and may too be involved in secondary membrane perforation after PFT-attack. GSDMD pores show non-selectivity on ion levels while MLKL pores have cation selective characteristic (Chen et al., 2016). The activation of GSDMD is triggered through proteolytic cleavage by caspase-1 or 11. Interestingly, caspase could also be activated by MLKL, and thereby lead to the activation of GSDMD (Conos et al., 2017; Kayagaki et al., 2015; Shi et al., 2015). Caspase cleaves off the C-terminus of GSDMD to allow the N-terminal to oligomerize and bind to inner leaflet of the plasma membrane (Ding et al., 2016). This mechanism can also attack mitochondrial membranes and bacteria (Liu et al., 2016). It is known that the leakage of potassium will trigger the activation of caspase (Walev, et al., 1995). Because K^+ efflux can be probably induced by all bacterial PFTs, it is possible that they could all trigger activation of GSDMD in susceptible host cells. In spite of this straightforward idea, until recently there have been no data directly showing that any PFT will trigger activation of GSDMD.

In a first set of experiments addressing the issue, we used lanthanides, which had been reported to block ion flux through GSDMD pores, one candidate endogenous pore former possibly contributing to the secondary effects of PFT. We noticed that lanthanides inhibited both the primary damage and repair responses induced by PhlyP. Why lanthanides reduced toxicity remains unclear, but it might be explained by some interference with activation of pro-PhlyP. This was suggested by the result that mature PhlyP (pro-toxin activated with trypsin) was less susceptible. Lanthanides (Gd^{3+} and La^{3+}) are known inhibitors of large, non-selective, cation selective membrane channels and have similar ion diameter as Ca^{2+} (Lewis and Spalding, 1998). Therefore, we sought a more specific approach to test whether small b-PFT could activate GSDMD.

By using fluorescence microscopy, we found in HaCaT cells that transiently transfected GSDMD-Flag(3) translocate to the cellular periphery upon treatment with α-toxin. In addition, there was massive formation of membrane protrusions, typically observed during pyroptotic cell death. As in earlier studies on GSDMD, we used overexpression of GSDMD, so it will require further work to verify the concept that small β-PFT can

trigger larger membrane pores and thereby induce Ca^{2+} influx by activating GSDMD in non-transfected cells.

The foregoing data indicated that small β-PFT might trigger endogenous channel-forming proteins like GSDMD. However, this did not satisfyingly explain influx of PI upon treatment with high concentrations of a small β-PFT (which per se does not permit influx of these markers), because ZVAD-FMK did not inhibit influx of this dye. However, there another possible explanation emerged. Thus, uncontrolled entry of water and ions into the target cell leads to cell swelling, which may ultimately lead to membrane rupture. Unchecked influx of water may happen through pores formed by PFTs or other channels. The mechanistic details of rupture induced by cellular osmotic swelling is not fully understood, and experimental approaches to investigate this process are limited. However, previous reports showed that glycine inhibits membrane rupture induced by cellular swelling (Petrat et al., 2011). Therefore, we used this method to study a possible involvement of rupture in cells treated with α-toxin. This approach demonstrated that the influx of PI into HaCaT cells upon treatment with comparably high concentrations of α-toxin could be partially inhibited by glycine, and is therefore probably a consequence of membrane rupture. That high concentrations of α-toxin lead to gross damage of the membrane is consistent with the finding that it also leads to the release of LDH, e.g. (Inoshima et al., 2011), a cytosolic protein, which cannot escape through pores formed by small β-PFT, GSDMD or MLKL. Whether toxin pores are sufficient to trigger rupture remains an open question.

The present data supports the idea that cellular channel forming proteins such as P2X, MLKL and GSDMD are activated by PFT. This in turn will impact the changes in ion fluxes and downstream events. Ultimately, it will also determine if, when and how a target cell will die. To date, it is not even excluded that endogenous pore forming proteins can, under certain circumstances, promote membrane repair rather than accelerating cell death: thus, it is conceivable that MLKL or GSDMD, triggered by a small β-PFT, which does not itself cause significant influx of Ca^{2+} could trigger CIDRE. One indication for such a scenario might be the effect of MLKL-inhibitor NSA on the viability of α-toxin treated HaCaT cells (von Hoven et al., 2019). Another example may be P2XR which have been proposed to enhance the lytic function of PFT: as shown in Fig. 18b, suramin, a broad spectrum inhibitor of P2X actually reduced the recovery of

potassium levels after PhlyP attack. This would suggest a protective function of P2X in this context. Moreover, ZVAD-FMK reduces cellular K^+ recovery in PhlyP-attacked cells (Fig. 28), raising the question whether this is due to the inhibition of GSDMD-activation or of other targets. More work is required to clarify whether a specific cellular channel will promote membrane repair after small β-PFT attack, or accelerate death. Even delaying cell death may be an advantage for a host, because it would allow for transmitting signals and mobilizing defence, as exemplified by recent studies showing that ESCRT-dependent exocytosis of MLKL pores delays necroptosis (Gong et al., 2017).

That endogenous pore formers may function as double-edged swords is suggested by the fact that they seem to serve both destructive functions and rescue processes together. This is exemplified by GSDMD: the drop of cytosolic potassium in response to a PFT would lead to the activation of caspases causing formation of GSDMD pores in the target membranes, and to pyroptosis. At the same time, these caspases will activate lipid synthesis pathways, which contribute to cellular membrane repair (Gurcel et al., 2006). An emerging theme here thus appears to be that molecules usually considered executioners of cell death may also help to delay it.

The present work also illustrates the power of small β-PFTs to study the role of secondary membrane damage for cell fate: CDC like SLO and LLO have been invaluable tools to study canonical, i.e., calcium-influx dependent membrane repair. They form large, nonselective pores, which permit influx of dyes and efflux of proteins from cells. This makes them highly accessible, in particular for imaging-based methods. However, their large pore size makes it extremely difficult to differentiate primary damage from the emerging array of secondary events due to endogenous pore formers channels and rupture. Because the various small β-PFTs differentially restrict the flux of dyes and marker-molecules, they will help us to untangle the true complexity of cellular responses to membrane damage.

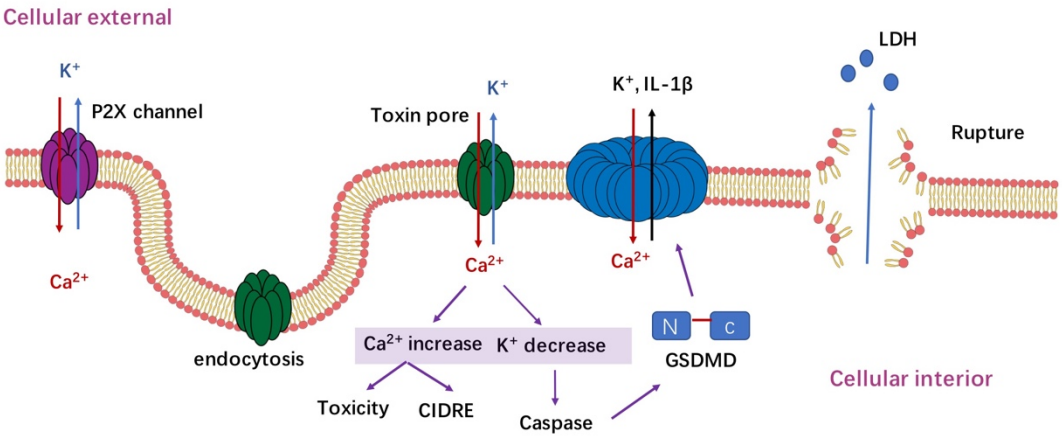

Figure 34: Secondary membrane damage may contribute to the effects of PFTs. The membrane damage caused by PFTs triggers efflux of potassium and a drop of ATP, and – depending on the PFT - influx of calcium ions. These events may activate endogenous membrane channel forming proteins, which are permeable for Ca^{2+} and PI, such as P2X, GSDMD and MLKL, to probably influence both toxic effects of PFTs and as well as membrane repair. When the cellular regulation mechanism of volume becomes overburdened, membrane rupture will lead to leakage of large molecules.

Appendix 1: Author Publications

- Gisela von Hoven, **Qianqian Qin**, Claudia Neukirch, Matthias Husmann, Nadja Hellmann. *S. aureus* α-toxin: small pore, large consequences[J]. *Biol Chem*, 2019 Sep 25;400(10):1261-1276.

- Gisela von Hoven, Amable J. Rivas, Claudia Neukirch, Martina Meyenburg, **Qianqian Qin**, Sapun Parekh, Nadja Hellmann, Matthias Husmann. Repair of a Bacterial Small β-Barrel Toxin Pore Depends on Channel Width[J]. *MBio*. 2017 Feb 14;8(1).

- Gisela von Hoven, Amable J. Rivas, Claudia Neukirch, Stefan Klein, Christian Hamm, **Qianqian Qin**, Martina Meyenburg, Sabine Füser, Paul Saftig, Nadja Hellmann, Rolf Postina, Matthias Husmann. Dissecting the role of ADAM10 as a mediumtor of *Staphylococcus aureus* α-toxin action[J]. *Biochem J*. 2016 Jul 1;473(13):1929-40.

- Amable J. Rivas, Gisela von Hoven, Claudia Neukirch, Martina Meyenburg, **Qianqian Qin**, Sabine Füser, Klaus Boller, Manuel L. Lemos, Carlos R. Osorio, Matthias Husmann. Phobalysin, a Small β-Pore-Forming Toxin of *Photobacterium damselae* subsp. *damselae*[J]. *Infect Immun*. 2015 Nov;83(11):4335-48.

Appendix 2: Author Contributions

Several data sets and corresponding figures contributed by others in the group, but published in work co-authored by the author of this thesis (QQ) are displayed in this thesis, because they underscore findings made by the author of the present thesis (QQ). This is also mentioned in the text, where appropriate. Data and corresponding display items of Figure 15d; Figure 16c; Figure 18a; Figure 20e; Figure 21b, c and e; parts of Figure 23a and b; parts of Figure 24a and 24b and c; Figure 25b were mainly contributed by [redacted] and [redacted]. Figures were published on journal *MBio*, American Society for Microbiology ("ASM"). (von Hoven et al., 2017). Original publication: von Hoven G, Rivas AJ, Neukirch C, Meyenburg M, **Qin Q**, et al. Repair of a Bacterial Small β-Barrel Toxin Pore Depends on Channel Width[J]. *MBio*. 2017 Feb 14;8(1).
Data and figure of Figure 29b and c were contributed by [redacted] and [redacted]. Figures were published in Biochemical Journal (von Hoven et al., 2016). Original publication: von Hoven, G., et al. (2016). Dissecting the role of ADAM10 as a mediumtor of Staphylococcus aureus alpha-toxin action[J]. *Biochem J.* 473(13): 1929-1940.
Figure 13a was contributed by [redacted] and [redacted]. Figures was published in journal Infection and Immunity® (IAI), American Society for Microbiology ("ASM") (Rivas et al., 2015). Original publication: Rivas AJ, von Hoven G, Neukirch C, Meyenburg M, Qin Q, et al. Phobalysin, a Small β-Pore-Forming Toxin of Photobacterium damselae subsp. damselae[J]. *Infect Immun*. 2015 Nov;83(11):4335-48.
The other figures of the Result sections were generated by Qianqian Qin. Introduction into methods, help and guidance by [redacted], [redacted], [redacted] is gratefully acknowledged.

Appendix 3: Image Copyright Statement

The permissions to adapt and use Fig. 1 and 3 in introduction part were granted by Openstax. Images are free to share and adapt under their licence terms (https://creativecommons.org/licenses/by/4.0/).

The permission to adapt and use Fig. 4 in introduction part was granted by journal *Trends in Cell Biology* with the copyright license number: 4721281171451 of the Copyright Clearance Center, Boston, MA, USA. Original publication: Kovacs, S. B. and E. A. Miao (2017). "Gasdermins: Effectors of Pyroptosis." *Trends Cell Biol* 27(9): 673-684.

The permission to adapt and use Fig. 5 was granted from journal *Molecular Cell* with copyright licence number: 4721290844947 of the Copyright Clearance Center, Boston, MA, USA. Original publication: Wang, H., et al. (2014). "Mixed lineage kinase domain-like protein MLKL causes necrotic membrane disruption upon phosphorylation by RIP3." *Mol Cell* 54(1): 133-146.

The permission to adapt and use Fig. 6 was granted from journal *Clinical and Vaccine Immunology* (CVI), American Society for Microbiology ("ASM"), which is an open access article distributed under the Creative Commons CC BY licence. Original publication: Fiaschi, L., et al. (2016). "Auto-Assembling Detoxified Staphylococcus aureus Alpha-Hemolysin Mimicking the Wild-Type Cytolytic Toxin." *Clin Vaccine Immunol* 23(6): 442-450.

The permission to adapt and use Fig. 7 was granted from journal *IUBMB Life* with copyright license number: 4707060307417 of the Copyright Clearance Center, Boston, MA, USA. Original publication: Kathuria, R. and K. Chattopadhyay (2018). "Vibrio cholerae cytolysin: Multiple facets of the membrane interaction mechanism of a beta-barrel pore-forming toxin." *IUBMB Life* 70(4): 260-266.

The permissions to use Fig. 8a-d were granted by journal *MBio*, American Society for Microbiology ("ASM"). which is an open access article distributed under the Creative Commons CC BY licence. Original publication: von Hoven G, Rivas AJ, Neukirch C, Meyenburg M, Qin Q, et al. "Repair of a Bacterial Small β-Barrel Toxin Pore Depends on Channel Width". *MBio*. 2017 Feb 14;8(1).

The permission to use Fig. 8e was granted by journal *Infection and Immunity* (IAI), American Society for Microbiology ("ASM"). Authors in ASM journals retain the right to republish discrete portions of his/her article in any other publication. For a full list of author rights, please see: http://journals.asm.org/site/misc/ASM_Author_Statement.xhtml. Original publication: Rivas AJ, von Hoven G, Neukirch C, Meyenburg M, Qin Q, et al. "Phobalysin, a Small β-Pore-Forming Toxin of Photobacterium damselae subsp. damselae". *Infect Immun*. 2015 Nov;83(11):4335-48.

The permission to adapt and use Fig. 11 was granted by journal *Cell Host & Microbe* with copyright license number: 4721340227396 of the Copyright Clearance Center, Boston, MA, USA. Original publication: Bischofberger, M., et al. (2012). "Pathogenic pore-forming proteins: function and host response." *Cell Host Microbe* 12(3): 266-275.

Appendix 4: Lists of Figures

Appendix 5: List of Tables

References

Achouak, W., Heulin, T., and Pages, J.M. (2001). Multiple facets of bacterial porins. FEMS Microbiol Lett *199*, 1-7.

Aglietti, R.A., Estevez, A., Gupta, A., Ramirez, M.G., Liu, P.S., Kayagaki, N., Ciferri, C., Dixit, V.M., and Dueber, E.C. (2016). GsdmD p30 elicited by caspase-11 during pyroptosis forms pores in membranes. Proc Natl Acad Sci U S A *113*, 7858-7863.

Andrin, C., Pinkoski, M.J., Burns, K., Atkinson, E.A., Krahenbuhl, O., Hudig, D., Fraser, S.A., Winkler, U., Tschopp, J., and Opas, M. (1998). Interaction between a Ca2+-binding protein calreticulin and perforin, a component of the cytotoxic T-cell granules. Biochemistry *37*, 10386-10394.

Arbuthnott, J.P., Freer, J.H., and Bernheimer, A.W. (1967). Physical states of staphylococcal alpha-toxin. J Bacteriol *94*, 1170-1177.

Baaske, R., Richter, M., Moller, N., Ziesemer, S., Eiffler, I., Muller, C., and Hildebrandt, J.P. (2016). ATP Release from Human Airway Epithelial Cells Exposed to Staphylococcus aureus Alpha-Toxin. Toxins (Basel) *8*.

Babiychuk, E.B., Monastyrskaya, K., and Draeger, A. (2008). Fluorescent annexin A1 reveals dynamics of ceramide platforms in living cells. Traffic *9*, 1757-1775.

Babiychuk, E.B., Monastyrskaya, K., Potez, S., and Draeger, A. (2009). Intracellular Ca(2+) operates a switch between repair and lysis of streptolysin O-perforated cells. Cell Death Differ *16*, 1126-1134.

Babiychuk, E.B., Monastyrskaya, K., Potez, S., and Draeger, A. (2011). Blebbing confers resistance against cell lysis. Cell Death Differ *18*, 80-89.

Barlic, A., Gutierrez-Aguirre, I., Caaveiro, J.M., Cruz, A., Ruiz-Arguello, M.B., Perez-Gil, J., and Gonzalez-Manas, J.M. (2004). Lipid phase coexistence favors membrane insertion of equinatoxin-II, a pore-forming toxin from Actinia equina. J Biol Chem *279*, 34209-34216.

Becker, R.E., Berube, B.J., Sampedro, G.R., DeDent, A.C., and Bubeck Wardenburg, J. (2014). Tissue-specific patterning of host innate immune responses by Staphylococcus aureus alpha-toxin. J Innate Immun *6*, 619-631.

Bergsbaken, T., Fink, S.L., and Cookson, B.T. (2009). Pyroptosis: host cell death and inflammation. Nature reviews Microbiology *7*, 99-109.

Berube, B.J., and Bubeck Wardenburg, J. (2013). Staphylococcus aureus alpha-toxin: nearly a

century of intrigue. Toxins (Basel) *5*, 1140-1166.

Bhakdi, S., Klonisch, T., Nuber, P., and Fischer, W. (1991). Stimulation of monokine production by lipoteichoic acids. Infection and immunity *59*, 4614-4620.

Bhakdi, S., and Tranum-Jensen, J. (1991). Alpha-toxin of Staphylococcus aureus. Microbiol Rev *55*, 733-751.

Bianco, F., Perrotta, C., Novellino, L., Francolini, M., Riganti, L., Menna, E., Saglietti, L., Schuchman, E.H., Furlan, R., Clementi, E.*, et al.* (2009). Acid sphingomyelinase activity triggers microparticle release from glial cells. EMBO J *28*, 1043-1054.

Bischofberger, M., Gonzalez, M.R., and van der Goot, F.G. (2009). Membrane injury by pore-forming proteins. Curr Opin Cell Biol *21*, 589-595.

Bischofberger, M., Iacovache, I., and van der Goot, F.G. (2012). Pathogenic pore-forming proteins: function and host response. Cell Host Microbe *12*, 266-275.

Bouillot, S., Reboud, E. and Huber, P. (2018). Functional Consequences of Calcium Influx Promoted by Bacterial Pore-Forming Toxins.Toxins *10(10)*, 387.

Braun, J.S., Hoffmann, O., Schickhaus, M., Freyer, D., Dagand, E., Bermpohl, D., Mitchell, T.J., Bechmann, I., and Weber, J.R. (2007). Pneumolysin causes neuronal cell death through mitochondrial damage. Infection and immunity *75*, 4245-4254.

Brito, C., Cabanes, D., Sarmento Mesquita, F., and Sousa, S. (2019). Mechanisms protecting host cells against bacterial pore-forming toxins. Cell Mol Life Sci *76*, 1319-1339.

Brown, B.S. (1996). Biological membranes (Biochemical Society).

Brown, D.A., and London, E. (2000). Structure and function of sphingolipid- and cholesterol-rich membrane rafts. J Biol Chem *275*, 17221-17224.

Bumba, L., Masin, J., Fiser, R., and Sebo, P. (2010). Bordetella adenylate cyclase toxin mobilizes its beta2 integrin receptor into lipid rafts to accomplish translocation across target cell membrane in two steps. PLoS Pathog *6*, e1000901.

Cabezas, S., Ho, S., Ros, U., Lanio, M.E., Alvarez, C., and van der Goot, F.G. (2017). Damage of eukaryotic cells by the pore-forming toxin sticholysin II: Consequences of the potassium efflux. Biochim Biophys Acta Biomembr *1859*, 982-992.

Cai, Z., Jitkaew, S., Zhao, J., Chiang, H.C., Choksi, S., Liu, J., Ward, Y., Wu, L.G., and Liu, Z.G. (2014). Plasma membrane translocation of trimerized MLKL protein is required for TNF-induced necroptosis. Nat Cell Biol *16*, 55-65.

Carmeille, R., Degrelle, S.A., Plawinski, L., Bouvet, F., Gounou, C., Evain-Brion, D., Brisson, A.R.,

and Bouter, A. (2015). Annexin-A5 promotes membrane resealing in human trophoblasts. Biochimica et biophysica acta *1853*, 2033-2044.

Cascales, E., Buchanan, S.K., Duche, D., Kleanthous, C., Lloubes, R., Postle, K., Riley, M., Slatin, S., and Cavard, D. (2007). Colicin biology. Microbiology and molecular biology reviews : MMBR *71*, 158-229.

Chakrabarti, S., Liehl, P., Buchon, N., and Lemaitre, B. (2012). Infection-induced host translational blockage inhibits immune responses and epithelial renewal in the Drosophila gut. Cell Host Microbe *12*, 60-70.

Chambers, R. and Chambers, E. L. (1961). Explorations into the Nature of the Living Cell. Harvard University Press Cambridge Massachusetts.

Chen, H.D., Kao, C.Y., Liu, B.Y., Huang, S.W., Kuo, C.J., Ruan, J.W., Lin, Y.H., Huang, C.R., Chen, Y.H., Wang, H.D.*, et al.* (2017). HLH-30/TFEB-mediumted autophagy functions in a cell-autonomous manner for epithelium intrinsic cellular defense against bacterial pore-forming toxin in C. elegans. Autophagy *13*, 371-385.

Chen, X., He, W.T., Hu, L., Li, J., Fang, Y., Wang, X., Xu, X., Wang, Z., Huang, K., and Han, J. (2016). Pyroptosis is driven by non-selective gasdermin-D pore and its morphology is different from MLKL channel-mediumted necroptosis. Cell Res *26*, 1007-1020.

Christie, M.P., Johnstone, B.A., Tweten, R.K., Parker, M.W., and Morton, C.J. (2018). Cholesterol-dependent cytolysins: from water-soluble state to membrane pore. Biophys Rev *10*, 1337-1348.

Conos, S.A., Chen, K.W., De Nardo, D., Hara, H., Whitehead, L., Nunez, G., Masters, S.L., Murphy, J.M., Schroder, K., Vaux, D.L.*, et al.* (2017). Active MLKL triggers the NLRP3 inflammasome in a cell-intrinsic manner. Proc Natl Acad Sci U S A *114*, E961-E969.

Corrotte, M., Fernandes, M.C., Tam, C., and Andrews, N.W. (2012). Toxin pores endocytosed during plasma membrane repair traffic into the lumen of MVBs for degradation. Traffic *13*, 483-494.

Corrotte, M., Almeida, P.E., Tam, C., Castro-Gomes, T., Fernandes, M.C., Millis, B.A., Cortez, M., Miller, H., Song, W., Maugel, T.K., et al. (2013). Caveolae internalization repairs wounded cells and muscle fibers. Elife *2*, e00926.

Dal Peraro, M., and van der Goot, F.G. (2016a). Pore-forming toxins: ancient, but never really out of fashion. Nature reviews Microbiology *14*, 77-92.

De, S., and Olson, R. (2011). Crystal structure of the Vibrio cholerae cytolysin heptamer reveals

common features among disparate pore-forming toxins. Proc Natl Acad Sci U S A *108*, 7385-7390.

Ding, J., Wang, K., Liu, W., She, Y., Sun, Q., Shi, J., Sun, H., Wang, D.C., and Shao, F. (2016). Pore-forming activity and structural autoinhibition of the gasdermin family. Nature *535*, 111-116.

Draeger, A., and Babiychuk, E.B. (2013). Ceramide in plasma membrane repair. Handb Exp Pharmacol, 341-353.

Dragneva, Y., Anuradha, C.D., Valeva, A., Hoffmann, A., Bhakdi, S., and Husmann, M. (2001). Subcytocidal attack by staphylococcal alpha-toxin activates NF-kappaB and induces interleukin-8 production. Infection and immunity *69*, 2630-2635.

Dunne, A., Ross, P.J., Pospisilova, E., Masin, J., Meaney, A., Sutton, C.E., Iwakura, Y., Tschopp, J., Sebo, P., and Mills, K.H. (2010). Inflammasome activation by adenylate cyclase toxin directs Th17 responses and protection against Bordetella pertussis. J Immunol *185*, 1711-1719.

Essmann, F., Bantel, H., Totzke, G., Engels, I.H., Sinha, B., Schulze-Osthoff, K., and Janicke, R.U. (2003). Staphylococcus aureus alpha-toxin-induced cell death: predominant necrosis despite apoptotic caspase activation. Cell Death Differ *10*, 1260-1272.

Estacion, M., Weinberg, J.S., Sinkins, W.G., and Schilling, W.P. (2003). Blockade of maitotoxin-induced endothelial cell lysis by glycine and L-alanine. Am J Physiol Cell Physiol *284*, C1006-1020.

Fernandez, L., and Hancock, R.E. (2012). Adaptive and mutational resistance: role of porins and efflux pumps in drug resistance. Clin Microbiol Rev *25*, 661-681.

Fiaschi, L., Di Palo, B., Scarselli, M., Pozzi, C., Tomaszewski, K., Galletti, B., Nardi-Dei, V., Arcidiacono, L., Mishra, R.P., Mori, E.*, et al.* (2016). Auto-Assembling Detoxified Staphylococcus aureus Alpha-Hemolysin Mimicking the Wild-Type Cytolytic Toxin. Clin Vaccine Immunol *23*, 442-450.

Fiser, R., Masin, J., Bumba, L., Pospisilova, E., Fayolle, C., Basler, M., Sadilkova, L., Adkins, I., Kamanova, J., Cerny, J.*, et al.* (2012). Calcium influx rescues adenylate cyclase-hemolysin from rapid cell membrane removal and enables phagocyte permeabilization by toxin pores. PLoS Pathog *8*, e1002580.

Fivaz, M., Vilbois, F., Thurnheer, S., Pasquali, C., Abrami, L., Bickel, P.E., Parton, R.G., and van der Goot, F.G. (2002). Differential sorting and fate of endocytosed GPI-anchored

proteins. EMBO J *21*, 3989-4000.

Forst, D., Welte, W., Wacker, T., and Diederichs, K. (1998). Structure of the sucrose-specific porin ScrY from Salmonella typhimurium and its complex with sucrose. Nat Struct Biol *5*, 37-46.

Fussle, R., Bhakdi, S., Sziegoleit, A., Tranum-Jensen, J., Kranz, T., and Wellensiek, H.J. (1981). On the mechanism of membrane damage by Staphylococcus aureus alpha-toxin. J Cell Biol *91*, 83-94.

Gadsby, D.C. (2009). Ion channels versus ion pumps: the principal difference, in principle. Nat Rev Mol Cell Biol *10*, 344-352.

Gekara, N.O., Westphal, K., Ma, B., Rohde, M., Groebe, L., and Weiss, S. (2007). The multiple mechanisms of Ca2+ signalling by listeriolysin O, the cholesterol-dependent cytolysin of Listeria monocytogenes. Cell Microbiol *9*, 2008-2021.

Gierok, P., Harms, M., Richter, E., Hildebrandt, J.P., Lalk, M., Mostertz, J., and Hochgrafe, F. (2014). Staphylococcus aureus alpha-toxin mediumtes general and cell type-specific changes in metabolite concentrations of immortalized human airway epithelial cells. PLoS One *9*, e94818.

Gilbert, R. (2002). Pore-forming toxins. Cellular and Molecular Life Sciences CMLS *59*, 832-844.

Gong, Y.N., Guy, C., Olauson, H., Becker, J.U., Yang, M., Fitzgerald, P., Linkermann, A., and Green, D.R. (2017). ESCRT-III Acts Downstream of MLKL to Regulate Necroptotic Cell Death and Its Consequences. Cell *169*, 286-300 e216.

Gonzalez, M.R., Bischofberger, M., Freche, B., Ho, S., Parton, R.G., and van der Goot, F.G. (2011). Pore-forming toxins induce multiple cellular responses promoting survival. Cell Microbiol *13*, 1026-1043.

Gonzalez, M.R., Bischofberger, M., Pernot, L., van der Goot, F.G., and Freche, B. (2008). Bacterial pore-forming toxins: the (w)hole story? Cell Mol Life Sci *65*, 493-507.

Gonzalez-Juarbe, N., Gilley, R.P., Hinojosa, C.A., Bradley, K.M., Kamei, A., Gao, G., Dube, P.H., Bergman, M.A., and Orihuela, C.J. (2015). Pore-Forming Toxins Induce Macrophage Necroptosis during Acute Bacterial Pneumonia. PLoS Pathog *11*, e1005337.

Gurcel, L., Abrami, L., Girardin, S., Tschopp, J., and van der Goot, F.G. (2006). Caspase-1 activation of lipid metabolic pathways in response to bacterial pore-forming toxins promotes cell survival. Cell *126*, 1135-1145.

Gutierrez, M. G., Saka, H.A., Chinen, I., Zoppino, F.C.M., Yoshimori, T., Bocco, J.L., Colombo,

M.I.(2007). Protective role of autophagy against *Vibrio cholerae* cytolysin, a pore-forming toxin from *V. cholerae*. Proc. Natl Acad. Sci. USA *104*, 1829–1834.

Hamon, M.A., Batsche, E., Regnault, B., Tham, T.N., Seveau, S., Muchardt, C., and Cossart, P. (2007). Histone modifications induced by a family of bacterial toxins. Proc Natl Acad Sci U S A *104*, 13467-13472.

Hamon, M.A., Ribet, D., Stavru, F., and Cossart, P. (2012). Listeriolysin O: the Swiss army knife of Listeria. Trends Microbiol *20*, 360-368.

Hardie, D.G., Ross, F.A., and Hawley, S.A. (2012). AMPK: a nutrient and energy sensor that maintains energy homeostasis. Nat Rev Mol Cell Biol *13*, 251-262.

Harshman, S., and Sugg, N. (1985). Effect of calcium ions on staphylococcal alpha-toxin-induced hemolysis of rabbit erythrocytes. Infection and immunity *47*, 37-40.

He, C., and Klionsky, D.J. (2009). Regulation mechanisms and signaling pathways of autophagy. Annu Rev Genet *43*, 67-93.

Hernandez, S.L., Nelson, M., Sampedro, G.R., Bagrodia, N., Defnet, A.M., Lec, B., Emolo, J., Kirschner, R., Wu, L., Biermann, H.*, et al.* (2019). Staphylococcus aureus alpha toxin activates Notch in vascular cells. Angiogenesis *22*, 197-209.

Heusser, S.A., Yoluk, O., Klement, G., Riederer, E.A., Lindahl, E., and Howard, R.J. (2016). Functional characterization of neurotransmitter activation and modulation in a nematode model ligand-gated ion channel. J Neurochem.

Hildebrand, A., Pohl, M., and Bhakdi, S. (1991). Staphylococcus aureus alpha-toxin. Dual mechanism of binding to target cells. J Biol Chem *266*, 17195-17200.

Hille, B. (1978). Ionic channels in excitable membranes. Current problems and biophysical approaches. Biophysical Journal *22*, 283.

Hille, B., and Catterall, W. (1994). Electrical excitability and ion channels.

Hoffmann, E.K., Lambert, I.H., and Pedersen, S.F. (2009). Physiology of cell volume regulation in vertebrates. Physiol Rev *89*, 193-277.

Hotze, E.M., and Tweten, R.K. (2012). Membrane assembly of the cholesterol-dependent cytolysin pore complex. Biochimica et biophysica acta *1818*, 1028-1038.

Huffman, D.L., Abrami, L., Sasik, R., Corbeil, J., van der Goot, F.G., and Aroian, R.V. (2004). Mitogen-activated protein kinase pathways defend against bacterial pore-forming toxins. Proc Natl Acad Sci U S A *101*, 10995-11000.

Husmann, M., Beckmann, E., Boller, K., Kloft, N., Tenzer, S., Bobkiewicz, W., Neukirch, C., Bayley,

H., and Bhakdi, S. (2009). Elimination of a bacterial pore-forming toxin by sequential endocytosis and exocytosis. FEBS Lett *583*, 337-344.

Husmann, M., Dersch, K., Bobkiewicz, W., Beckmann, E., Veerachato, G., and Bhakdi, S. (2006). Differential role of p38 mitogen activated protein kinase for cellular recovery from attack by pore-forming S. aureus alpha-toxin or streptolysin O. Biochem Biophys Res Commun *344*, 1128-1134.

Iacovache, I., Degiacomi, M.T., Pernot, L., Ho, S., Schiltz, M., Dal Peraro, M., and van der Goot, F.G. (2011). Dual chaperone role of the C-terminal propeptide in folding and oligomerization of the pore-forming toxin aerolysin. PLoS Pathog *7*, e1002135.

Iacovache, I., van der Goot, F.G., and Pernot, L. (2008). Pore formation: an ancient yet complex form of attack. Biochimica et biophysica acta *1778*, 1611-1623.

Idone, V., Tam, C., Goss, J.W., Toomre, D., Pypaert, M., and Andrews, N.W. (2008). Repair of injured plasma membrane by rapid Ca2+-dependent endocytosis. J Cell Biol *180*, 905-914.

Im, S.S., and Osborne, T.F. (2012). Protection from bacterial-toxin-induced apoptosis in macrophages requires the lipogenic transcription factor sterol regulatory element binding protein 1a. Mol Cell Biol *32*, 2196-2202.

Imre, G., Heering, J., Takeda, A.N., Husmann, M., Thiede, B., zu Heringdorf, D.M., Green, D.R., van der Goot, F.G., Sinha, B., Dotsch, V.*, et al.* (2012). Caspase-2 is an initiator caspase responsible for pore-forming toxin-mediumted apoptosis. EMBO J *31*, 2615-2628.

Inoshima, I., Inoshima, N., Wilke, G.A., Powers, M.E., Frank, K.M., Wang, Y., and Bubeck Wardenburg, J. (2011). A Staphylococcus aureus pore-forming toxin subverts the activity of ADAM10 to cause lethal infection in mice. Nat Med *17*, 1310-1314.

Inoshima, N., Wang, Y., and Bubeck Wardenburg, J. (2012). Genetic requirement for ADAM10 in severe Staphylococcus aureus skin infection. J Invest Dermatol *132*, 1513-1516.

Jiang, R., Taly, A., Lemoine, D., Martz, A., Cunrath, O., and Grutter, T. (2012). Tightening of the ATP-binding sites induces the opening of P2X receptor channels. EMBO J *31*, 2134-2143.

Jimenez, A.J., Maiuri, P., Lafaurie-Janvore, J., Divoux, S., Piel, M., and Perez, F. (2014). ESCRT machinery is required for plasma membrane repair. Science *343*, 1247136.

Johnson, B.B., and Heuck, A.P. (2014). Perfringolysin O structure and mechanism of pore formation as a paradigm for cholesterol-dependent cytolysins. Subcell Biochem *80*, 63-81.

Jonas, D., Walev, I., Berger, T., Liebetrau, M., Palmer, M., and Bhakdi, S. (1994). Novel path to apoptosis: small transmembrane pores created by staphylococcal alpha-toxin in T lymphocytes evoke internucleosomal DNA degradation. Infect Immun *62*, 1304-1312.

Jover, E., Tawk, M.Y., Laventie, B.J., Poulain, B., and Prevost, G. (2013). Staphylococcal leukotoxins trigger free intracellular Ca(2+) rise in neurones, signalling through acidic stores and activation of store-operated channels. Cell Microbiol *15*, 742-758.

Kacprzyk-Stokowiec, A., Kulma, M., Traczyk, G., Kwiatkowska, K., Sobota, A., and Dadlez, M. (2014). Crucial role of perfringolysin O D1 domain in orchestrating structural transitions leading to membrane-perforating pores: a hydrogen-deuterium exchange study. J Biol Chem *289*, 28738-28752.

Kaiser, W.J., Sridharan, H., Huang, C., Mandal, P., Upton, J.W., Gough, P.J., Sehon, C.A., Marquis, R.W., Bertin, J., and Mocarski, E.S. (2013). Toll-like receptor 3-mediumted necrosis via TRIF, RIP3, and MLKL. J Biol Chem *288*, 31268-31279.

Kaiser, W.J., Upton, J.W., and Mocarski, E.S. (2008). Receptor-interacting protein homotypic interaction motif-dependent control of NF-kappa B activation via the DNA-dependent activator of IFN regulatory factors. J Immunol *181*, 6427-6434.

Kao, C.Y., Los, F.C., Huffman, D.L., Wachi, S., Kloft, N., Husmann, M., Karabrahimi, V., Schwartz, J.L., Bellier, A., Ha, C.*, et al.* (2011). Global functional analyses of cellular responses to pore-forming toxins. PLoS Pathog *7*, e1001314.

Kathuria, R., and Chattopadhyay, K. (2018). Vibrio cholerae cytolysin: Multiple facets of the membrane interaction mechanism of a beta-barrel pore-forming toxin. IUBMB Life *70*, 260-266.

Kayagaki, N., Stowe, I.B., Lee, B.L., O'Rourke, K., Anderson, K., Warming, S., Cuellar, T., Haley, B., Roose-Girma, M., Phung, Q.T.*, et al.* (2015). Caspase-11 cleaves gasdermin D for non-canonical inflammasome signalling. Nature *526*, 666-671.

Kennedy, C.L., Smith, D.J., Lyras, D., Chakravorty, A., and Rood, J.I. (2009). Programmed cellular necrosis mediumted by the pore-forming alpha-toxin from Clostridium septicum. PLoS Pathog *5*, e1000516.

Keyel, P.A., Loultcheva, L., Roth, R., Salter, R.D., Watkins, S.C., Yokoyama, W.M., and Heuser, J.E. (2011). Streptolysin O clearance through sequestration into blebs that bud passively from the plasma membrane. J Cell Sci *124*, 2414-2423.

Khilwani, B., Mukhopadhaya, A., and Chattopadhyay, K. (2015). Transmembrane oligomeric

form of Vibrio cholerae cytolysin triggers TLR2/TLR6-dependent proinflammatory responses in monocytes and macrophages. Biochem J *466*, 147-161.

Kim G.H., Klotchkova T.A., Kang Y.-M. (2001) Life without a cell membrane: regeneration of protoplasts from disintegrated cells of the marine green alga Bryopsis plumosa. J Cell Sci *114*, 2009–2014.

Kitur, K., Parker, D., Nieto, P., Ahn, D.S., Cohen, T.S., Chung, S., Wachtel, S., Bueno, S., and Prince, A. (2015). Toxin-induced necroptosis is a major mechanism of Staphylococcus aureus lung damage. PLoS Pathog *11*, e1004820.

Kitur, K., Wachtel, S., Brown, A., Wickersham, M., Paulino, F., Penaloza, H.F., Soong, G., Bueno, S., Parker, D., and Prince, A. (2016). Necroptosis Promotes Staphylococcus aureus Clearance by Inhibiting Excessive Inflammatory Signaling. Cell Rep *16*, 2219-2230.

Kloft, N., Busch, T., Neukirch, C., Weis, S., Boukhallouk, F., Bobkiewicz, W., Cibis, I., Bhakdi, S., and Husmann, M. (2009). Pore-forming toxins activate MAPK p38 by causing loss of cellular potassium. Biochem Biophys Res Commun *385*, 503-506.

Kloft, N., Neukirch, C., Bobkiewicz, W., Veerachato, G., Busch, T., von Hoven, G., Boller, K., and Husmann, M. (2010). Pro-autophagic signal induction by bacterial pore-forming toxins. Med Microbiol Immunol *199*, 299-309.

Kloft, N., Neukirch, C., Von Hoven, G., Bobkiewicz, W., Weis, S., Boller, K., Husmann, M. (2012). A subunit of eukaryotic translation initiation factor 2α–phosphatase (CreP/PPP1R15B) regulates membrane traffic. *J. Biol. Chem* 287, 35299–35317.

Knapp, O., Maier, E., Mkaddem, S.B., Benz, R., Bens, M., Chenal, A., Geny, B., Vandewalle, A., and Popoff, M.R. (2010). Clostridium septicum alpha-toxin forms pores and induces rapid cell necrosis. Toxicon *55*, 61-72.

Koebnik, R., Locher, K.P., and Van Gelder, P. (2000). Structure and function of bacterial outer membrane proteins: barrels in a nutshell. Mol Microbiol *37*, 239-253.

Kondos, S.C., Hatfaludi, T., Voskoboinik, I., Trapani, J.A., Law, R.H., Whisstock, J.C., and Dunstone, M.A. (2010). The structure and function of mammalian membrane-attack complex/perforin-like proteins. Tissue Antigens *76*, 341-351.

Kovacs, S.B., and Miao, E.A. (2017). Gasdermins: Effectors of Pyroptosis. Trends Cell Biol *27*, 673-684.

Krantz, B. A., Melnyk, R. A., Zhang, S., Juris, S. J., Lacy, B. D., Wu, Z. Y., Finkelstein, A., Collier, R. J. (2005). A Phenylalanine Clamp Catalyzes Protein Translocation Through the Anthrax

Toxin Pore. Science 309, 777–781.

Kristan, K.C., Viero, G., Dalla Serra, M., Macek, P., and Anderluh, G. (2009). Molecular mechanism of pore formation by actinoporins. Toxicon *54*, 1125-1134.

Lakey, J.H., and Slatin, S.L. (2001). Pore-forming colicins and their relatives. Curr Top Microbiol Immunol *257*, 131-161.

Lamkanfi, M., and Dixit, V.M. (2014). Mechanisms and functions of inflammasomes. Cell *157*, 1013-1022.

LaRocca, T.J., Stivison, E.A., Hod, E.A., Spitalnik, S.L., Cowan, P.J., Randis, T.M., and Ratner, A.J. (2014). Human-specific bacterial pore-forming toxins induce programmed necrosis in erythrocytes. MBio *5*, e01251-01214.

Lasek, W., and Malejczyk, J. (2007). Mechanizmy cytotoksyczności limfocytów. Immunologia Gołąb J, Jakóbisiak M, Lasek W, Stokłosa T (eds) PWN, Warszawa, 241-249.

Law, R.H., Lukoyanova, N., Voskoboinik, I., Caradoc-Davies, T.T., Baran, K., Dunstone, M.A., D'Angelo, M.E., Orlova, E.V., Coulibaly, F., Verschoor, S.*, et al.* (2010). The structural basis for membrane binding and pore formation by lymphocyte perforin. Nature *468*, 447-451.

Lee, K.Z., Lestradet, M., Socha, C., Schirmeier, S., Schmitz, A., Spenle, C., Lefebvre, O., Keime, C., Yamba, W.M., Bou Aoun, R.*, et al.* (2016). Enterocyte Purge and Rapid Recovery Is a Resilience Reaction of the Gut Epithelium to Pore-Forming Toxin Attack. Cell Host Microbe *20*, 716-730.

Lehmann, C., Zeis, M., Schmitz, N., and Uharek, L. (2000). Impaired binding of perforin on the surface of tumor cells is a cause of target cell resistance against cytotoxic effector cells. Blood *96*, 594-600.

Lein, M., deRonde, B.M., Sgolastra, F., Tew, G.N., and Holden, M.A. (2015). Protein transport across membranes: Comparison between lysine and guanidinium-rich carriers. Biochimica et biophysica acta *1848*, 2980-2984.

Lewis, B.D., and Spalding, E.P. (1998). Nonselective block by La3+ of Arabidopsis ion channels involved in signal transduction. J Membr Biol *162*, 81-90.

Liang, X., and Ji, Y. (2006). Alpha-toxin interferes with integrin-mediumted adhesion and internalization of Staphylococcus aureus by epithelial cells. Cell Microbiol *8*, 1656-1668.

Linhartova, I., Bumba, L., Masin, J., Basler, M., Osicka, R., Kamanova, J., Prochazkova, K., Adkins, I., Hejnova-Holubova, J., Sadilkova, L.*, et al.* (2010). RTX proteins: a highly diverse family

secreted by a common mechanism. FEMS Microbiol Rev *34*, 1076-1112.

Liu, C.C., Young, L.H., and Young, J.D. (1996). Lymphocyte-mediumted cytolysis and disease. N Engl J Med *335*, 1651-1659.

Liu, X., Zhang, Z., Ruan, J., Pan, Y., Magupalli, V.G., Wu, H., and Lieberman, J. (2016). Inflammasome-activated gasdermin D causes pyroptosis by forming membrane pores. Nature *535*, 153-158.

Locovei, S., Scemes, E., Qiu, F., Spray, D.C., and Dahl, G. (2007). Pannexin1 is part of the pore forming unit of the P2X(7) receptor death complex. FEBS Lett *581*, 483-488.

Lodish, H., Berk, A., and Zipursky, S. (2000). Molecular cell biology 4th edition.

Martin, C.J., Peters, K.N., and Behar, S.M. (2014). Macrophages clean up: efferocytosis and microbial control. Curr Opin Microbiol *17*, 17-23.

Mathur, A., Feng, S., Hayward, J.A., Ngo, C., Fox, D., Atmosukarto, II, Price, J.D., Schauer, K., Martlbauer, E., Robertson, A.A.B.*, et al.* (2019). A multicomponent toxin from Bacillus cereus incites inflammation and shapes host outcome via the NLRP3 inflammasome. Nat Microbiol *4*, 362-374.

McCormack, R., de Armas, L., Shiratsuchi, M., and Podack, E.R. (2013a). Killing machines: three pore-forming proteins of the immune system. Immunol Res *57*, 268-278.

McCormack, R., de Armas, L.R., Shiratsuchi, M., Ramos, J.E., and Podack, E.R. (2013b). Inhibition of intracellular bacterial replication in fibroblasts is dependent on the perforin-like protein (perforin-2) encoded by macrophage-expressed gene 1. J Innate Immun *5*, 185-194.

McCoy, A.J., Koizumi, Y., Toma, C., Higa, N., Dixit, V., Taniguchi, S., Tschopp, J., and Suzuki, T. (2010). Cytotoxins of the human pathogen Aeromonas hydrophila trigger, via the NLRP3 inflammasome, caspase-1 activation in macrophages. Eur J Immunol *40*, 2797-2803.

McLarnon, J.G. (2005). Purinergic mediumted changes in Ca2+ mobilization and functional responses in microglia: effects of low levels of ATP. J Neurosci Res *81*, 349-356.

McNeil, A.K., Rescher, U., Gerke, V., and McNeil, P.L. (2006). Requirement for annexin A1 in plasma membrane repair. J Biol Chem *281*, 35202-35207.

McNeil, P.L., and Steinhardt, R.A. (2003). Plasma membrane disruption: repair, prevention, adaptation. Annu Rev Cell Dev Biol *19*, 697-731.

Michel, A.D., Grahames, C.B., and Humphrey, P.P. (1996). Functional characterisation of P2

purinoceptors in PC12 cells by measurement of radiolabelled calcium influx. Naunyn Schmiedebergs Arch Pharmacol *354*, 562-571.

Miller, C.M., Boulter, N.R., Fuller, S.J., Zakrzewski, A.M., Lees, M.P., Saunders, B.M., Wiley, J.S., and Smith, N.C. (2011). The role of the P2X(7) receptor in infectious diseases. PLoS Pathog *7*, e1002212.

Morgan BP, Luzio JP, Campbell AK. (1986). Intracellular Ca2+ and cell injury: a paradoxical role of Ca2+ in complement membrane attack. Cell Calcium 7, 399–411.

Moschioni, M., Tombola, F., de Bernard, M., Coelho, A., Zitzer, A., Zoratti, M., and Montecucco, C. (2002). The Vibrio cholerae haemolysin anion channel is required for cell vacuolation and death. Cell Microbiol *4*, 397-409.

Nagamune, K., Yamamoto, K., Naka, A., Matsuyama, J., Miwatani, T., and Honda, T. (1996). In vitro proteolytic processing and activation of the recombinant precursor of El Tor cytolysin/hemolysin (pro-HlyA) of Vibrio cholerae by soluble hemagglutinin/protease of V. cholerae, trypsin, and other proteases. Infection and immunity *64*, 4655-4658.

Nakae, T. (1976). Identification of the outer membrane protein of E. coli that produces transmembrane channels in reconstituted vesicle membranes. Biochem Biophys Res Commun *71*, 877-884.

North, R.A. (2002). Molecular physiology of P2X receptors. Physiol Rev *82*, 1013-1067.

Nygard Skalman, L., Holst, M.R., Larsson, E., and Lundmark, R. (2018). Plasma membrane damage caused by listeriolysin O is not repaired through endocytosis of the membrane pore. Biol Open *7*.

Olson, R., and Gouaux, E. (2005). Crystal structure of the Vibrio cholerae cytolysin (VCC) pro-toxin and its assembly into a heptameric transmembrane pore. J Mol Biol *350*, 997-1016.

Olson, R., Nariya, H., Yokota, K., Kamio, Y., and Gouaux, E. (1999). Crystal structure of staphylococcal LukF delineates conformational changes accompanying formation of a transmembrane channel. Nat Struct Biol *6*, 134-140.

Opota, O., Vallet-Gely, I., Vincentelli, R., Kellenberger, C., Iacovache, I., Gonzalez, M.R., Roussel, A., van der Goot, F.G., and Lemaitre, B. (2011). Monalysin, a novel ss-pore-forming toxin from the Drosophila pathogen Pseudomonas entomophila, contributes to host intestinal damage and lethality. PLoS Pathog *7*, e1002259.

Osickova, A., Masin, J., Fayolle, C., Krusek, J., Basler, M., Pospisilova, E., Leclerc, C., Osicka, R., and Sebo, P. (2010). Adenylate cyclase toxin translocates across target cell membrane without forming a pore. Mol Microbiol *75*, 1550-1562.

Osinska, I., Popko, K., and Demkow, U. (2014). Perforin: an important player in immune response. Cent Eur J Immunol *39*, 109-115.

Parker, M.W., and Feil, S.C. (2005). Pore-forming protein toxins: from structure to function. Progress in biophysics and molecular biology *88*, 91-142.

Paul, K., and Chattopadhyay, K. (2014). Pre-pore oligomer formation by Vibrio cholerae cytolysin: insights from a truncated variant lacking the pore-forming pre-stem loop. Biochem Biophys Res Commun *443*, 189-193.

Petrat, F., Drowatzky, J., Boengler, K., Finckh, B., Schmitz, K.J., Schulz, R., and de Groot, H. (2011). Protection from glycine at low doses in ischemia-reperfusion injury of the rat small intestine. Eur Surg Res *46*, 180-187.

Petrie, E.J., Czabotar, P.E., and Murphy, J.M. (2019). The Structural Basis of Necroptotic Cell Death Signaling. Trends Biochem Sci *44*, 53-63.

Potez, S., Luginbuhl, M., Monastyrskaya, K., Hostettler, A., Draeger, A., and Babiychuk, E.B. (2011). Tailored protection against plasmalemmal injury by annexins with different Ca2+ sensitivities. J Biol Chem *286*, 17982-17991.

Powers, M.E., Becker, R.E., Sailer, A., Turner, J.R., and Bubeck Wardenburg, J. (2015). Synergistic Action of Staphylococcus aureus alpha-Toxin on Platelets and Myeloid Lineage Cells Contributes to Lethal Sepsis. Cell Host Microbe *17*, 775-787.

Powers, M.E., Kim, H.K., Wang, Y., and Bubeck Wardenburg, J. (2012). ADAM10 mediumtes vascular injury induced by Staphylococcus aureus alpha-hemolysin. J Infect Dis *206*, 352-356.

Radin, J.N., Gonzalez-Rivera, C., Ivie, S.E., McClain, M.S., and Cover, T.L. (2011). Helicobacter pylori VacA induces programmed necrosis in gastric epithelial cells. Infection and immunity *79*, 2535-2543.

Rai, A.K., and Chattopadhyay, K. (2015a). Revisiting the membrane interaction mechanism of a membrane-damaging beta-barrel pore-forming toxin Vibrio cholerae cytolysin. Mol Microbiol *97*, 1051-1062.

Rai, A.K., and Chattopadhyay, K. (2015b). Vibrio cholerae cytolysin: structure-function mechanism of an atypical beta-barrel pore-forming toxin. Adv Exp Med Biol *842*, 109-

125.

RamaKrishnan, A.M., and Sankaranarayanan, K. (2016). Understanding autoimmunity: The ion channel perspective. Autoimmun Rev.

Rassow, J. (2011). Helicobacter pylori vacuolating toxin A and apoptosis. Cell Commun Signal *9*, 26.

Reboud, E., Bouillot, S., Patot, S., Beganton, B., Attree, I., and Huber, P. (2017). Pseudomonas aeruginosa ExlA and Serratia marcescens ShlA trigger cadherin cleavage by promoting calcium influx and ADAM10 activation. PLoS Pathog *13*, e1006579.

Reddy, A., Caler, E.V., and Andrews, N.W. (2001). Plasma membrane repair is mediated by Ca(2+)-regulated exocytosis of lysosomes. Cell *106*, 157-169.

Rivas, A.J., Lemos, M.L., and Osorio, C.R. (2013). Photobacterium damselae subsp. damselae, a bacterium pathogenic for marine animals and humans. Front Microbiol *4*, 283.

Rivas, A.J., von Hoven, G., Neukirch, C., Meyenburg, M., Qin, Q., Fuser, S., Boller, K., Lemos, M.L., Osorio, C.R., and Husmann, M. (2015). Phobalysin, a Small beta-Pore-Forming Toxin of Photobacterium damselae subsp. damselae. Infection and immunity *83*, 4335-4348.

Rodriguez, A., Webster, P., Ortego, J., and Andrews, N.W. (1997). Lysosomes behave as Ca2+-regulated exocytic vesicles in fibroblasts and epithelial cells. J Cell Biol *137*, 93-104.

Rojko, N., Dalla Serra, M., Macek, P., and Anderluh, G. (2016). Pore formation by actinoporins, cytolysins from sea anemones. Biochimica et biophysica acta *1858*, 446-456.

Ron, D., and Walter, P. (2007). Signal integration in the endoplasmic reticulum unfolded protein response. Nat Rev Mol Cell Biol *8*, 519-529.

Rossjohn, J., Feil, S.C., McKinstry, W.J., Tweten, R.K., and Parker, M.W. (1997). Structure of a cholesterol-binding, thiol-activated cytolysin and a model of its membrane form. Cell *89*, 685-692.

Russo, H.M., Rathkey, J., Boyd-Tressler, A., Katsnelson, M.A., Abbott, D.W., and Dubyak, G.R. (2016). Active Caspase-1 Induces Plasma Membrane Pores That Precede Pyroptotic Lysis and Are Blocked by Lanthanides. J Immunol *197*, 1353-1367.

Saka, H.A., Gutierrez, M.G., Bocco, J.L., and Colombo, M.I. (2007). The autophagic pathway: a cell survival strategy against the bacterial pore-forming toxin Vibrio cholerae cytolysin. Autophagy *3*, 363-365.

Savinov, S.N., and Heuck, A.P. (2017). Interaction of Cholesterol with Perfringolysin O: What

Have We Learned from Functional Analysis? Toxins (Basel) *9*.

Schirmer, T., Keller, T.A., Wang, Y.F., and Rosenbusch, J.P. (1995). Structural basis for sugar translocation through maltoporin channels at 3.1 A resolution. Science *267*, 512-514.

Schoenauer, R., Atanassoff, A.P., Wolfmeier, H., Pelegrin, P., Babiychuk, E.B., and Draeger, A. (2014). P2X7 receptors mediumte resistance to toxin-induced cell lysis. Biochimica et biophysica acta *1843*, 915-922.

Schoenauer, R., Larpin, Y., Babiychuk, E.B., Drucker, P., Babiychuk, V.S., Avota, E., Schneider-Schaulies, S., Schumacher, F., Kleuser, B., Koffel, R*., et al.* (2019). Down-regulation of acid sphingomyelinase and neutral sphingomyelinase-2 inversely determines the cellular resistance to plasmalemmal injury by pore-forming toxins. FASEB J *33*, 275-285.

Schreiber, R.D., Morrison, D.C., Podack, E.R., and Muller-Eberhard, H.J. (1979). Bactericidal activity of the alternative complement pathway generated from 11 isolated plasma proteins. J Exp Med *149*, 870-882.

Schuchman, E.H. (2010). Acid sphingomyelinase, cell membranes and human disease: lessons from Niemann-Pick disease. FEBS Lett *584*, 1895-1900.

Schuler, G.D., Boguski, M.S., Stewart, E.A., Stein, L.D., Gyapay, G., Rice, K., White, R.E., Rodriguez-Tome, P., Aggarwal, A., Bajorek, E*., et al.* (1996). A gene map of the human genome. Science *274*, 540-546.

Schwiering, M., Husmann, M., and Hellmann, N. (2017). P2X-Receptor Antagonists Inhibit the Interaction of S. aureus Hemolysin A with Membranes. Toxins (Basel) *9*.

Shatursky, O., Heuck, A.P., Shepard, L.A., Rossjohn, J., Parker, M.W., Johnson, A.E., and Tweten, R.K. (1999). The mechanism of membrane insertion for a cholesterol-dependent cytolysin: a novel paradigm for pore-forming toxins. Cell *99*, 293-299.

Shi, J., Zhao, Y., Wang, K., Shi, X., Wang, Y., Huang, H., Zhuang, Y., Cai, T., Wang, F., and Shao, F. (2015). Cleavage of GSDMD by inflammatory caspases determines pyroptotic cell death. Nature *526*, 660-665.

Shinkai, Y., Takio, K., and Okumura, K. (1988). Homology of perforin to the ninth component of complement (C9).

Singer, S.J., and Nicolson, G.L. (1972). The fluid mosaic model of the structure of cell membranes. Science *175*, 720-731.

Skals, M., Leipziger, J., and Praetorius, H.A. (2011). Haemolysis induced by alpha-toxin from Staphylococcus aureus requires P2X receptor activation. Pflugers Arch *462*, 669-679.

Skocaj, M., Yu, Y., Grundner, M., Resnik, N., Bedina Zavec, A., Leonardi, A., Krizaj, I., Guella, G., Macek, P., Kreft, M.E., *et al.* (2016). Characterisation of plasmalemmal shedding of vesicles induced by the cholesterol/sphingomyelin binding protein, ostreolysin A-mCherry. Biochimica et biophysica acta *1858*, 2882-2893.

Smets, B., Ghillebert, R., De Snijder, P., Binda, M., Swinnen, E., De Virgilio, C., and Winderickx, J. (2010). Life in the midst of scarcity: adaptations to nutrient availability in Saccharomyces cerevisiae. Curr Genet *56*, 1-32.

Solovyova, A.S., Nollmann, M., Mitchell, T.J., and Byron, O. (2004). The solution structure and oligomerization behavior of two bacterial toxins: pneumolysin and perfringolysin O. Biophys J *87*, 540-552.

Song, G., Ouyang, G., Bao, S. (2005). The activation of Akt/PKB signaling pathway and cell survival. *J Cell Mol Med* 9, 59–71.

Soong, G., Chun, J., Parker, D., and Prince, A. (2012). Staphylococcus aureus activation of caspase 1/calpain signaling mediumtes invasion through human keratinocytes. J Infect Dis *205*, 1571-1579.

Srivastava, S.S., Pany, S., Sneh, A., Ahmed, N., Rahman, A., and Musti, K.V. (2009). Membrane bound monomer of Staphylococcal alpha-hemolysin induces caspase activation and apoptotic cell death despite initiation of membrane repair pathway. PLoS One *4*, e6293.

Stillwell, W. (2013). An introduction to Biological Membranes. Academic Press.

Stanisstreet. M. (1982) Calcium and wound healing in xenopus early embryos. Journal of embryology and experimental morphology. Vol 67, 195-205.

Subramanyam, P., and Colecraft, H.M. (2015). Ion channel engineering: perspectives and strategies. J Mol Biol *427*, 190-204.

Tam, C., Idone, V., Devlin, C., Fernandes, M.C., Flannery, A., He, X., Schuchman, E., Tabas, I., and Andrews, N.W. (2010). Exocytosis of acid sphingomyelinase by wounded cells promotes endocytosis and plasma membrane repair. J Cell Biol *189*, 1027-1038.

Thelestam, M., and Mollby, R. (1983). Survival of cultured cells after functional and structural disorganization of plasma membrane by bacterial haemolysins and phospholipases. Toxicon *21*, 805-815.

Togo, T., Krasieva, T.B., and Steinhardt, R.A. (2000). A decrease in membrane tension precedes successful cell-membrane repair. Mol Biol Cell *11*, 4339-4346.

Tweten, R.K. (2005). Cholesterol-dependent cytolysins, a family of versatile pore-forming

toxins. Infection and immunity *73*, 6199-6209.

Uhlen, P., Laestadius, A., Jahnukainen, T., Soderblom, T., Backhed, F., Celsi, G., Brismar, H., Normark, S., Aperia, A., and Richter-Dahlfors, A. (2000). Alpha-haemolysin of uropathogenic E. coli induces Ca2+ oscillations in renal epithelial cells. Nature *405*, 694-697.

Usmani, S.M., von Einem, J., Frick, M., Miklavc, P., Mayenburg, M., Husmann, M., Dietl, P., and Wittekindt, O.H. (2012). Molecular basis of early epithelial response to streptococcal exotoxin: role of STIM1 and Orai1 proteins. Cell Microbiol *14*, 299-315.

Valeva, A. Walev, I., Gerber, A., Klein, J., Palmer, M., Bhakdi, S. (2000). Staphylococcal alpha-toxin: repair of a calcium-impermeable pore in the target cell membrane. *Mol. Microbiol* 36, 467–476.

von Hoven, G., Qin, Q., Neukirch, C., Husmann, M., and Hellmann, N. (2019). Staphylococcus aureus alpha-toxin: small pore, large consequences. Biol Chem *400*, 1261-1276.

von Hoven, G., Rivas, A.J., Neukirch, C., Klein, S., Hamm, C., Qin, Q., Meyenburg, M., Fuser, S., Saftig, P., Hellmann, N*., et al.* (2016). Dissecting the role of ADAM10 as a mediumtor of Staphylococcus aureus alpha-toxin action. Biochem J *473*, 1929-1940.

von Hoven, G., Rivas, A.J., Neukirch, C., Meyenburg, M., Qin, Q., Parekh, S., Hellmann, N., and Husmann, M. (2017). Repair of a Bacterial Small beta-Barrel Toxin Pore Depends on Channel Width. MBio *8*.

Walev, I., Bhakdi, S.C., Hofmann, F., Djonder, N., Valeva, A., Aktories, K., and Bhakdi, S. (2001). Delivery of proteins into living cells by reversible membrane permeabilization with streptolysin-O. Proc Natl Acad Sci U S A *98*, 3185-3190.

Walev, I., Martin, E., Jonas, D., Mohamadzadeh, M., Muller-Klieser, W., Kunz, L., and Bhakdi, S. (1993). Staphylococcal alpha-toxin kills human keratinocytes by permeabilizing the plasma membrane for monovalent ions. Infection and immunity *61*, 4972-4979.

Walev, I., Palmer, M., Martin, E., Jonas, D., Weller, U., Hohn-Bentz, H., Husmann, M., and Bhakdi, S. (1994). Recovery of human fibroblasts from attack by the pore-forming alpha-toxin of Staphylococcus aureus. Microb Pathog *17*, 187-201.

Walev, I., Reske, K., Palmer, M., Valeva, A., and Bhakdi, S.(1995). Potassium‐inhibited processing of IL‐1 beta in human monocytes. EMBO J *14*, 1607-1614.

Wang, H., Sun, L., Su, L., Rizo, J., Liu, L., Wang, L.F., Wang, F.S., and Wang, X. (2014). Mixed lineage kinase domain-like protein MLKL causes necrotic membrane disruption upon

phosphorylation by RIP3. Mol Cell *54*, 133-146.

Wang, K., Li, J., Degterev, A., Hsu, E., Yuan, J., and Yuan, C. (2007). Structure-activity relationship analysis of a novel necroptosis inhibitor, Necrostatin-5. Bioorg Med Chem Lett *17*, 1455-1465.

Watson, H. (2015). Biological membranes. Essays Biochem *59*, 43-69.

Wickham, S.E., Hotze, E.M., Farrand, A.J., Polekhina, G., Nero, T.L., Tomlinson, S., Parker, M.W., and Tweten, R.K. (2011). Mapping the intermedilysin-human CD59 receptor interface reveals a deep correspondence with the binding site on CD59 for complement binding proteins C8alpha and C9. J Biol Chem *286*, 20952-20962.

Wiles, T.J., Dhakal, B.K., Eto, D.S., and Mulvey, M.A. (2008). Inactivation of host Akt/protein kinase B signaling by bacterial pore-forming toxins. Mol Biol Cell *19*, 1427-1438.

Wiles, T.J., and Mulvey, M.A. (2013). The RTX pore-forming toxin alpha-hemolysin of uropathogenic Escherichia coli: progress and perspectives. Future microbiology *8*, 73-84.

Wilke, G.A., and Bubeck Wardenburg, J. (2010). Role of a disintegrin and metalloprotease 10 in Staphylococcus aureus alpha-hemolysin-mediumted cellular injury. Proc Natl Acad Sci U S A *107*, 13473-13478.

Willison, J.H., and Johnston, G.C. (1985). Ultrastructure of Saccharomyces cerevisiae strain AG1-7 and its responses to changes in environment. Can J Microbiol *31*, 109-118.

Wolfmeier, H., Radecke, J., Schoenauer, R., Koeffel, R., Babiychuk, V.S., Drucker, P., Hathaway, L.J., Mitchell, T.J., Zuber, B., Draeger, A.*, et al.* (2016). Active release of pneumolysin prepores and pores by mammalian cells undergoing a Streptococcus pneumoniae attack. Biochimica et biophysica acta *1860*, 2498-2509.

Wolfmeier, H., Schoenauer, R., Atanassoff, A.P., Neill, D.R., Kadioglu, A., Draeger, A., and Babiychuk, E.B. (2015). Ca(2)(+)-dependent repair of pneumolysin pores: A new paradigm for host cellular defense against bacterial pore-forming toxins. Biochimica et biophysica acta *1853*, 2045-2054.

Yang, S.T., Kreutzberger, A.J.B., Lee, J., Kiessling, V., and Tamm, L.K. (2016). The role of cholesterol in membrane fusion. Chem Phys Lipids *199*, 136-143.

Young, J., Cohn, Z.A., and Podack, E.R. (1986). The ninth component of complement and the pore-forming protein (perforin 1) from cytotoxic T cells: structural, immunological, and functional similarities. Science *233*, 184-190.

Yuldasheva, L.N., Merzlyak, P.G., Zitzer, A.O., Rodrigues, C.G., Bhakdi, S., and Krasilnikov, O.V. (2001). Lumen geometry of ion channels formed by Vibrio cholerae EL Tor cytolysin elucidated by nonelectrolyte exclusion. Biochimica et biophysica acta *1512*, 53-63.

Zhang, Y., Chen, X., Gueydan, C., and Han, J. (2018). Plasma membrane changes during programmed cell deaths. Cell Res *28*, 9-21.

Zitzer, A., Harris, J.R., Kemminer, S.E., Zitzer, O., Bhakdi, S., Muething, J., and Palmer, M. (2000). Vibrio cholerae cytolysin: assembly and membrane insertion of the oligomeric pore are tightly linked and are not detectably restricted by membrane fluidity. Biochimica et biophysica acta *1509*, 264-274.

Zitzer, A., Wassenaar, T.M., Walev, I., and Bhakdi, S. (1997). Potent membrane-permeabilizing and cytocidal action of Vibrio cholerae cytolysin on human intestinal cells. Infection and immunity *65*, 1293-1298.

Zitzer, A., Zitzer, O., Bhakdi, S., and Palmer, M. (1999). Oligomerization of Vibrio cholerae cytolysin yields a pentameric pore and has a dual specificity for cholesterol and sphingolipids in the target membrane. J Biol Chem *274*, 1375-1380.